UNIVERSIDADE FEDERAL DE PERNAMBUCO
CENTRO DE TECNOLOGIA E GEOCIÊNCIAS
PROGRAMA DE PÓS-GRADUAÇÃO EM GEOCIÊNCIAS
DEPARTAMENTO DE GEOLOGIA

WILLIAN ALEXANDRE LIMA DE MOURA

ESTRATIGRAFIA QUÍMICA E ESPECTRAL DA FORMAÇÃO ESTIVA (ALBIANO SUPERIOR-TURONIANO) DA BACIA PERNAMBUCO, NE DO BRASIL

Dissertação de Mestrado

Recife
2020

WILLIAN ALEXANDRE LIMA DE MOURA

ESTRATIGRAFIA QUÍMICA E ESPECTRAL DA FORMAÇÃO ESTIVA (ALBIANO SUPERIOR-TURONIANO) DA BACIA PERNAMBUCO, NE DO BRASIL

Dissertação de mestrado apresentada ao Programa de Pós Graduação em Geociências como requisito parcial para obtenção do grau de Mestre em geociências.

Área de concentração: Geologia sedimentar e ambiental

Orientador (a): Prof.Dr. Mário de Lima Filho PPGEOC-UFPE

Coorientadores (a): Prof.Dr. João Adauto de Souza Neto PPGEOC-UFPE

Dra. Rosa Elvira Correa Pabón ITV-VALE-PROFICAN

Recife

2020

Catalogação na fonte:
Bibliotecário Josias Machado, CRB-4 / 1690

M929e Moura, William Alexandre Lima de.
Estratigrafia química e espectral da formação estiva (Albiano superior-turoniano) da Bacia Pernambuco, NE do Brasil. / Willian Alexandre Lima de Moura. – 2020.
132 f.: il., figs.

Orientador: Prof. Dr. Mario de Lima Filho.
Coorientador: Prof. Dr. João Adauto de Souza Neto.
Coorientadora: Prof.ª Dra. Rosa Elvira Correa Pabón.
Dissertação (Mestrado) – Universidade Federal de Pernambuco. CTG. Programa de Pós-Graduação em Geociências, Recife, 2020.
Inclui referências.

1. Geociências. 2. Sistemas carbonáticos. 3. Geoquímica. 4. Espectroscopia de reflectância. 5. Formação estiva. 6. Bacia Pernambuco. I. Lima Filho, Mario de (orientador). II. Souza Neto, João Adauto de (coorientador). Pabón, Rosa Elvira Correa. III. (coorientador). III. Título.

UFPE

551 CDD (22. ed.) BCTG/2022-227

WILLIAN ALEXANDRE LIMA DE MOURA

ESTRATIGRAFIA QUÍMICA E ESPECTRAL DA FORMAÇÃO ESTIVA (ALBIANO SUPERIOR-TURONIANO) DA BACIA PERNAMBUCO, NE DO BRASIL

Dissertação apresentada ao Programa de Pós-Graduação em Geociências da Universidade Federal de Pernambuco, Centro de Tecnologia e Geociências, como requisito parcial para a obtenção do título de Mestre em Geociências. Área de Concentração: Geologia Sedimentar e Ambiental.

Aprovada em: 09/11/2020

BANCA EXAMINADORA

Prof. Dr. João Adauto de Souza Neto (Coorientador)
Universidade Federal de Pernambuco

Prof. Dr. Virgínio Henrique de Miranda Lopes Neumann (Examinador Interno)
Universidade Federal de Pernambuco

Prof. Dr. René Rodrigues (Examinador Externo)
Universidade do Estado do Rio de Janeiro

AGRADECIMENTOS

Agradeço a minha família, por todo o apoio durante a minha vida principalmente nos meus anos de graduação e de pós-graduação. É uma honra e orgulho ter vocês como família.

Agradeço ao CNPq pela concessão da bolsa de mestrado, instituição esta que precisa ser respeitada e defendida com todo ardor, neste momento de destruição da nossa soberania nacional. A Petrobras S.A pela realização da sondagem estratigráfica 1 LABIO PE 1, no âmbito do projeto “Bioestratigrafia da Bacia Pernambuco”. Devidos agradecimentos ao Laboratório de Quimioestratigrafia da UERJ na pessoa do Prof. Dr. René Rodrigues pela realização das análises de COT e ST. Também agradeço ao LABOQUIM e ao prof. Dr. Manuel Flores (DOCEAN) e dos técnicos Keyla e Bruno pela realização das análises isotópicas.
Ao IG UNICAMP na pessoa do professor Carlos Roberto de Souza. A prof. Dr. Thais Carrino (UFPE) e Rosa Pabón (ITV) pelo apoio na realização das análises espectrais e de imageamento hiperespectral.

Aos amigos que a geologia e a vida me proporcionaram: Márcio, Lilia, Isis, Kátia, Pamy, Rodrigo, Mateus, Pablo, Igor, Douglas, Jefferson, Phelps, João Maria, Diego, Ian, Flávia, Léo, Alcione, Vivian, Caio, Gabi, Diogo, Alan, Thalita, Daniel selva, Pierre, Stephany, Jailson, Sara, João Carlos. Isabela. Ainda agradeço aos membros do A.A. Diniz, Daniel, Tiago, Rafael, Luis, Cayo, Gabriel, Andres, Zarzar, Salviano, Luana. Sempre grato por todos os momentos de dificuldade mais principalmente aos momentos de alegria (e quantos momentos!). Também agradeço a minha grande amiga e geóloga Rizelda Regadas por todos os conselhos e amizade. A Thaisa Moura pela amizade de longas datas. Aos amigos da Checkmat Recife e ao Mestre Alexandre Xavier por todos os ensinamentos ao longo desse último ano.

Aos professores do Departamento de Geologia e do PPGEOC meu muito obrigado por todo o aprendizado e ensinamentos ao longo dos anos de graduação e de pós-graduação. Em especial aos profs. Andres, Gorki, Paula, Osvaldo, Carlinda, Gelson, Sônia, Virginio, Antônio, Anelise, Ignez, Lúcia, Tiago, Sérgio, Thais, Marcelo.

Meu muito obrigado aos prof. Adauto e ao Prof. Mário pela orientação, paciência, ensinamentos, amizade durante minha formação ao longo de todos esses anos, o que me tornei como pessoa e como profissional se deve sobretudo a vocês. Também agradeço aos membros do Laboratório de Geoquímica Aplicada ao Petróleo: Thales, Aline, Acauã, Gabriel, Bruno, Josy. Aos amigos do CRCN-CNEN Crescêncio, Ana Cláudia, Gilberto, Alex, Mariana, Déric, Elvis, Bethania.

Obrigado!

“Do ser ao pó, é só carbono
Solene, terreno, imenso
Perene, pequeno, humano”

(Lenine)

RESUMO

A Bacia Pernambuco é uma das bacias marginais do Atlântico Sul, formada durante a quebra do supercontinente Gondwana na era mesozoica. Este estudo foi desenvolvido em um ambiente carbonático intensamente dolomitizadas da Formação Estiva, depositadas durante a fase drifte (Albiano superior-Turoniano). Foram determinados os aspectos petrográficos, as assinaturas espectrais, e os teores geoquímicos de carbono orgânico total, enxofre total e nitrogênio total, bem como os isótopos estáveis de carbono orgânico (13C/12C) e nitrogênio (15N/14N) na sondagem estratigráfica 1 LABIO PE 1. Foram identificados: dolowackestones e dolopackestones com pelóides e siliciclásticos, margas, folhelhos e arenitos calcíferos como principais litologias bem como a ocorrência de veios ricos em calcita. As concentrações de COT (0.19 e 3.6%) e ST (0,02 e 1,32%) sugerem deposição desde condições de água doce à água salina (marinho). Já a relação entre δ13C e a razão TOC/TN sugerem uma matéria orgânica rica em fitoplâncton marinho e plantas terrestres tipo C3. Assinaturas geoquímicas de δ13Corg entre -24,65 e -18,51‰ e de δ15N entre +0,93 e +5,44‰, sugerem que o intervalo estratigráfico estudado foi depositado durante o evento de anoxia global 2, ocorrido na passagem Cenomaniano-Turoniano (~94Ma). As assinaturas espectrais das litologias existentes na sondagem apresentaram as seguintes feições: os dolomitos apresentaram feição assimétrica em ~2320nm, relacionado a interação C-O; já os folhelhos possuem assinatura simétrica em ~2210nm, relacionado a interação Al-OH e a presença de ilita-smectita como principais argilominerais. Já as margas possuem duas feições características em ~2210nm relacionado a interação Al-OH e ~2320nm relacionado a C-O. Os veios de calcita apresentaram feições em 2340nm relacionados a interação C-O. Foram diferenciadas três sequências estratigráficas de terceira ordem, limitadas pela superfície de inundação máxima (SIM). Cada sequência está limitada por superfícies de inundação máxima, marcados por valores de COT de até 3,6%. O aumento de argila marcado pela absorção em 2210nm foi também relacionado a superfícies de inundação máxima.

Palavras-chave: sistemas carbonáticos; geoquímica; espectroscopia de reflectância; formação estiva; bacia Pernambuco.

ABSTRACT

The Pernambuco Basin is one of the most marginal sedimentary basins of the South Atlantic, formed during the Gondwana breakup in the Mesozoic era. This study was developed in carbonate environments intensely dolomitized of the Estiva Formation, deposited during the drift phase (late Albian to Turonian ages). It was determined the petrographic features, spectral signatures, and the geochemical data of Total Organic Carbon (TOC), Total Sulphur (TS), and Total Nitrogen (TN), as well as the carbon ($^{13}C/^{12}C$) and nitrogen isotopes ($^{15}N/^{14}N$) on the 1 LABIO PE 1 well. It was characterized dolowackestones and dolopackestones with peloids and siliciclastics, marls, shales, as well as carbonate-sandstones, as the main lithologies, calcite veins are also observed. The TOC concentration (0.19 e 3.6%) and the TS concentration (0.02 e 1.32%) suggest deposition from freshwater to saline waters (marine). On the other hand, the δ13C and the TOC/TN ratio suggest marine phytoplankton and C3 land plants as the main source of the organic matter. The $\delta^{13}C_{org}$ signature between -24.65 and -18.51‰ and the bulk $\delta^{15}N$ between +0.93 and +5.44‰, indicates that the investigated section was deposited during the oceanic anoxic event 2 occurred during the Cenomanian-Turonian boundary (~94Ma). The spectral signatures of the lithologies on the studied well present those features: the dolostones presents an asymmetrical absorption feature into 2320 nm related to C-O bonds, the shales asymmetrical feature into 2210 nm associated with Al-OH bonds, and illite and smectite as the main clay content. The marls present both absorption features into 2320nm and 2210nm, as well as the calcite veins an absorption feature into 2340nm also related to C-O bonds. It was differentiated three sequences bounded by the maximum flooding surfaces (MFS) marked by TOC values until 3.6%. The increase of argilosity marked by 2210nm absorption feature was also related to the MFS.

Keywords: carbonate environments; geochemistry; reflectance spectroscopy; estiva formation; Pernambuco basin

LISTA DE ILUSTRAÇÕES

SUMÁRIO

1 INTRODUÇÃO

O presente capítulo apresenta o estado da arte da geologia da Bacia Pernambuco e sua relação regional com as demais bacias sedimentares do Nordeste e seu embasamento cristalino. Também são apresentados o estado da arte sobre dolomitas e o processo de dolomitização em ambientes carbonáticos e a aplicação da técnica de espectroscopia de reflectância em rochas sedimentares.

1.1 Formação das bacias sedimentares do Nordeste brasileiro

O processo de formação das bacias sedimentares do Nordeste (Figura 1) se estabelece após os estágios finais de colisão e formação do supercontinente Gondwana no início do paleozoico (~540Ma). Inicialmente a sedimentação ocorreu por processos de sinéclise (Mabessoone & Neumann, 2005). Este processo ocorrido durante o ordoviciano superior-siluriano (460-415 Ma) foi responsável pela formação de extensas bacias sedimentares a exemplo da Bacia do Parnaíba, com a deposição do grupo Serra Grande (formações Ipu, Tianguá e Jaicós), (Caputo & Lima, 1984). Ainda durante o Paleozoico (Jurássico 200-145Ma) se estabeleceu no Nordeste um rifte estreito de direção NW-SE denominada de depressão afrobrasileira responsável pela deposição de sedimentos lacustres (Ponte & Ponte Filho, 1996). E formação das bacias de Sergipe-Alagoas, Jatobá, Tucano, Araripe e Parnaíba. A fase rifte é atribuída pós-período jurássico (Moulin et al., 2010), devido a esforços de direção NW-SE responsável pela geração dos principais braços de rifte e ruptura do supercontinente Gondwana (Matos, 1999).

Figura 1: Mapa geológico da Província Borborema, com destaque para as bacias sedimentares do NE e a influência de zonas de cisalhamento no controle tectônico. As bacias com sedimentação paleozoica estão diferenciadas das bacias cretáceas.

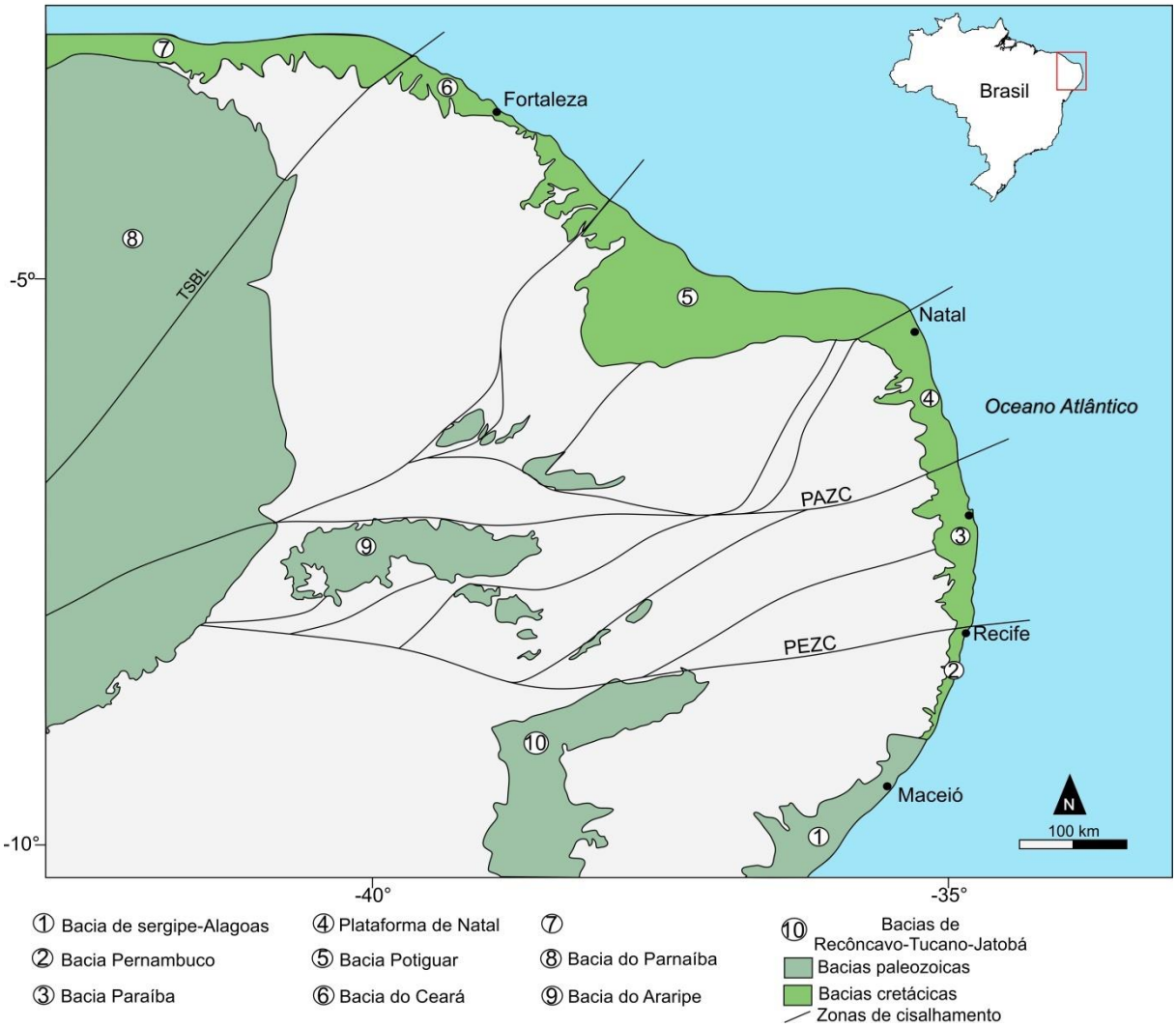

Fonte: Geobank CPRM (disponível em: http://geobank.cprm.gov.br/)

MATOS (1999) relaciona a herança do embasamento cristalino e de suas estruturas (e.g. Zonas de Cisalhamento) na acomodação e formação dos riftes intracontinentais. Este autor ainda relaciona o desenvolvimento de manifestações magmáticas e fases deformacionais. Matos (1999) descreve a evolução e formação das bacias sedimentares do Nordeste em quatro etapas: sin-rifte I; sin-rifte IIa; sin-rifte IIb; sin-rifte IIc. Estas etapas serão descritas a seguir.

Sin-rifte I: Está relacionada ao período Jurássico Superior (161-145Ma), através do desenvolvimento da depressão afro-brasileira, com processos de

sinéclise. Neta etapa sedimentação lacustre é observada ao longo de bacias sedimentares como Araripe com a deposição da Formação Missão Velha; Jatobá e Tucano com a deposição da Formação Aliança; Sergipe-Alagoas e a deposição da Formação Bananeiras (Figura 2A).

Sin-rifte IIa: Está relacionada ao período Berriasiano Inferior (145-140Ma), onde esforços extensionais de direção NW-SE gerou reativação das estruturas NW-SE por falhas normais e processos de transtensão das estruturas NE-SW e E-W. Esta atividade fori responsável pela formação dos riftes de Sergipe-Alagoas-Gabão (GSA) e Recôncavo-Tucano-Jatobá (RTJ), estes acomodados por geometria de meio-grábens. Nestas bacias sedimentares esta etapa é marcada pela deposição de sedimentos em sistemas de leques aluviais e sistemas fluviais como a Formações Itaparica-Candeias nas bacias do Recôncavo-Tucano-Jatobá; e Barra de Itiúba na Bacia de Sergipe Alagoas (Figura 2B).

Sin-rifte IIb: Ainda relacionado a esforços extensionais de direção NW-SE, durante o Valaginiano-Hautereviano (140-130Ma). Esta etapa marca a consolidação dos riftes de GSA e RTJ, além de um novo braço de rifte de direção NE-SW denominado Cariri-Potiguar (CP), responsável pela sedimentação nas bacias de Iguatu, Rio do Peixe, Araripe (Figura 2C).

Sin-rifte IIc: Esta etapa ocorrida durante o Barreminano (130-126Ma). Nesta etapa o avanço do rifte nas bacias do grupo GSA se estabeleceu com elevadas taxas de sedimentação. O rifte CP é abortado e a o rifte se propaga na direção bacias do grupo GSA (Figura 2D).

Figura 2: Modelo de evolução geológica para o NE brasileiro durante o Jurássico Superior até o Barremiano, Adaptado de MATOS (1999).

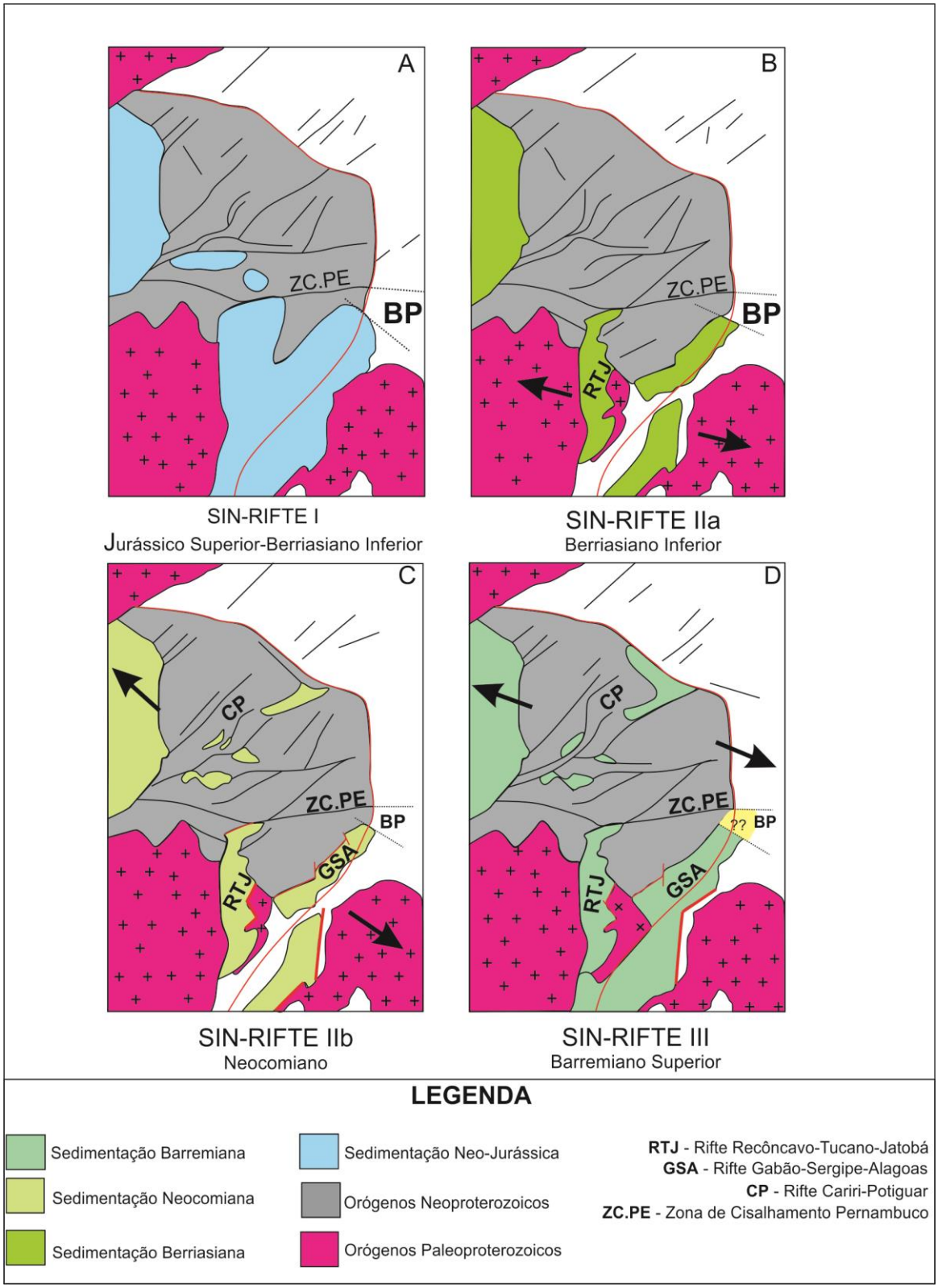

Fonte: Adaptado de MATOS (1999).

1.2 Bacia Pernambuco

Neste tópico serão descritos os principais trabalhos envolvendo a Bacia Pernambuco e o conhecimento geológico relacionado à esta bacia.

1.2.1 Evolução tectônica da Bacia Pernambuco

A Bacia Pernambuco, foi definida inicialmente como sub-bacia do Cabo como parte da Bacia Pernambuco-Paraíba (Alheiros & Ferreira, 1989) Entretanto após os estudos de LIMA FILHO (1998), esta fração geológica foi individualizada, ganhando o status de Bacia Pernambuco. Para este autor a Bacia Pernambuco fica limitada pela Zona de Cisalhamento Pernambuco e o Alto Estrutural de Maragogi Barreiros (Figura 3). A Bacia Pernambuco é uma bacia sedimentar tipo rifte associada aos processos de quebra do subcontinente Gondwana. Para LIMA FILHO (1998), esta bacia sedimentar possui características estruturais e estratigráficas similares às demais bacias marginais localizadas a sul, estando compartimentada por grábens e limitada por falhas normais de alto ângulo e falhas de transferência com grandes e profundos depocentros, enquanto a Bacia Paraíba possui um arcabouço em forma de rampa (Barbosa et al., 2007).

Figura 3: Mapa geológico da Província Borborema com destaque as bacias sedimentares do NE. Estão subdivididas as bacias que apresentam sedimentação paleozoica das bacias que apresentam sedimentação apenas cretácicas.

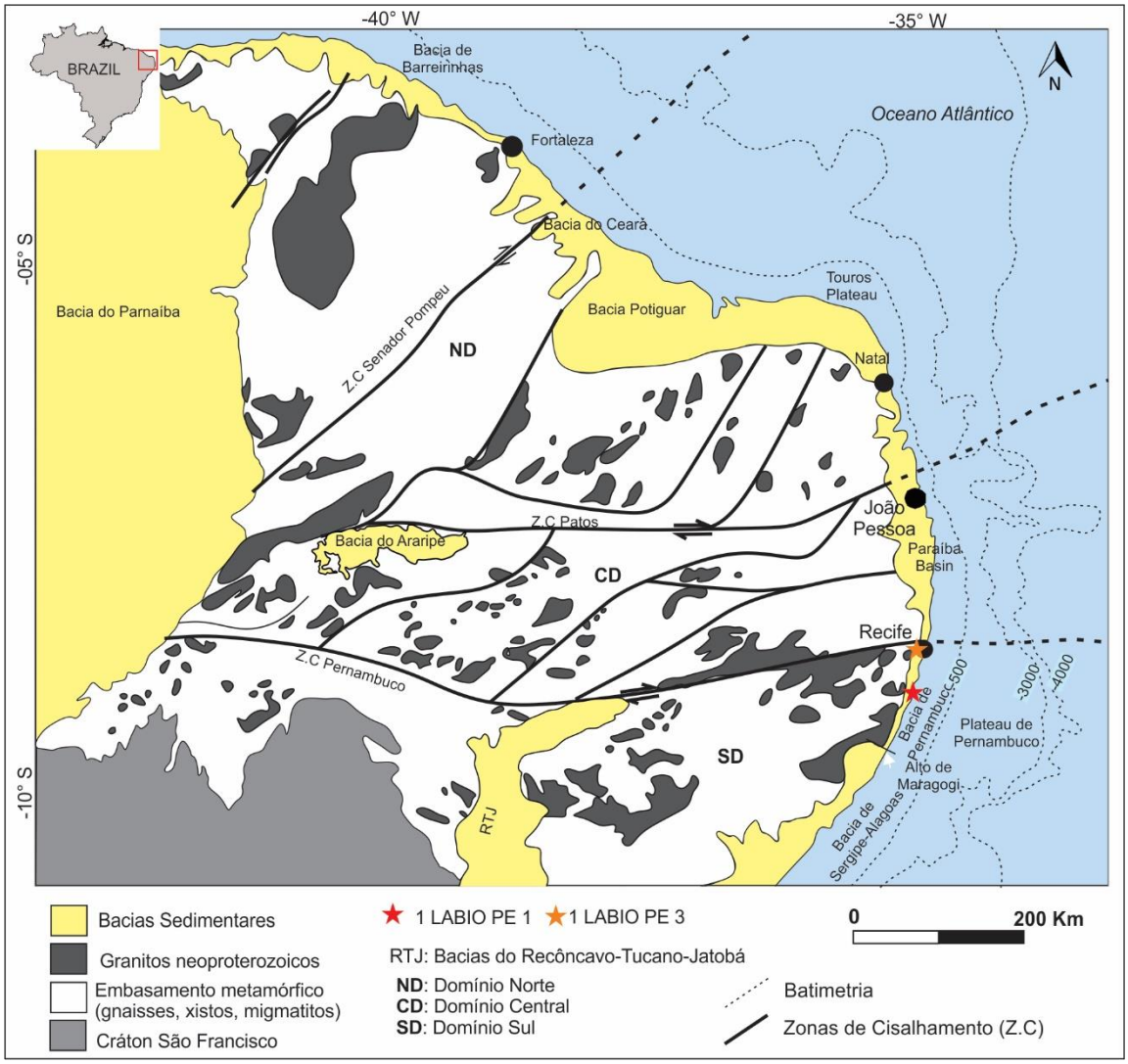

Fonte: geobank CPRM (disponível em: http://geobank.cprm.gov.br/)

LIMA FILHO (1998) JARDIM DE SÁ et al. (2003) e CORREIA FILHO (2017) compartimentam a Bacia Pernambuco em duas sub-bacias, a primeira a bacia interna (*onshore*) limitada ao leste pelo embasamento cristalino da Província Borborema e controlada por falhas normais de alto ângulo com direção NE-SW e falhas de transferência com componentes normais cuja direção é NW-SE. Ao oeste está limitada pelo Alto Estrutural de Maracatu. Esta importante estruturação subdivide a bacia interna da bacia externa, denominado de Platô de Pernambuco (Morais, 2008). Este setor da Bacia Pernambuco (*offshore*) possui pouco

conhecimento geológico devido à falta de sondagens estratigráficas, sendo seu conhecimento limitado através de linhas sísmicas e correlação com sondagens da bacia interna (Figura 4).

Figura 4: Compartimentação tectônica da Bacia Pernambuco e sua localização em relação as bacias marginais da margem leste do NE. Ainda se destaca os dados de batimetria e a indicação do Alto Estrutural de Maracatu.

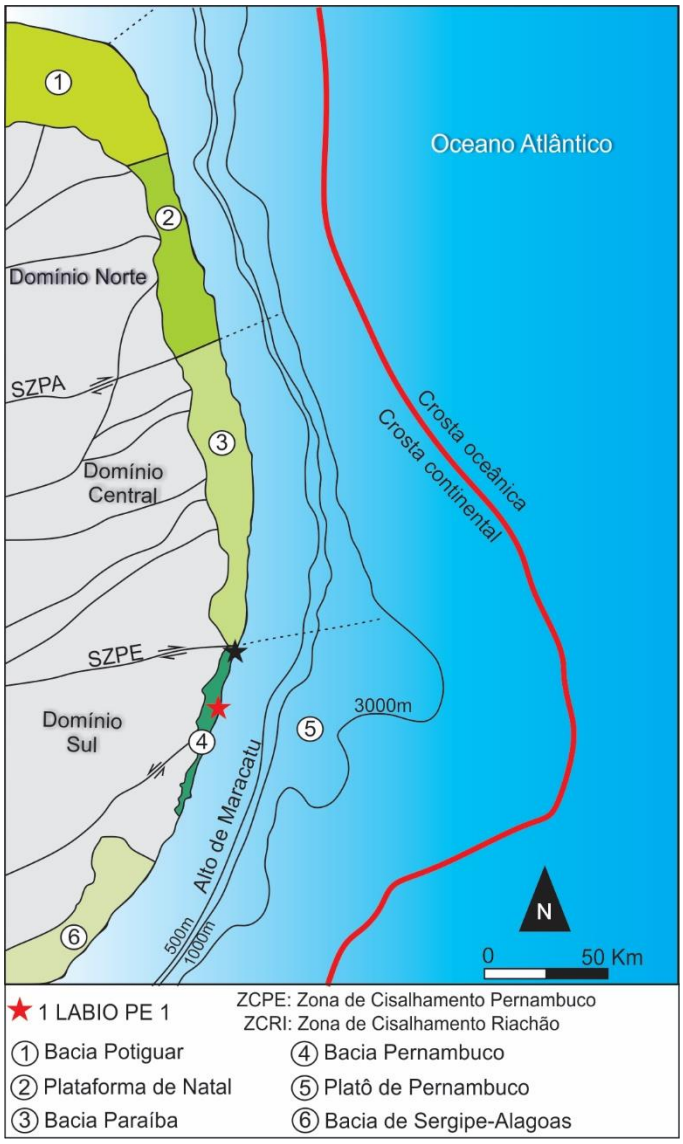

Fonte: Adaptado de BUARQUE et al. (2016)

A Bacia Externa, também denominada de Platô de Pernambuco está compartimentada por três grábens, a saber: gráben de Itapuama, gráben de Tamandaré e o gráben externo do Platô (Oliveira, 2013). Estando limitada pelo Alto

Estrutural vulcânico de Gaibu, localizado na área central desta sub-bacia e o Alto de Itamaracá com lineamento NW-SE, limitando com a Bacia Paraíba (Figura 5).

Figura 5: Compartimentação estrutural da Bacia Pernambuco e seus principais depocentros, em destaque os do Platô de Pernambuco. A linha de costa está destacada em vermelho.

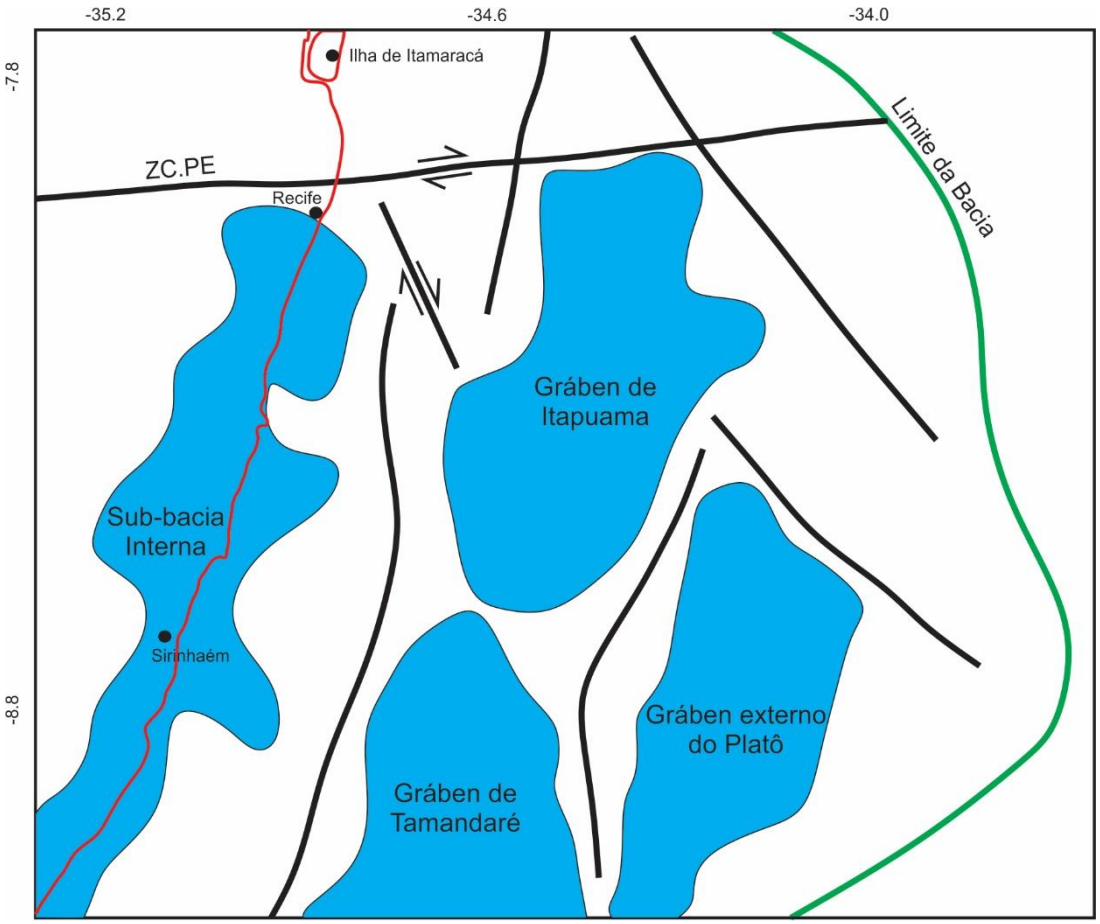

Fonte: Adaptado de OLIVEIRA (2013).

A bacia interna é subdividida em três principais grábens, a saber: Gráben de Sirinhaém, Gráben do Cupe e Gráben de Piedade (Figura 6). Os grábens de Sirinhaém e do Cupe possuem como características presença de depocentros profundos (estimados por gravimetria em 3500 metros) e através de poços de aproximadamente 2950 metros (Sondagem exploratória 2-CP-01-PE; Maia, 2012). Estes grábens são limitados por altos vulcânicos, que se alojaram ao longo de estruturas Pré-Cambrianas e falhas normais. A zona de Cisalhamento Pernambuco possui papel importante na propagação do rifte, esta estrutura pretérita, atenuou os

esforços, retardando a continuação do rifte em direção a Bacia Paraíba. Além disto, se comportou como um alto estrutural, conforme mostrado nos trabalhos de LIMA FILHO (1998), JARDIM DE SÁ et al. (2003), BARBOSA & LIMA FILHO (2005) e CORREIA FILHO (2017).

Figura 6: Compartimentação estrutural da Região interna da Bacia Pernambuco, em destaque a localização da sondagem estratigráfica 1 LABIO PE 1.

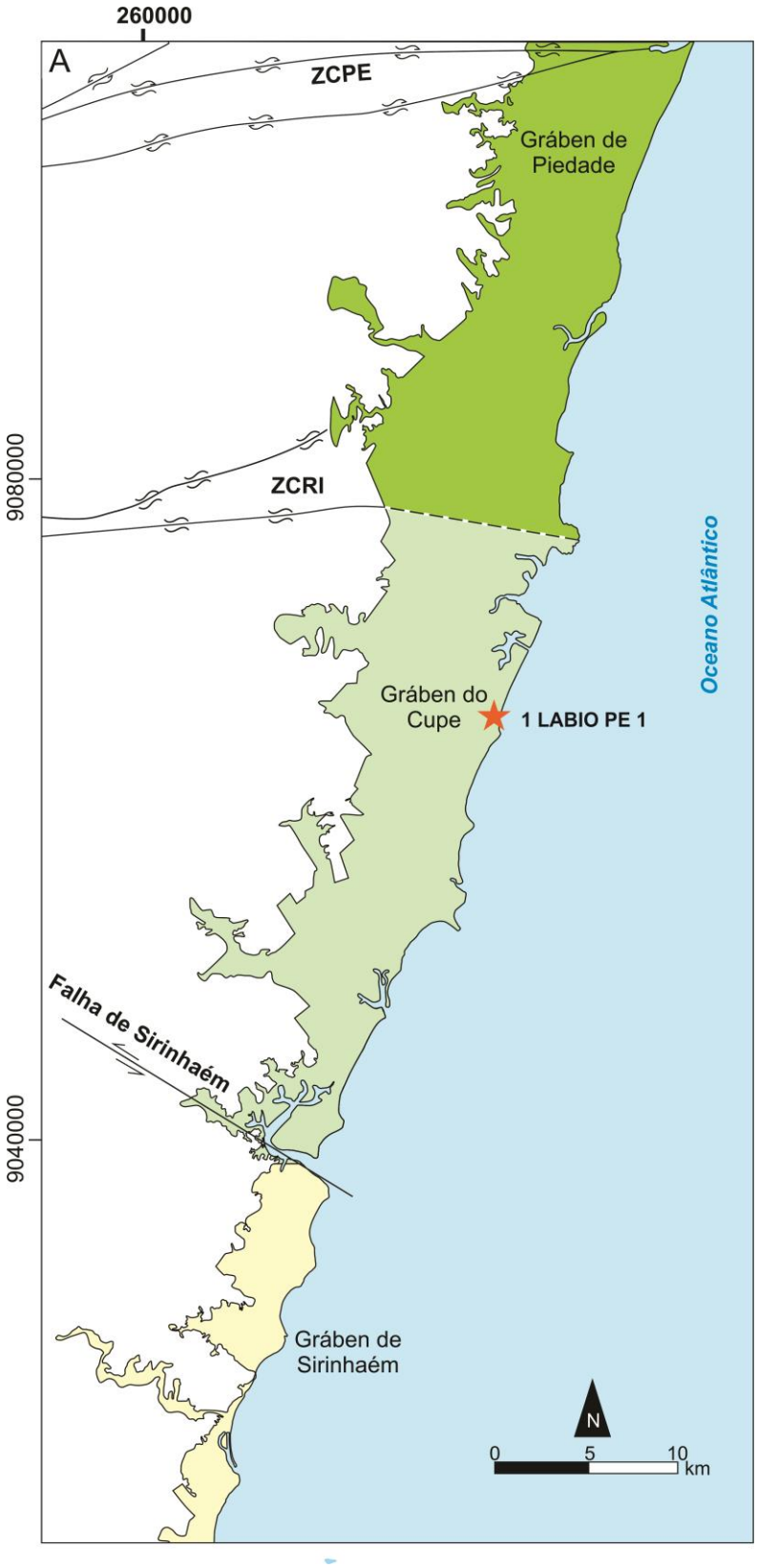

Fonte: Adaptado de CORREIA FILHO (2017).

1.2.2 Revisão Estratigráfica

Como já mencionado LIMA FILHO (1998) propôs formalmente a primeira carta estratigráfica da Bacia Pernambuco. Este autor propõe a sedimentação inicial da Formação Cabo, marcada por ortoconglomerados, arenitos arcosianos, siltitos, argilitos e folhelhos depositados em sistemas de leques aluviais a lacustres. Para LIMA FILHO (1998) a Formação Cabo abrange toda a fase rifte da Bacia Pernambuco, correspondendo à deposição desde o Aptiano Inferior até o Cenomaniano. A formação Cabo ocorre associada às falhas de borda da bacia que criaram espaços de acomodação favorecendo a deposição em de alta energia por processos gravitacionais em condições subaéreos. Esta unidade varia gradualmente para ambientes lacustres, onde foram depositados sedimentos mais finos, como siltitos, argilitos e folhelhos. MAIA (2012) em sua revisão estratigráfica nesta bacia menciona a descoberta de níveis carbonáticos e evaporíticos na sondagem estratigráfica 2-CP-01-PE. A autora correlaciona esta ocorrência ao topo da Formação Cabo, marcado como Aptiano-superior. Entretanto MAIA (2012) subdivide esta unidade em três formações, restringindo a Formação Cabo até o Aptiano Superior. Para a MAIA (2012) o intervalo correspondente ao Albiano Inferior e Médio (acima da camada se evaporitos) deve ser denominado de Formação Suape. A Formação Suape é marcada pela deposição de sedimentos em sistemas fluviais entrelaçados com fácies lacustres. Esta unidade passa a corresponder à fase rifte II, subdividida por uma discordância intra-rifte reconhecida através de linhas sísmicas e afloramentos. Não obstante, durante o Albiano é marcado por intensa atividade vulcânica, denominado de Província Magmática do Cabo (Long et al., 1986 Sial et al., 1987) ou Suite Magmática Ipojuca (Lima Filho, 1998; Lima Filho & Szatmari, 2002). Os depósitos vulcanoclásticos e vulcanogênicos, que ocorrem devido às atividades vulcânicas são tratados por LIMA FILHO (1998) e MAIA (2012) como pertencentes à Formação Algodoais, depositados durante o Santoniano-Campaniano, entretanto SANTANA (2016) e CORREIA FILHO (2017) relacionam estes depósitos ao Albiano e incorporam a Formação Suape.

De acordo com MAIA (2012) ocorre no Albiano Superior a Formação Paraíso, correspondente a uma fase de *sag*, com acomodação tectônica durante a fase pós-rifte, em ambiente siliciclástico marinho restrito. A sedimentação carbonática, ocorre

durante a fase drifte, estando associada à Formação Estiva relacionada a calcários, margas e folhelhos negros, intensamente dolomitizados e sulfetados (Tomé et al., 2006) associados a tratos de sistema de mar alto (Córdoba et al., 2007).

Recentemente, LIMA FILHO et al. (2017) através de sondagens estratigráficas na borda norte da Bacia Pernambuco menciona a presença de carbonatos crono-correlacionados às formações Gramame (Maastritchiano) da Bacia Paraíba e a Formação Marituba (Paleoceno-Eoceno) da Bacia Sergipe-Alagoas, entretanto estas unidades necessitam ser formalmente propostas e individualizadas na Bacia Pernambuco.

CÓRDOBA et al. (2007) MORAIS (2008) e CORREIA FILHO (2017) ainda relacionam a presença da Formação Calumbi, crono-correlacionada a da Bacia Sergipe-Alagoas (Oligoceno), sendo estes depósitos reconhecidos através de linhas sísmicas e na região do Platô de Pernambuco. Nesta pesquisa será utilizada, com algumas modificações, a proposta estratigráfica de CORREIA FILHO (2017), Figura 7, para o setor *onshore*. Aqui a Formação Paraíso será incorporada como fácies siliciclásticas da Formação Estiva. As unidades estratigráficas serão detalhadas a seguir.

Figura 7: Diagrama das principais cartas estratigráficas recentemente propostas para o setor interno da Bacia Pernambuco.

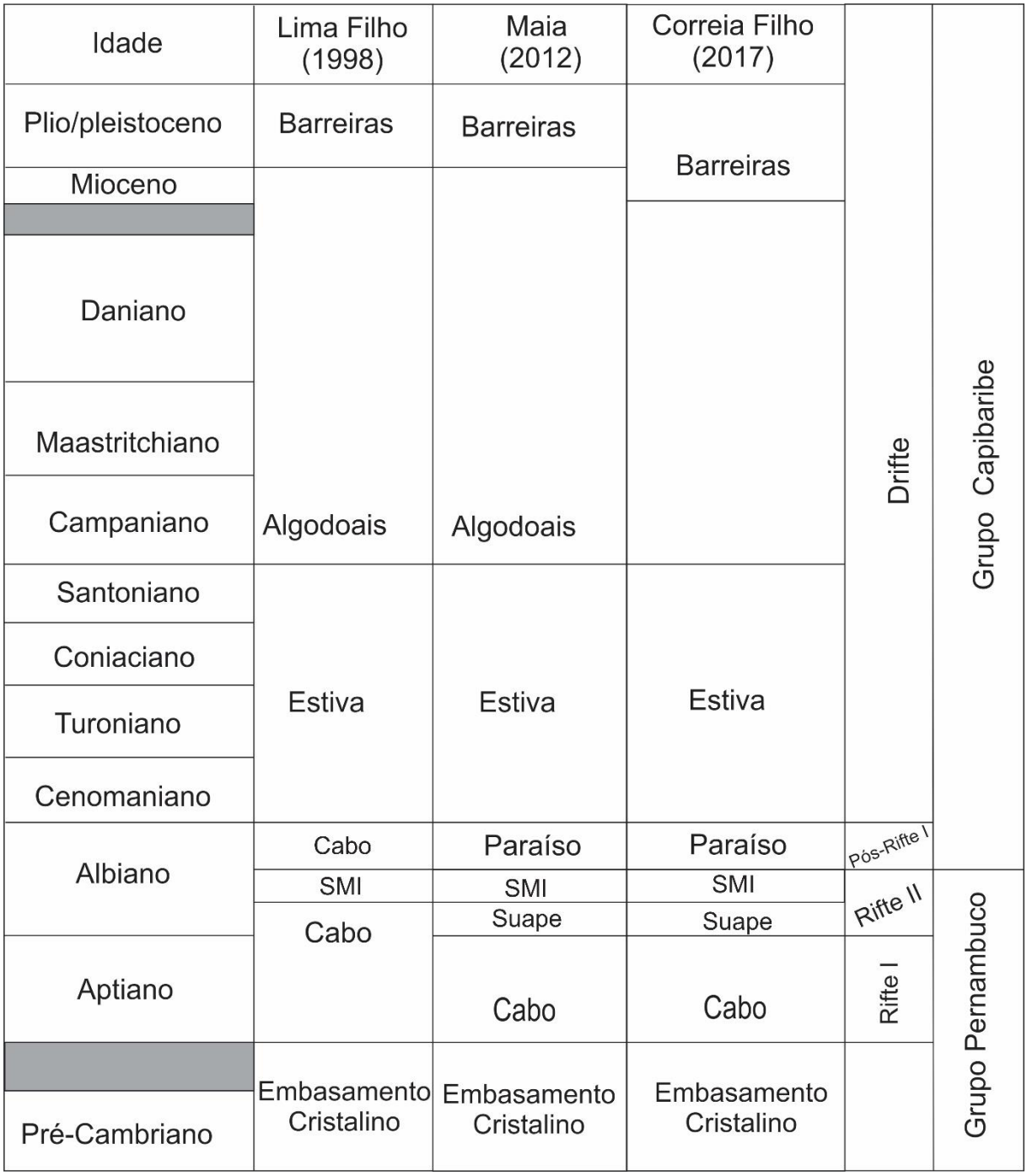

Fonte: LIMA FILHO (1998), MAIA (2012) e CORREIA FILHO (2017).

1.2.2.1 Formação Cabo

Como mencionado no capítulo anterior à sedimentação na Bacia Pernambuco possui sedimentação inicial durante o Barremiano (?) - Aptiano. Esta sedimentação ocorre com depósitos de ortoconglomerados polimíticos, arenitos arcosianos e argilitos (Figura 8A-8C) relacionados à sedimentação em sistemas de leques aluviais que gradam para depósitos em sistemas lacustres. Não obstante são reconhecidos através de linhas sísmicas e algumas amostras de poços níveis descontínuos de depósitos de sal: gipsita (Maia, 2012; Correia Filho et al., 2019) crono-correlacionados à deposição da camada de sal existente nas bacias marginais e em bacias interiores, relacionados ao Aptiano superior.

Figura 8: Painel das principais litologias encontradas na Formação Cabo. (A) Ortoconglomerado polimítico com clastos decimétricos tamanho seixos a bloco. (B) Arenito arcosiano com fácies conglomeráticas. (C) Argilito verde.

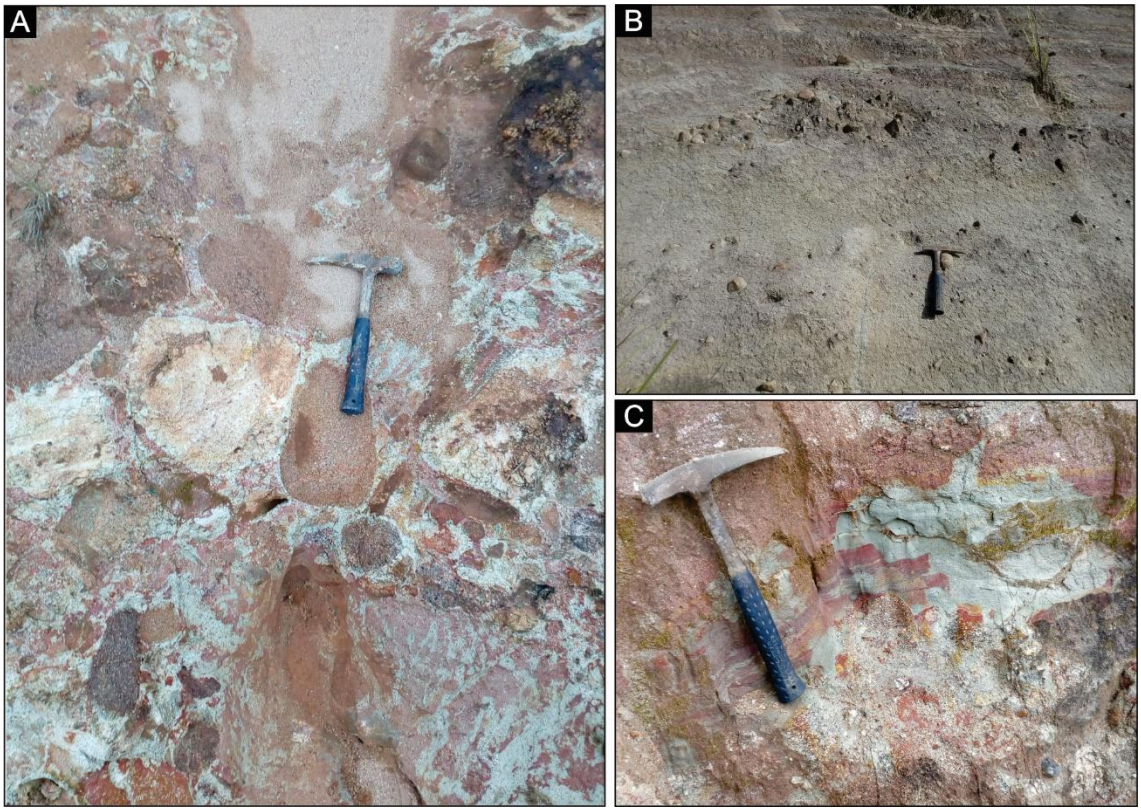

Fonte: O autor

1.2.2.2 Formação Suape

A Formação Suape foi incorporada a carta estratigráfica da Bacia Pernambuco por MAIA (2012). Esta unidade corresponde a arenitos, argilitos e sedimentos vulcanoclásticos e vulcanogênicos relacionados ao retrabalhamento de rochas da Suite Magmática Ipojuca (Maia, 2012; Santana, 2016). Esta unidade é datada do Albiano Inferior pela palinozona P-280 (Lima Filho & Silva Santos, 2001). Ocorre nesta unidade intercalação de sedimentos com rochas vulcânicas (em sua maioria traquitos) com morfologia de derrames, sugerindo depósitos sub-aéreos com contemporâneo retrabalhamento dos sedimentos por processos fluviais (Santana, 2016). Além disto, geometria de canais entrelaçados, e pacotes tabulares de argilitos também são evidenciados, indicando um sistema fluvial entrelaçado migrando para sistemas lacustres (Figura 9; Maia, 2012).

Figura 9: Principais aspectos geológicos da Formação Suape. (A) Contato entre arenito e traquito (SMI). (B, C) Retrabalhamento vulcanoclástico por processos fluviais. (D) Painel representativo mostrando geometria de canal (linha discontínua vermelha) e derrames vulcânicos.

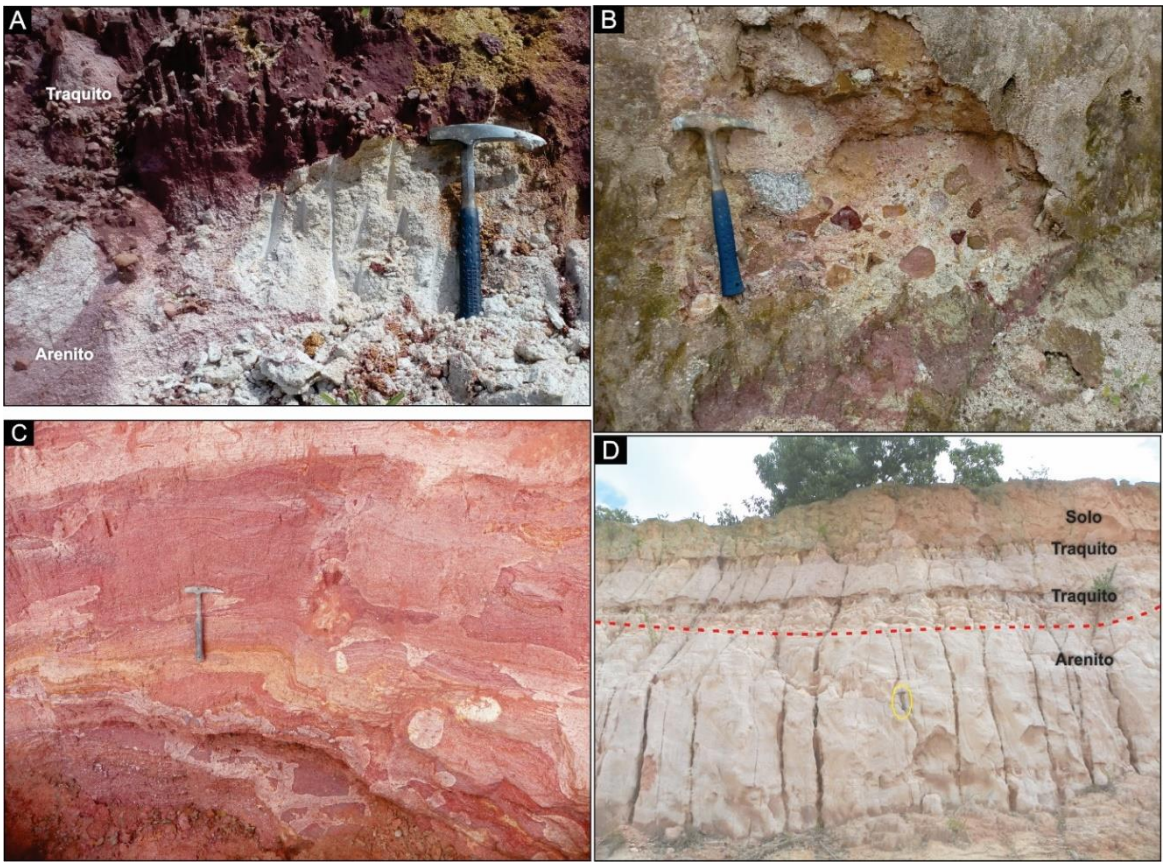

Fonte: O autor

1.2.2.3 Suite Magmática Ipojuca

A Suite Magmática Ipojuca (SMI) é a expressão geológica de uma pluma mantélica existente no NE brasileiro (Long et al., 1986). Esta pluma atuou na Bacia Pernambuco durante o Albiano (110-102Ma) conforme dados geocronológicos obtidos por $^{40}Ar/^{39}Ar$ em sanidina; (Lima Filho & Szatimari, 2002; Nascimento, 2003). Ocorrem na forma de derrames, sills, plugs, diques e domos, afetando diretamente as formações Cabo e Suape (Maia, 2012; Santana, 2016). Em termos de litologia são descritos desde basaltos, traquibasaltos, traquiandesitos, traquitos, riolitos lém do granito sub-vulcânico do Cabo (Figura 10). O magmatismo da SMI é de caráter alcalino, os basaltos possuem assinatura de basaltos de margem continental (CMB) com assinatura isotópica do manto empobrecido (Nascimento, 2003). Além disto, um

pulso juvenil datado por U-Pb em apatita com 72 ±10Ma (LA-ICP-MS) foi reconhecido no alto estrutural do Cabo de Santo Agostinho (Nascimento, 2018). Esta manifestação vulcânica está associada a atividades pós-rifte relacionado à reativação maastritchiniana. Entretanto esta expressão vulcânica é pouco reconhecida na região *onshore*, sendo mais expressiva e reconhecidas através de linhas sísmicas *offshore*, conforme mostrado por VARELA et al. (2016).

Figura 10: Estampa dos principais aspectos da Suite Magmática Ipojuca (SMI). (A) Riolito maciço. (B) Dique de traquibasalto. (C) Derrame de traquito. (D) Derrame de basalto.

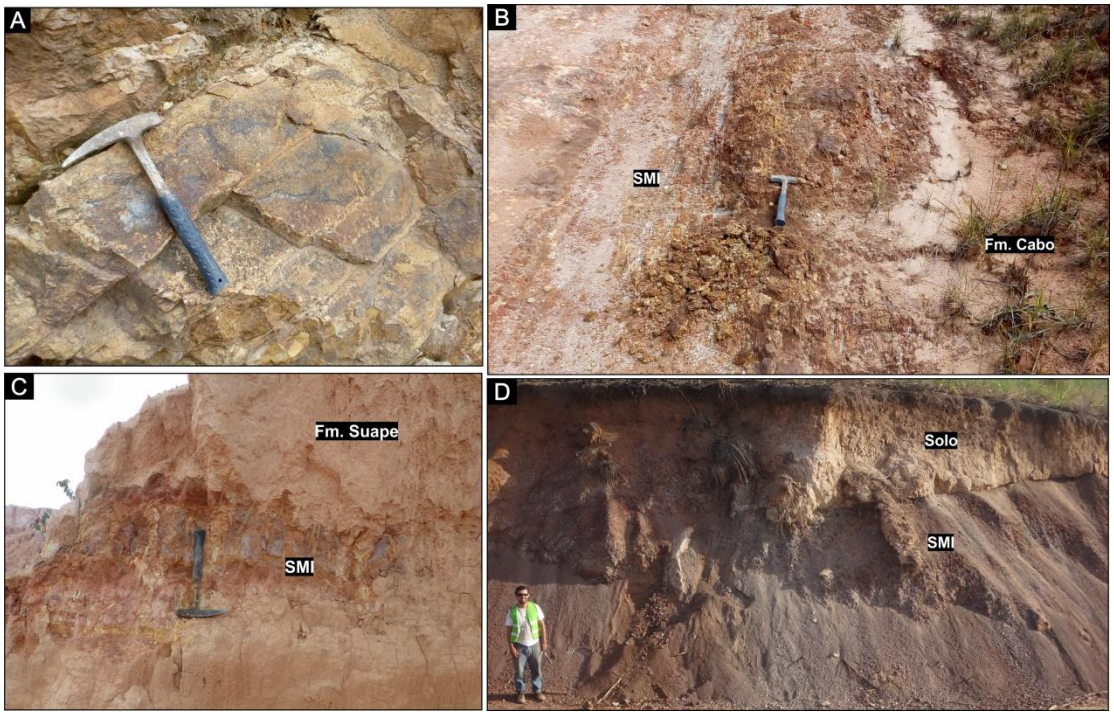

Fonte: O autor. A figura D foi cedida por I.M.G.Silva.

1.2.2.4 Formação Estiva

A Formação Estiva foi reconhecida pelos trabalhos pioneiros de OLIVEIRA & LEONARDOS (1946). A sua expressão na Bacia Pernambuco é pouco reconhecida com afloramentos pouco expressivos e representativos (Figura 11), sendo sua existência mais reconhecida através de sondagens estratigráficas. A formação Estiva é composta por calcários dolomitizados, margas, folhelhos e arenitos relacionados a uma rampa carbonática rasa com aporte intenso aporte de

sedimentos continentais (Lima Filho, 1998; Tomé et al., 2006). Estes calcários encontram-se intensamente piritizados por influência diagenética. FERREIRA (2009) estudou o conteúdo palinológico desta formação, atribuiu uma sedimentação marinha rasa, com influência de pólens continentais além de palinomórfos paleozoicos advindos da Bacia de Sergipe Alagoas além de condições marinhas normais. ARAÚJO (2014) também estudou o intervalo estratigráfico relacionado à Formação Estiva na região extremo norte da Bacia Pernambuco no furo 1 LABIO PE 3 (Furo IATE). Nesta sondagem a Formação Estiva é composta por sedimentos siliciclasticos. A autora ainda estudou a deposição de 1,2 metros de folhelhos negros, com teores de Carbono Orgânico Total (COT) de até 1,8% e valores de $\delta^{13}C$ entre -23 e -22‰.

RAMIREZ et al. (2018) também estudando este intervalo estratigráfico na mesma sondagem estratigráfica, atribuiu através do conteúdo palinológico associação transicional a marinha. RIEDEL et al. (2019) investigando eventos anóxicos na Bacia Pernambuco encontrou baixos valores de P_{org} da ordem de 0,16 e 0,33 µmol/g, relacionando a deposição destes ao evento de anoxia global ocorrido durante o Albiano-Cenomaniano (Evento Bonarelli). MOURA et al. (2020) estudando folhelhos negros na sondagem estratigráfica 1 LABIO PE 1 associou a deposição destes a condições sub-óxicas à anóxicas em um ambiente marinho raso.

Figura 11: Afloramento da Formação Estiva, apresentando calcários dolomitizados e fraturados.

Fonte. O.J.Correia Filho

1.2.2.5 Formação Barreiras

A Formação Barreiras ocorre na Bacia Pernambuco associada aos altos estruturais (Correia Filho, 2017). Esta unidade compreende arenitos, argilitos e folhelhos, associados a uma sedimentação fluvial com algumas fácies marinhas. Corresponde ao registro de variação relativa do nível do mar durante o Oligoceno-Mioceno (~23Ma). Esta unidade ocorre ainda intensamente falhada devido a reativações cenozoicas das estruturas geológicas pré-cambrianas (Rossetti et al., 2013).

1.3 Estudos espectrais em ambientes sedimentares

O emprego de técnicas espectrais em ambientes sedimentares se dá como uma ferramenta integrada principalmente no reconhecimento de assinaturas minerias e composicionais (Kurz et al., 2011, 2012; Coulter et al. 2017).

No contexto da Geologia Sedimentar, foi cunhado o termo “Estratigrafia Espectral” introduzido nas geociências por LANG (1991), este termo refere-se à aplicação de tecnologias espectrais em problemas estratigráficos. No caso do estudo feito por LANG (1991) foram aplicadas técnicas espectrais no estudo de planetas extraterrestres, desenvolvidos pela Agência Espacial Americana (NASA).

O estudo espectral de rochas carbonáticas na faixa do visível ao infravermelho de ondas curtas foi inicialmente realizado por HUNT & SALISBURY (1971). Estes autores identificaram a ocorrência de feições de absorção derivadas da vibração de moléculas de C-O na região do infravermelho de ondas curtas (SWIR: 1001-2500 nm) e indicaram comprimentos de onda específicos para separação entre calcita (absorção em cerca de 2340 nm), dolomita (absorção em ~2320 nm), rodocrosita (~2310 nm) siderita (~2305 nm) e argilominerais (absorção em cerca de 2200-2210 nm). Já a técnica de imageamento hiperespectral é ainda pouco explorada em estudos de ambientes carbonáticos, destacando-se os trabalhos de KURZ et al. (2011, 2012) e de ZAINI et al. (2014), nos quais foi possível realizar a caracterização composicional de rochas carbonáticas e de processos de interação hidrotermal, e diagenéticos/substituição química (*e.g* Ca por Mg).

1.4 Dolomitas e o processo de dolomitização

O termo dolomito é uma homenagem ao geólogo francês *Deodat Guy de Dolomieu* (1750–1801), que primeiro descreveu este tipo de rocha nos Alpes Tiroleanos (Noroeste da Áustria). Um dolomito é uma rocha composta basicamente por mineral de dolomita.

Dolomitas são um carbonato de cálcio e magnésio ($CaMg(CO_3)_2$, e consiste numa alternância estrutural dos elementos químicos Ca e Mg separado por camadas de CO_3. Apesar da comum ocorrência de dolomitos no registro geológico, desde o Arqueano até o Holoceno, a precipitação da dolomita por processos naturais é pouco entendida, sendo a transformação calcita-dolomita associada a estágios

diagenéticos num processo denominado de dolomitização. Um dos argumentos que postulam a abundante ocorrência de dolomitos no ambiente sedimentar antigos é a mudança da razão Mg/Ca da água do mar, ao longo do tempo geológico, ou a influência de organismos microbianos (Warren, 2000). Dolomitos são geralmente relacionados a ambientes costeiros, em salmouras hipersalinas a partir de águas esquizohalinas (Hardie, 1987, Warren, 2002). Entretanto, depósitos associados a ambientes marinhos “normais” e lacustres são descritos (e.g. Machel, 2004; Gregg et al., 2015).

A origem da dolomita no ambiente sedimentar é pouco conhecida devido a um problema de cinética química, num termo designado por LAND (1980) como “O problema da Dolomitização” que impede a precipitação durante a deposição, pincipalmente em sistemas carbonáticos modernos (e.g. Land, 1980), onde são raras as ocorrências de dolomita deposicional. A dolomitização pode afetar um determinado depósito carbonático de diferentes formas: pervarziva e ou como veios em fissuras. A dolomitização pode ainda modificar toda a textura deposicional do carbonato, sendo classificada como dolomita mimica; e ainda preservar alguns “fantasmas” ou relictos deposicionais (e.g. peloides, ooides, bioclastos) classificando a dolomita como não-mimica (Sibley, 1978; Sibley & Gregg, 1987; Gregg et al., 2015). Ainda são descritos e classificados por SIBLEY (1978) e SIBLEY & GREGG, 1987, tipos de texturas para dolomitos:

1) Dolomita tipo planar-e (ou idiomórfica) e planar-s (subidiomórfica) que constituem de cristais euédricos à subédricos de dolomitas, geralmente relacionados a baixas temperaturas de fluidos (até 50ºC);
2) Dolomita não planar constituída de cristais anédricos, em contatos lobados ou serrados e o não planar tipo sela (ou *saddle*) geralmente associado a poros e possuem formas de pontas.

O processo de formação e precipitação da dolomita deve ocorrer em condições subsupeficiais sob circulação e refluxo de fluidos (Warren, 2000). Os Modelos de dolomitização são sumarizados por WARREN (2000).

Modelo em ambiente evaporitico: São formados em ambientes de sabka, inframaré e lagunas hipersalinas. Este tipo de ambiente é um dos poucos em que existem condições químicas para a precipitação da dolomita autigênica. Isto se dá devido a precipitação da aragonita e gipsita anidrita que condicionam o aumento da razão Mg/Ca. Outro fator a ser considerado é a presença de SO_4^{2-} que induz a precipitação da dolomita.

Modelo de infiltração por refluxo: Também formados em ambientes de inframaré e recifes, esta modelo de dolomitização se dá pela infiltração de fluidos ricos em Mg, que por diferença de densidade com a água do mar acabam infiltrando por meio de fraturas.

Modelo de zona de mistura: Este processo se dá em condições rasas onde existe a mistura de águas meteóricas com águas salinas que resultaria num fluido saturado em Mg favorecendo a precipitação de dolomita.

Modelo de águas marinhas: Neste modelo de dolomitização águas de origem marinha (frias) percolam pelos sedimentos e devido à presença de condições geotérmicas abaixo das plataformas carbonáticas, este fluido marinho é aquecido em um sistema de convecção, denominado de convecção de Kohout, gerando a dolomitização.

1.5 Objetivos

Promover uma melhor compreensão dos aspectos litológicos, texturais, diagenéticos e paleodeposicionais referentes à deposição dos sedimentos carbonáticos relacionados à Formação Estiva, Bacia Pernambuco, NE do Brasil.

1.5.1 Objetivos Específicos

- Obter dados petrográficos em rochas da Formação Estiva associadas a um intervalo de um testemunho de sondagem;

- Utilizar a técnica de espectroscopia de refletância no intervalo estratigráfico correspondente à Formação Estiva, de modo a relacionar as principais fases minerais existentes;
- Aplicar o imageamento hiperespectral em *plugs* de testemunho de sondagem referente a rochas da Formação Estiva, de modo a relacionar as principais características mineralógicas e texturais existentes;
- Aplicar geoquímica de carbono orgânico, enxofre e nitrogênio bem como o emprego dos isótopos estáveis de carbono e nitrogênio, visando caracterizar a distribuição temporal de seus constituintes geoquímicos;
- Integrar os dados obtidos de modo a caracterizar, com maior acurácia, aspectos litológicos, sedimentólogicos e estratigráficos das rochas da Formação Estiva.

2 MATERIAL E MÉTODOS

Neste capítulo serão descritos todos os procedimentos metodológicos utilizados nesta pesquisa.

2.4 Descrição da sondagem estratigráfica e amostragem

A sondagem estratigráfica utilizada denominada 1 LABIO PE 1, está localizada conforme as coordenadas UTM. 25L 281523E; 9064610N, perfurado no ano de 2014, localizada na Praia do Cupe, a cerca de 60 Km ao sul da cidade de Recife, conforme indicado na figura 6. As caixas contendo os testemunhos estão armazenadas no Laboratório de Geologia Sedimentar e Ambiental (LAGESE). O intervalo correspondente a Formação Estiva compreende uma espessura de cerca de 30m de comprimento, e possui uma taxa de recuperação média de 80% (Figura 12). A descrição da sondagem se deu com materiais usuais de descrição de rocha, além de HCl a 10% e HCl a 50%, para diferenciação entre calcita e dolomita. Na etapa descritiva foi utilizada a classificação de GRABAU (1904) para rochas carbonáticas.

Figura 12: Testemunhos da sondagem estratigráfica 1 LABIO PE 1.

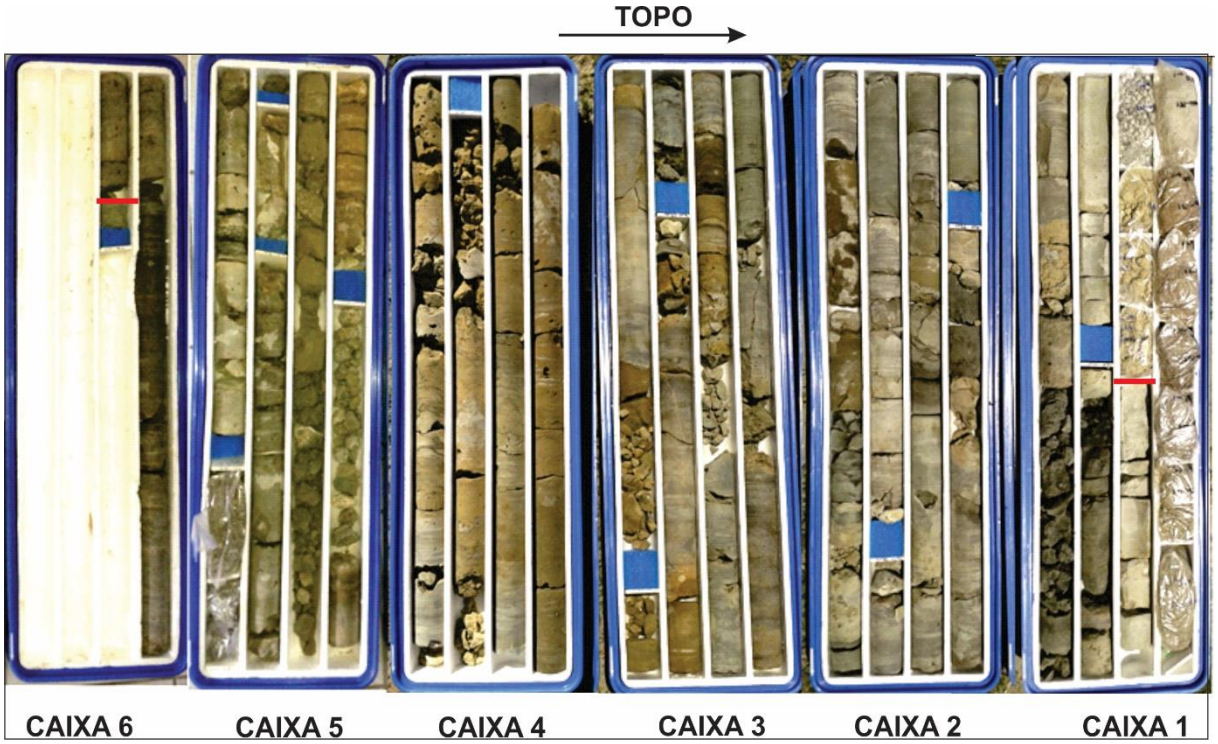

Fonte: M.F. Lima Filho

A amostragem se deu para diferentes técnicas analíticas, a saber: petrografia, espectroscopia de reflectância, imageamento hiperspectral, além de Carbono Orgânico Total (COT), Enxofre Total (ST), Nitrogênio Total (NT) assim como Isótopos de carbono orgânico e nitrogênio, nas amostras com acumulações de matéria orgânica. Foi utilizado um espaçamento entre as amostras, conforme mostrado na figura 13.

Figura 13: Perfil descritivo da sondagem estratigráfica 1LABIO PE 1, com a indicação da amostragem para análises petrográficas, espectrais e geoquimicas.

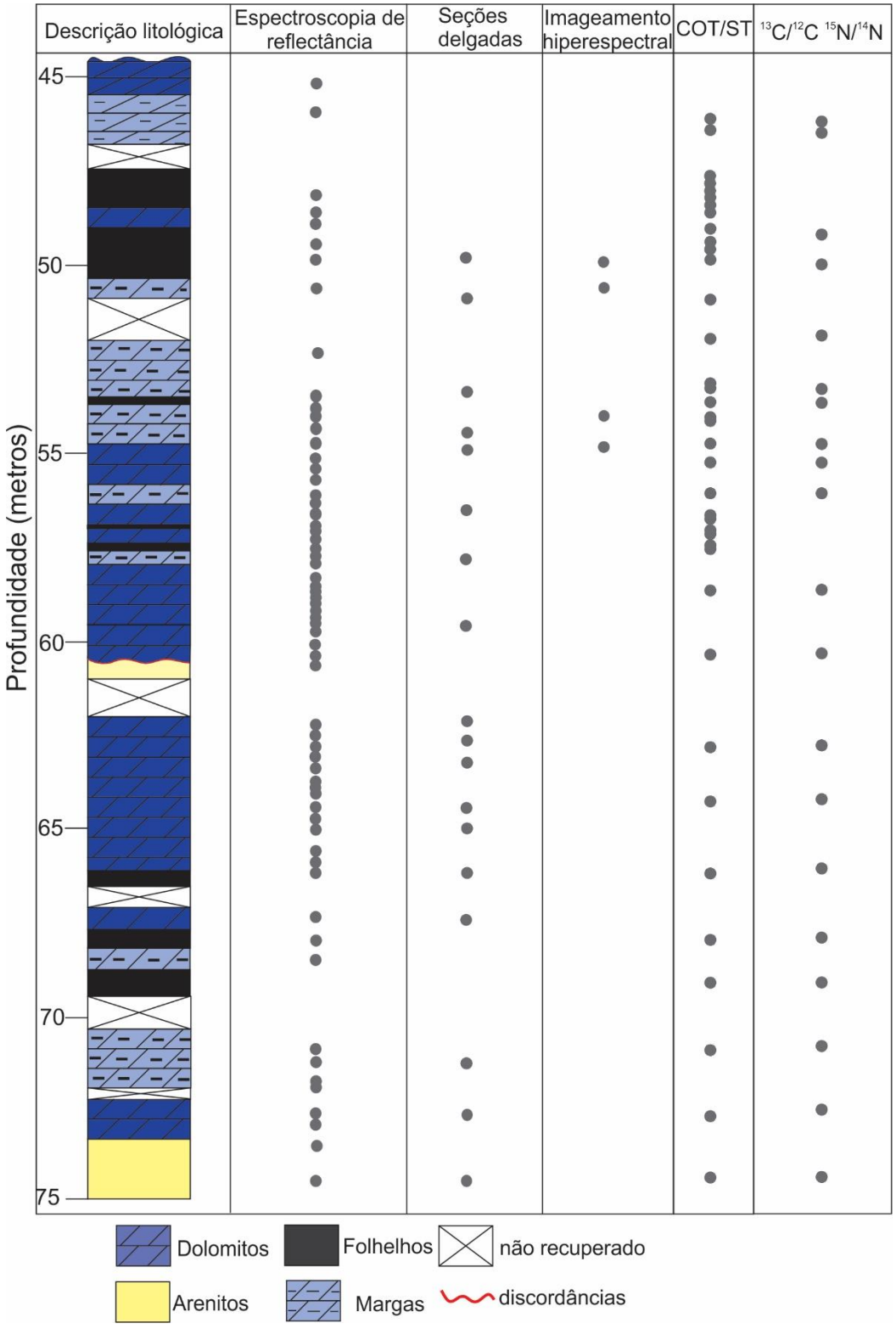

Fonte: O autor

2.5 Análises Petrográficas

Com base em amostras representativas do intervalo estratigráfico de estudo, 19 seções delgadas foram confeccionadas no Laboratório de Confecção de Lâminas Delgadas do Departamento de Geologia (DGEO) da UFPE. As lâminas foram descritas utilizando um microscópio ZEISS modelo SCOPE A1, com câmera acoplada, pertencente ao Laboratório de Petrologia Sedimentar do LAGESE. Nesta etapa de investigação as amostras de rochas carbonáticas foram descritas conforme a classificação de ENBRY & KLOVAN (1979) observando os critérios texturais existentes. Devido ao atual estágio diagenético, pelo processo de dolomitização, foi utilizada a classificação de SIBLEY & GREGG (1978) para descrição textural de dolomitas. As 19 amostras foram adicionalmente investigadas utilizando um microscópio de catodoluminescência, modelo CL8200 pertencente ao mesmo laboratório, para melhor descrição de processos diagenéticos e mineralogia.

2.6 Espectroscopia de Reflectância

Foram analisadas 65 amostras foram encaminhadas apara análises pontuais de espectroscopia de reflectância. Foi utilizado um espectroradiômetro FieldSpec® 4 Standard Resolution, pertencente ao Instituto de Geociências da Universidade de Campinas (UNICAMP). O instrumento FieldSpec® 4 Standard Resolution opera na faixa de 350 a 2500 nm, e possui 2152 canais espectrais com resolução espectral de 3 nm na faixa do VNIR (visível ao infravermelho próximo: 350-1000 nm), e de 10 nm na faixa do SWIR (infravermelho de ondas curtas: 1001-2500 nm) para determinação das principais feições de absorção dos minerais existentes nas amostras (calcita, dolomita, argilominerais).

2.7 Imageamento Hiperespectral

Foram imageadas quatro (4) amostras representativas com o uso de duas câmeras imageadoras hiperespectrais da HySpex, um operando na faixa de 400-

1000 nm em 186 canais (câmera VNIR-1800) e outra registrando radiação refletida no intervalo de 930-2500 nm (câmera SWIR-384), abrangendo 288 canais espectrais. Os imageamentos foram realizados considerando-se altura do sensor de 30 cm e campos de visada de 16-17°, de forma que as imagens possuem pixels de cerca de 1 mm. Além do imageamento das amostras de rocha, foram adquiridas medidas de refletância do padrão branco (Spectralon®) para posterior transformação empírica dos dados brutos para refletância. Esta etapa analítica foi realizada no Laboratório de Sensoriamento Remoto de SENAI-CIMATEC (Bahia).

2.8 Análises de Carbono Orgânico Total e Enxofre Total

As amostras analisadas para carbono orgânico e enxofre total foram previamente atacadas com ácido clorídrico (HCL) a 1M por 24% para remoção do carbonato. As amostras foram analisadas com um analisador elementar LECO CS-356 do Laboratório de Geoquímica da Universidade do Estado do Rio de Janeiro (UERJ).

2.9 Isótopos de Carbono Orgânico e Nitrogênio Total

Previamente a análise, as 22 amostras selecionadas foram acidificadas com HCl 1 M por 24 h. A análise elementar e isotópica foi conduzida utilizando um analisador elementar EuroVector (EA3000) acoplado a um espectrômetro de massas de razão isotópica *Delta V Advantage* (Thermo Scientific), pertencente ao Laboratório de Oceanografia Química (LOQUIM) do Departamento de Oceanografia Química da UFPE. O analisador elementar foi configurado com um reator CHN preenchido com óxido de cromo, fios de cobre reduzido e óxido de cobalto prateado; uma armadilha para adsorção da água (perclorato de magnésio) e uma coluna de separação cromatográfica. A quantificação da massa de NT e CO nas amostras foram conduzidas a partir da construção de uma curva analítica ($R^2 \geq 0,995$) utilizando como material de referência (MR) o sedimento B2151 (*Elemental Microanalysis*, N = 0,52%; C = 7,45%, $\delta^{13}C$ = -28,85 ‰; $\delta^{15}N$ +4,32 ‰). Durante

análise, o cilindro de referência para análise isotópica do CO_2 [CO_2 com alta pureza (5.0)] apresentou $\delta^{13}C$ médio igual a -27,44 ‰ e $\delta^{15}N$ +4,00 ‰.

3 RESULTADOS

Este capítulo trata-se de dois artigos científicos, utilizando-se todos os dados obtidos na pesquisa no âmbito da presente dissertação. O primeiro encontra-se em vias de submissão ao peródico internacional *Journal of South American Earth Science*. Este artigo trata de proposta paleogeográfica para a Bacia Pernambuco durante o Albiano superior-Turoniano, contém os resultados referentes à descrição de petrografia, concentração elementar de carbono, enxofre e nitrogênio e isótopos de carbono e nitrogênio, além da assinatura geoquímica durante o evento de anoxia global ocorrido durante a passagem Cenomaniano-Turoniano. O segundo manuscrito aceito no periódico internacional Journal of *South American Earth Science* sob D.O.I 10.1016/j.jsames.2022.103831 contempla os dados de espetroscopia de reflectância, e imageamento hiperespectral tratando de uma proposta de utilização sistemática de espectroscopia em sistemas carbonáticos bem como as facilidades e limitações desta técnica.

3.1 Artigo 1

The Oceanic Anoxic Event 2 record during the Cenomanian-Turonian boundary in the Pernambuco Basin (northeast, Brazil)

Willian Alexandre Lima de Moura[1,3*] João Adauto Souza Neto[1,2,3] René Rodrigues[4] Thales Lúcio[1,3] Mário Ferreira de Lima Filho[1,2,3]

[1] Programa de Pós-Graduação em Geociências, Universidade Federal de Pernambuco: Avenida da Arquitetura S/N, Cidade Universitária, Recife, 50740-550, Brasil

[2] Departamento de Geologia, Universidade Federal de Pernambuco: Avenida da Arquitetura S/N, Cidade Universitária, Recife, 50740-550, Brasil

[3] Laboratório de Geoquímica Aplicada ao Petróleo-Instituto de Pesquisa em Petróleo e Energia: Avenida da Arquitetura S/N, Cidade Universitária, Recife, 50740-550, Brasil

[4] Departamento de Estratigrafia e Paleontologia-DEPA, Universidade do Estado do Rio de Janeiro (UERJ): Rua São Francisco, 524-Maracanã, Rio de Janeiro, 20550-900, Brasil

Author corresponding[*]

W. A. L. Moura - alexandrewillian1995@gmail.com

ORCID ID: http://orcid.org/0000-0002-1471-3752

ABSTRACT

Since the late Albian in the Pernambuco Basin, lithological record was formed that corresponds to the post-rift to drift phases, which are associated with carbonate and siliciclastic deposits, and the establishment of marine sedimentation. Herein, we present both petrographic and geochemical data from 1 LABIO PE 1 well, in order to investigate the Oceanic Anoxic Event (OAE 2) record that occurred during the Cenomanian-Turonian boundary in the Pernambuco Basin. The studied section is composed predominantly of dolostones, marls, sandstones, and shales with microbial influences, and a greater siliciclastic supply. Besides that, the investigated rocks show Total Organic Carbon (TOC) values ranging from 0.19 to 3.60% Total Sulfur (TS) values from 0.02 to 1.20%, and Total Nitrogen (TN) values from 0.01 to 0.08%. The $\delta^{13}C_{org}$ data ranged from -24.65 to -18.89‰, which suggest both terrestrial plants and marine algae contributions. The bulk $\delta^{15}N$ shows values ranging from +0.93 to +5.44‰, which suggest N_2 fixation and a nitrification process, caused by loss of oxygen in the water column to denitrification process due to increase of anoxia. The influence of OAE 2 in the basin promoted a positive incursion in the $\delta^{13}C_{org}$ pattern in order of ca. -20.50‰, and organic carbon accumulation. Furthermore, that event was probably triggered due to Tethyan seawater and the volcanic-magmatic activity of the Santa Helena hotspot in the northeast, Brazil.

Keywords: Estiva Formation; OAE 2; Drift stage; C-N isotopes; Geochemistry.

1 INTRODUCTION

In the Mesozoic era, the Earth experienced oceanographic, and climatic changes, as a result of Gondwana supercontinent break-up (Huber et al., 2002; Norris et al., 2002; Haq et al., 2014). Some paleogeographical and paleoenvironmental reconstruction have been made through some sedimentary basins worldwide (*e.g.* Razin et al., 2010; Scotese and Moore, 2014; Perez-Dias and Eagles, 2017; Sherata et al., 2019; Ladant et al., 2020).

Specifically, during the upper Cretaceous period, some process, such as sea-level highstand, biotic crisis, enhanced of bioproductivity, and high levels of atmospheric CO_2, have been recorded worldwide (*e.g.* Schlanger and Jenkys, 1976; Jenkys, 1980, 2010; Mort et al., 2007; Haq, 2014). Consequently, the sea-level rise resulted in greenhouse warming, and increase of anoxia along the oceans, leading an organic carbon burial, and consequently widespread of organic-rich rock deposition (Schlanger and Jenkys, 1976; Jenkys, 1980, 2010, 2017).

Ocean Anoxic events (OAE) are global events of environmental perturbations characterized by the increase of low-oxygen zones, and widespread of black shales and organic-rich carbonates deposition in the oceans, which are associated with the carbon and nitrogen cycle perturbation leading to a positive carbon isotope excursion (CIE), and were common throughout the Phanerozoic Eon (*cf*. Schlanger and Jenkys, 1976; Jenkys, 1980, 2010). The OAE 2 occurred during the Cenomanian-Turonian boundary and was first identified by Schlanger and Jenkys (1976) in the Livello Bonarelli area, Italy. As it is well known, the anoxic events have been linked to a global warming caused by the emission of CO_2 to the atmosphere mainly due to increase of volcanic activity (Turgeon and Creaser, 2008; van Helmond et al., 2013; Robinson et al., 2017).

In the Brazilian marginal basins, the paleogeographical reconstruction (Figure 1) suggests marine conditions from the early to middle Albian ages dominated by marine carbonate platforms (*e.g*. Macaé group in the Campos Basin; Riachuelo Formation in the Sergipe-Alagoas Basin; Milani et al., 2007) and an influence through the Tethys seawater (Dias Brito, 1994; Perez-Dias and Eagles, 2017; Silva-Jr. et al., 2020). In addition, the seafloor spreading and oceanic crust formation, caused by the end of rift activities that culminated with the Gondwana break-up have been recorded (Matos, 1999; Mohriak and Leroy, 2012; Caixeta et al., 2015).

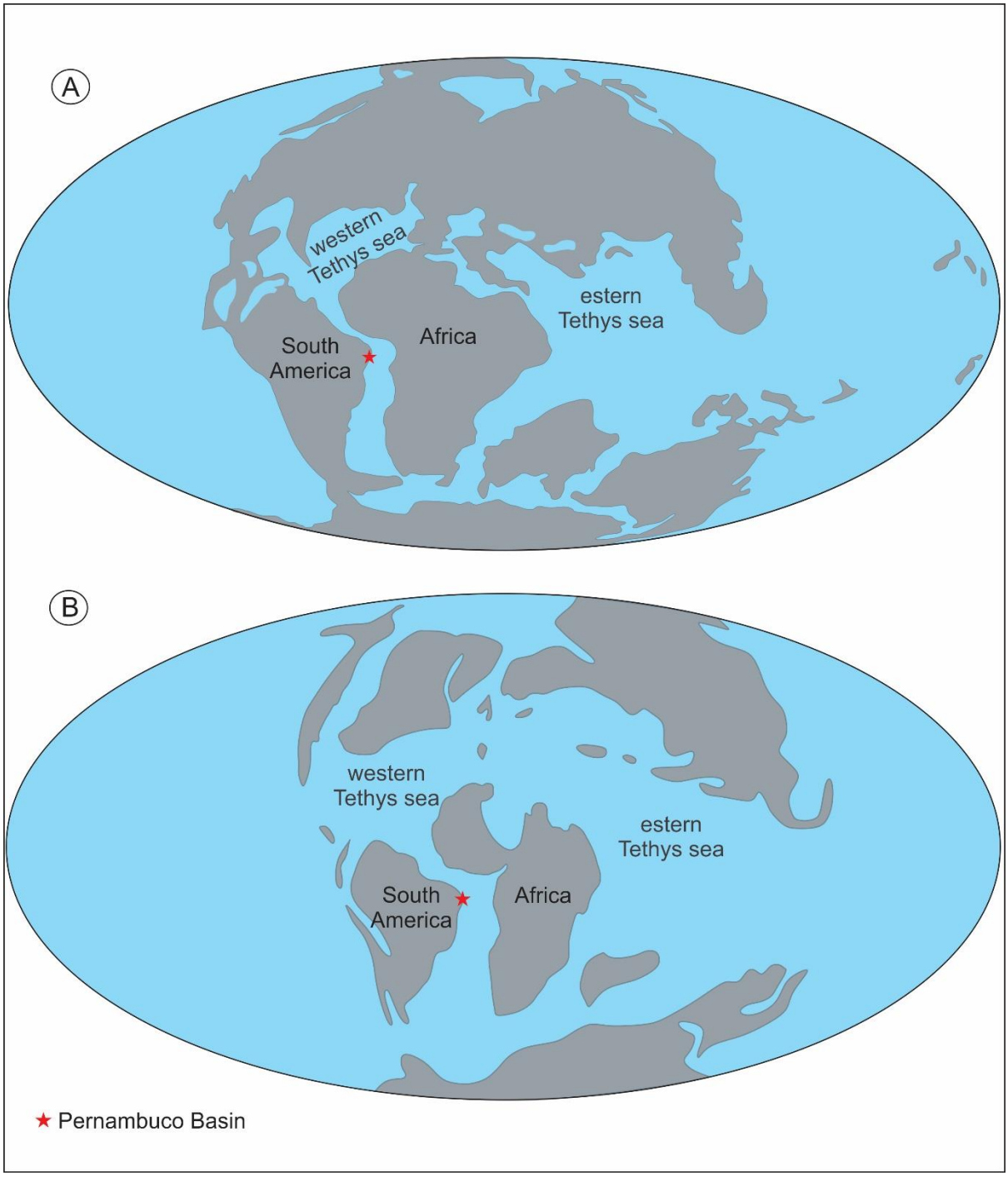

Figure 1. Paleogeographic map reconstruction. (A) From late Albian age (100 Ma); (B) From Cenomanian-Turonian boundary (~94 Ma); with the location of Pernambuco Basin, (adapted from online version http://www.odsn.de/odsn/services/paleomap/) from Hay et al. (1999) and Scotese (2014).

The Cenomanian-Turonian period have been recognized as an important geochronological interval due to the great organic matter accumulation and therefore its significant potential for petroleum generation. For this reason, it needs to be

highlighted and has been studied in some Brazilian sedimentary basins (*e.g.* Milani et al., 2007; Okubo et al., 2015; Valle et al., 2019; Dantas and Holz, 2020). However, this paleogeographic scenario is poorly understood in the Pernambuco Basin mainly due to the lack of outcrops.

For this reason, the aim of this paper is to improve the current knowledge of the late Albian to Turonian interval in the Pernambuco Basin, and consequent implications of the expression of global anoxic events, mainly the record of OAE-2 and the latest activities of the Gondwana break-up.

2 GEOLOGICAL SETTING

The Pernambuco Basin comprises one of the main sedimentary basins formed during the Gondwana break-up on South American plate during the Aptian-Albian ages (Lima-Filho, 1998; Barbosa et al., 2014). This basin is controlled by graben and horst systems (Correia-Filho, 2017) promoted by reactivation of Neoproterozoic shear zones, which acted as topographic highs, and thus directly influenced sedimentation settings (Figure 2A).

In the Pernambuco Basin, the sedimentation (Figure 2B) began with polymitic clast-supported conglomerate, arcosian sandstone, and green shales rocks deposited from alluvial fan systems of the Cabo Formation during the late Barremian(?) to Aptian ages, in the rift I stage (Lima-Filho, 1998; Barbosa et al., 2014). The rift II stage is marked by braided-type fluvial environment (sandstones and claystone) of the Suape Formation on middle Albian age (Maia, 2012). This fluvial sedimentation was developed contemporaneously with the volcanic-magmatic activity of Ipojuca Magmatic Suite during the middle to late Albian from 104.6 Ma to 100.2 Ma ($^{40}Ar/^{39}Ar$ in sanidine; Nascimento, 2003, 2004) with peak of ages in 102±1 Ma. This magmatic suite comprises basalts, rhyolites, trachytes, and trachybasalts, which affect the basin in the form of dykes, lava flows and domes (Nascimento, 2003). In addition, there is record of a younger pulse during Maastrichtian (72±10 Ma by LA-ICP-MS U-Pb apatite; Nascimento, 2018) related to post-rift volcanism that is mainly observed affecting the lithological content in the offshore region of the Pernambuco Basin (Buarque et al., 2016). The opening of marine sedimentation has been associated with post rift transitional deposits during a sag phase (late Albian age) represented by Paraíso Formation, composed of sandstones, mudstones, and

shales associated with estuarine to deltaic environment (Maia, 2012). However, the existence of this stratigraphic unit has been discussed by Lima-Filho et al. (2019) mainly based on the absence of representative outcrops and the occurrence in the wells as was described. The carbonate rocks of Estiva Formation characterize the beginning of the drift stage in the Pernambuco Basin, which is marked by a regional discordance between the rift units (Lima-Filho, 1998). Based in the paleontological content, the depositional ages have been related to late Albian to Turonian (*cf.* Beurlen and Cobra, 1960; Lima and Pedrão, 1989; Lima-Filho, 1998; Lima Filho and Silva-Santos, 2001; Araújo, 2014), and a deposition under shallow water conditions in a restricted marine environment (Tomé et al., 2006). The diagenesis affected these rocks, generating pyritization of organic matter, as well as an extensive and pervasive dolomitization (Tomé et al., 2006).

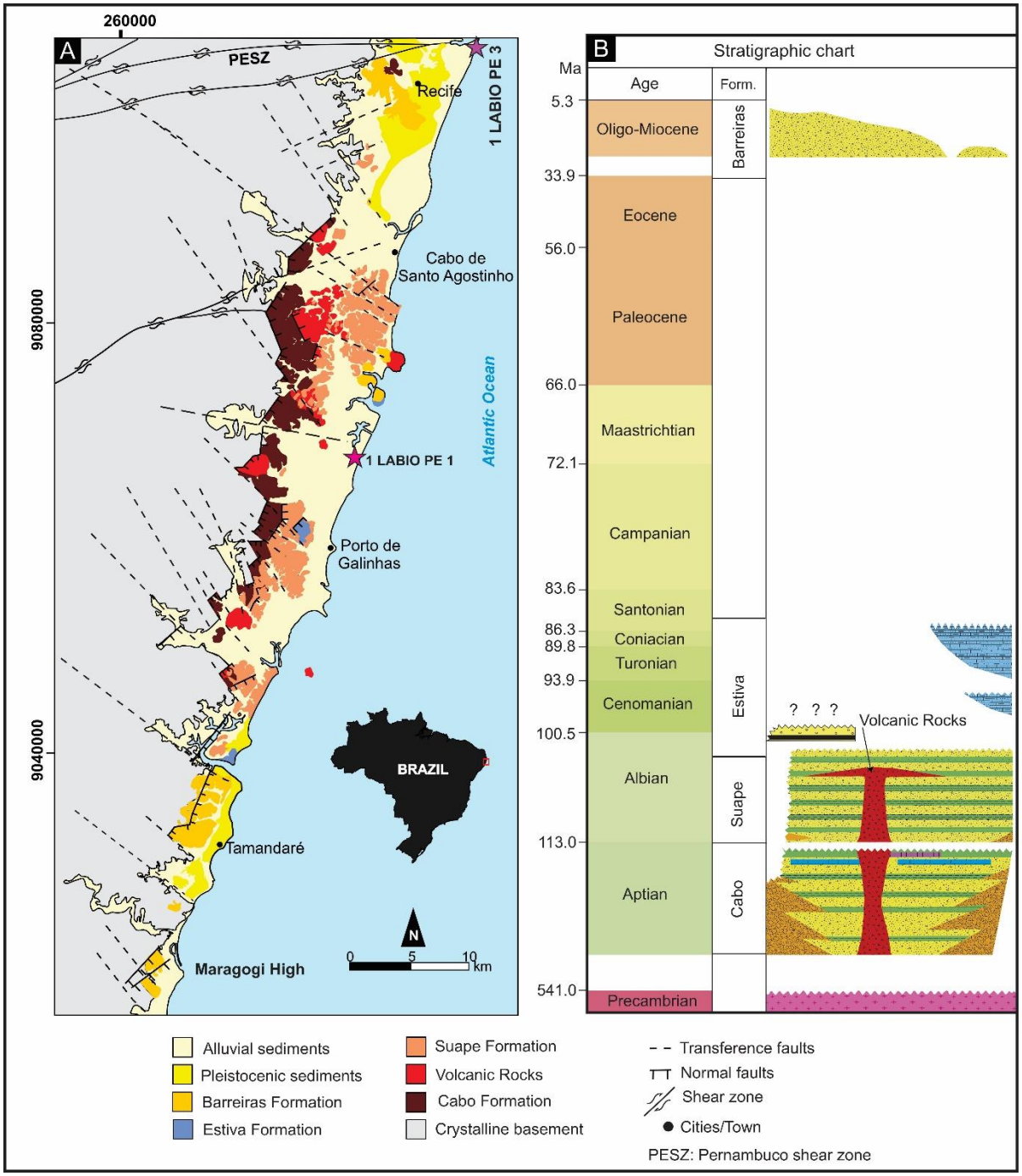

Figure 2. (A) Geological map of Pernambuco Basin, with the location of LABIO PE wells (simplified from Correia Filho, 2017). (B) Stratigraphic chart of the onshore region of the Pernambuco Basin (adapted from Maia, 2012).

3 MATERIAL AND METHODS

For this study, detailed stratigraphic log descriptions, as well as geochemical, and C-N isotope analyses of representative samples of the LABIO drilling project (1 LABIO PE 1 well) on the Cupe Beach (Figures 2 and 3), were used. The cores are

stored in the laboratory of Sedimentary and Environmental Geology (LAGESE) of the Federal University of Pernambuco (UFPE-Brazil). The core description was performed to show the high-frequency sedimentological changes, lithologies, textural aspects, and macrofossil contents, based on the classification of Grabau (1904). After that, nineteen representative samples were selected for microscopic analyses. The thin section was analyzed observing primary and diagenetic constituents, clay content, structures, and textures, based on the textural classification of Dunham (1962) and Embry and Klovan (1971), and classification of dolomite according to Sibley and Gregg (1978). The analytical techniques were performed on LAGESE using a Zeiss (SCOPE A1) microscope coupled with an imaging camera. In addition, some representative thin sections were also analyzed under cathodoluminescence, using the Cambridge Image Technology Ltd. (CITL) CL8200 model coupled to an optical microscope.

Total organic carbon (TOC) was determined in 36 samples and total sulfur (TS) in 24 samples, using a LECO® (CS-632) total analyzer of the Laboratory of Chemostratigraphy and Organic Geochemistry of the Rio de Janeiro State University (UERJ).

The carbon and nitrogen isotopes, as well as total nitrogen (TN) contents were determined in 23 representative samples by an Eurovector (EA3000) elemental analyzer with a mass spectrometer coupled to isotope ratio Delta-V Advantage of the Laboratory of Chemical Oceanography (LOQUIM) of the Federal University of Pernambuco (UFPE). The elemental analyzer was configured with a CHN reactor filled with chromium oxide, copper wires, cobalt oxide, and a water trap with magnesium perchlorate. The masses of TN and C_{org} and their respective isotopes were quantified by the analytical curve ($R2 \geq 0.995$) using a standard material B2151 (N = 0.52%; C = 7.45%. $\delta^{13}C$ = -28.85‰). During the analysis, the standard high purity CO_2 showed an average of $\delta^{13}C$ equal to -27.44‰. An individual $\delta^{13}C$ measure of the pure CO_2 standard was -28.73 ± 0.19‰, whereas the value certified is -28.85‰.

4 RESULTS

Herein, we describe all results obtained.

4.1 Sedimentological description of 1 LABIO PE 1 well

The Estiva Formation in 1 LABIO PE 1 well, is predominantly composed of carbonate and marl rocks, intensely dolomitized with subordinated shales and sandstones (Figure 3). Due to intense lithological variation, some intervals were detailed (Figure 3A, 3B). The sedimentary structures recorded in the well are described in detail in Table 1. The relatively low micropaleontological content in the studied well do not permit a better biostratigraphic resolution. However, a correlation was made, based on previous studies (*cf.* Lima and Pedrão, 1989; Lima-Filho and Silva-Santos, 2001; Araújo). that correlated the Estiva Formation from late Albian to Turonian ages

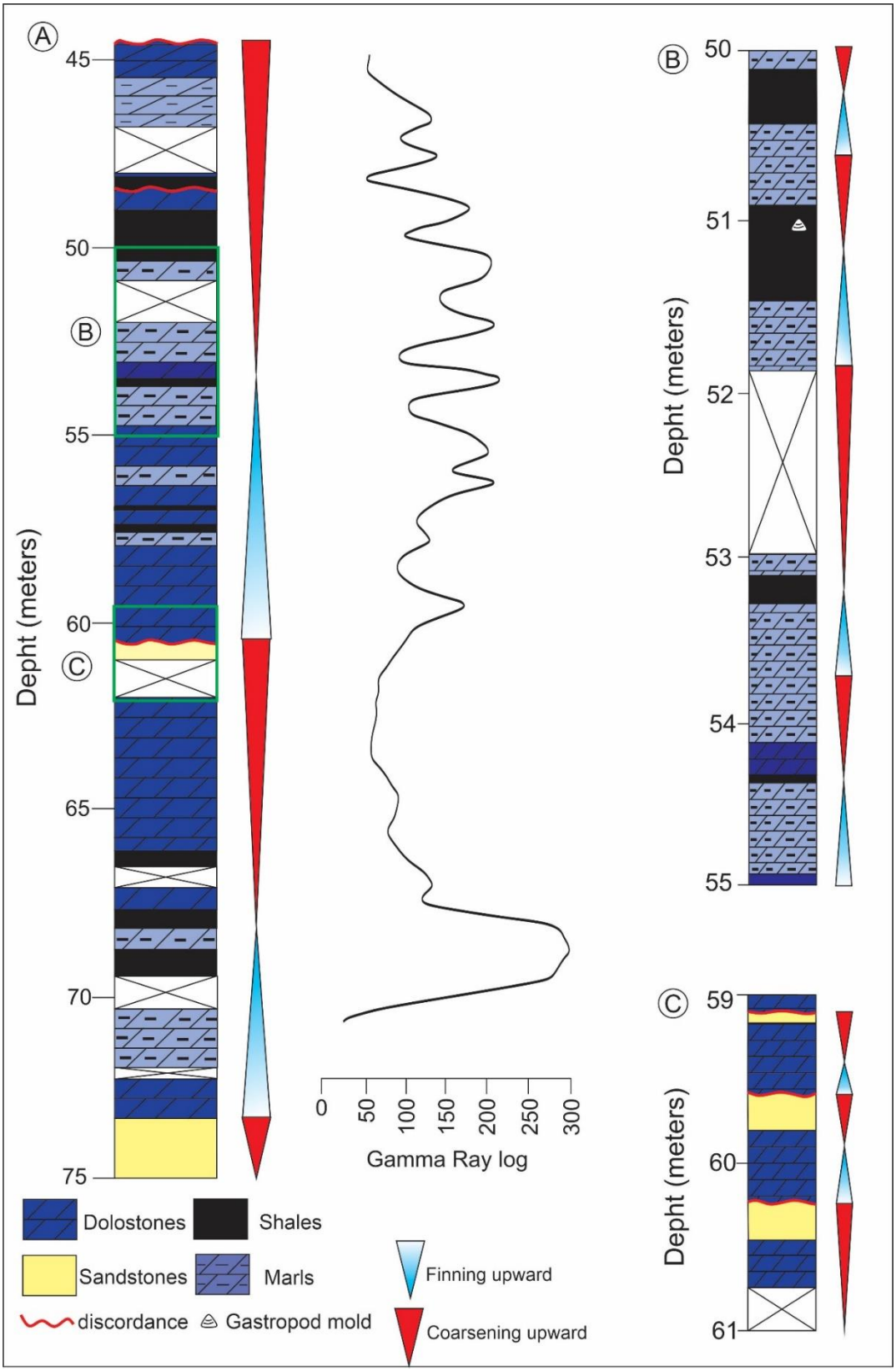

Figure 3. (A) Simplified geological profile of 1 LABIO PE 1 well; (B,C) Detailed geological description of the 1 LABIO PE 1 well.

Table 1: Description of sedimentary structures recorded in the 1 LABIO PE 1 well.

Sedimentary features	
i	Discordant contact between a dolostone and a shale sample with presence of a gastropod mold (Figure 4A)
ii	Bioclastic molds in a dolostone indicating proliferation of organisms (Figure 4B);
iii	Convolute structures on marl layers indicating fluidization contemporaneously to deposition (Figure 4C);
iv	Bivalve shells in a gray to black shale rock (Figure 4D);
v	Presence of vuggy porosity, suggesting karstification conditions and good potential for reservoir rock (Figure 4E)
vi	Presence of microbial structures (Figure 5A)
vii	Discordant contact between a sandstone and a dolostone (Figure 5B)
xiii	Massive sandstone with woody fragments (Figures 5C, 5D)
ix	Wavy/flaser lamination by fine sand intercalated with mud, indicating an energy variation (Figure 5E)
x	Sandstone with cross-bedding stratification associated with high energy conditions (Figure 5F).

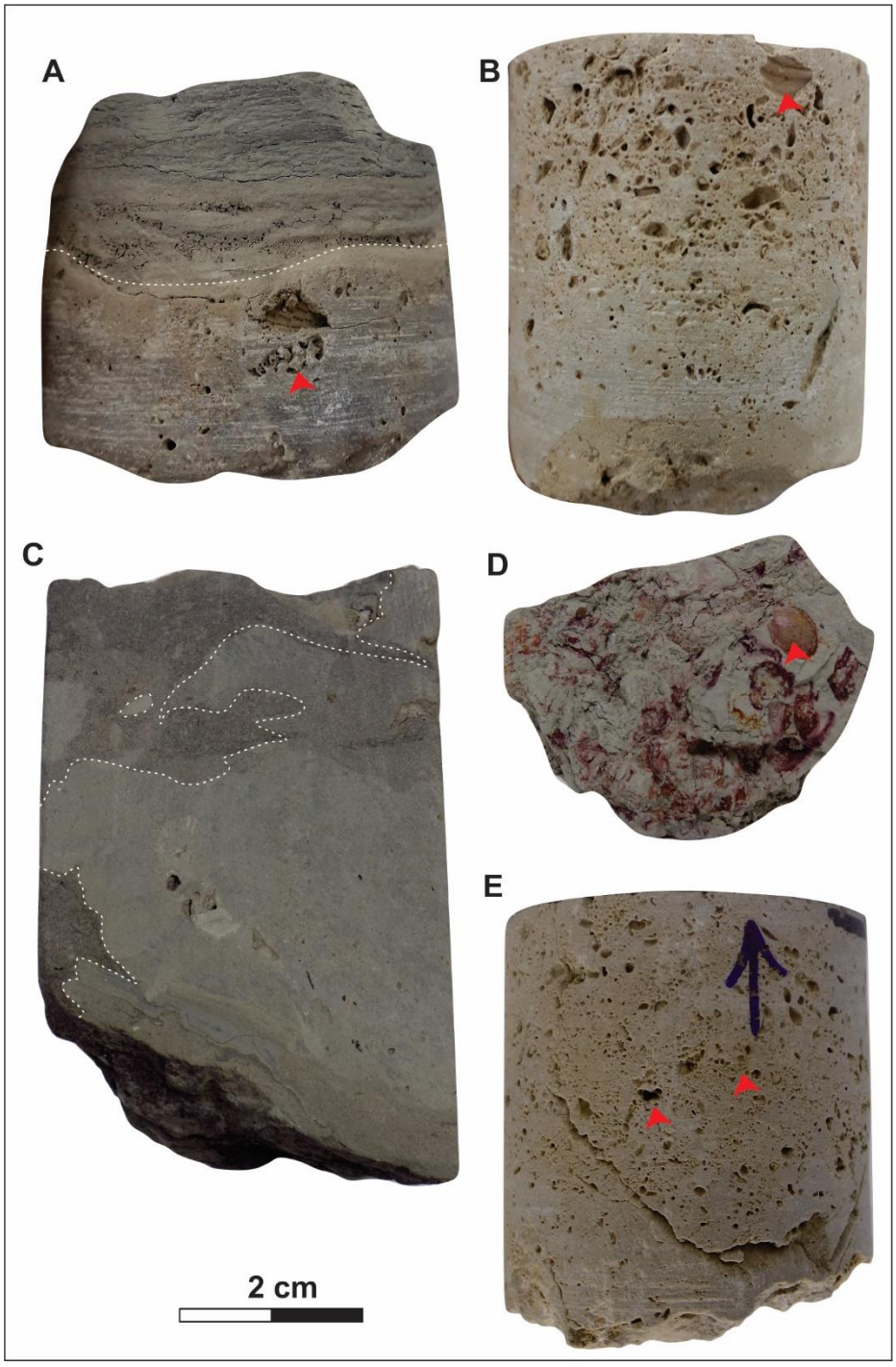

Figure 4. Representative core samples of the Estiva Formation. (A) Discordant contact between a dolostone (base) and a shale (top), detail of gastropod mold is present. (B) Massive bioclastic dolostone with disarticulated shells. (C) Marl with convolute stratification (white discontinued lines). (D) Detail of bivalve shell in a shale sample. (E) Bioclastic dolostone with intense bioturbation.

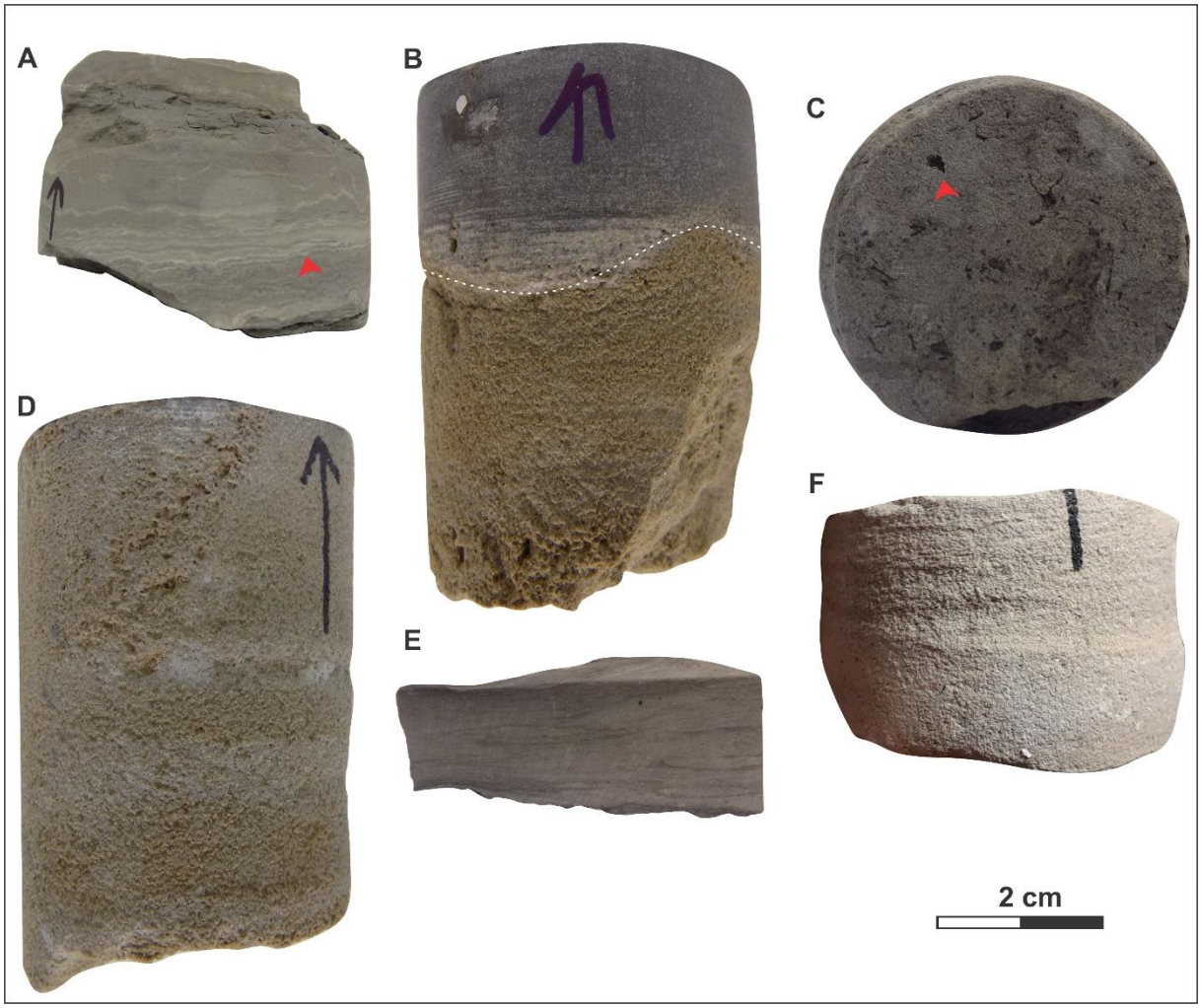

Figure 5. Representative core samples of the Estiva Formation. (A) microbialites marked by organic-rich levels and carbonate intercalations. (B) Discordant contact between dolostone (top) and sandstone (base). (C) Plant fragments in a sandstone sample. (D) Massive sandstone. (E) Wavy/flaser lamination. (F) Sandstone with cross-bedding stratification.

4.2 Petrographic features

4.2.1 The siliciclastic interval

The representative thin sections of the siliciclastic interval of the Estiva Formation are marked by the presence of dolomite-sandstones and shales. The framework of the samples is mainly composed of monocrystalline (~60 %) and polycrystalline (~20 %) quartz (Figures 6A, 6B) and plagioclase (~20 %). Organic matter occurs disseminated through the pore space and is intensely substituted by pyrite (Figures 6A-6B). The quartz grains are subangular to angular, poorly to well-sorted (Figures 6A-6D), with good preservation of the feldspar grains (Figure 6E), indicating short

distance of the sedimentary transport and/or rapid burial. Microcrystalline dolomite (10-30 %) usually occurs as cement filling the interstitial space between quartz-rich sand grains (Figure 6F). This dolomite cement was interpreted as a result of diagenetic alteration from an original calcite cementation

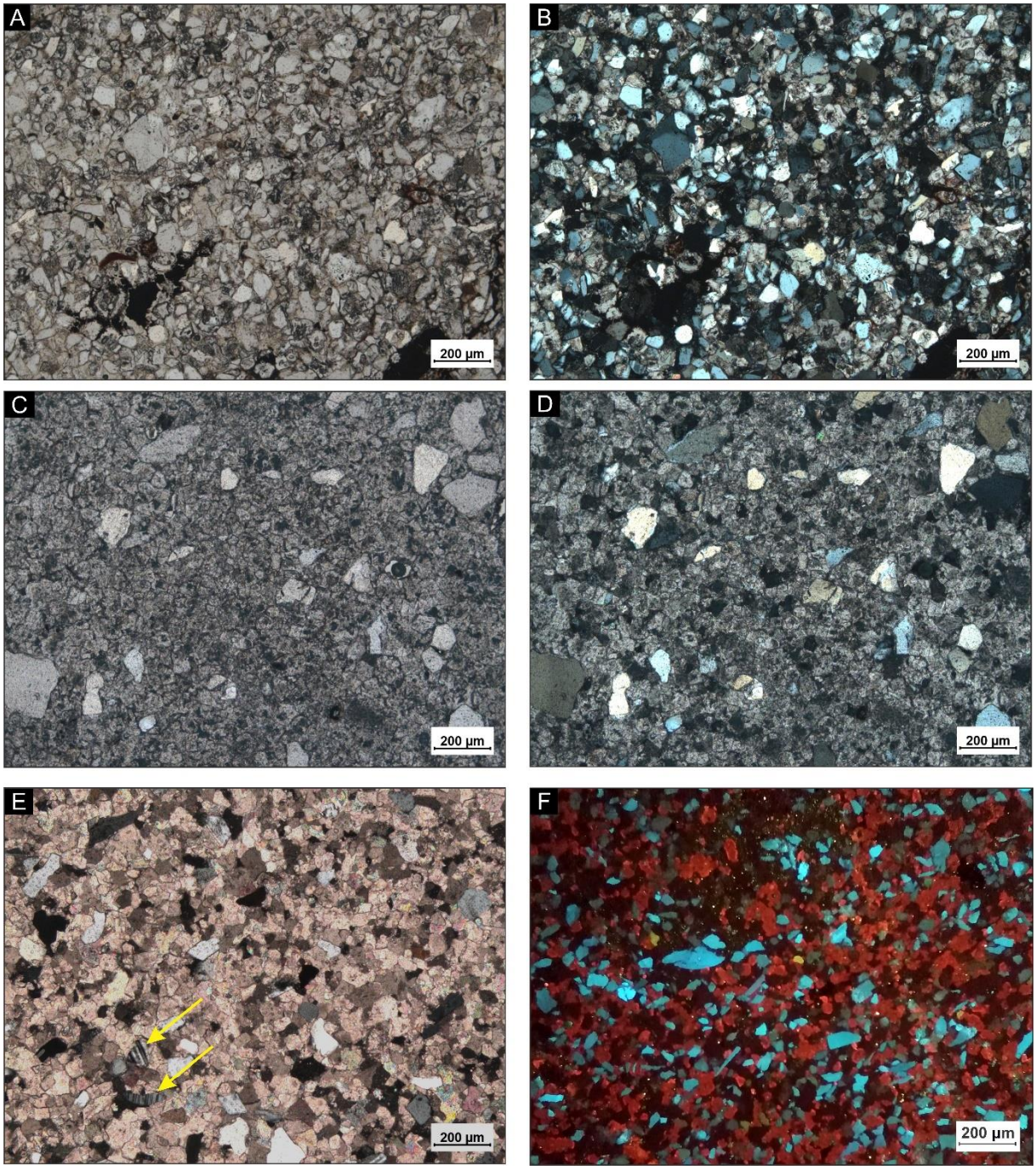

Figure 6. Photomicrographs of the siliciclastic interval from Estiva Formation. (A, B) Medium to well-sorted sandstone with organic matter and sulfide filling the pore space. (C, D) Detail of angulous quartz grains with dolomite cement in a dolomite-

sandstone; (E) Detail of preserved plagioclase grains (yellow arrows); (F) Detail of dolomite-sandstone under cathodoluminescence microscopy indicating the dolomite cement (red color) and igneous (?) quartz grains (blue color).

4.2.2 The carbonate interval

Most of thin sections of this interval contain dolomite with crystalline textures. The depositional textures were affected by the dolomitization process. Siliciclastic grains are also present in the investigated samples and indicate a greater influence of continental sediments during the carbonate deposition. The decrease of detrital sediments towards the top of the sequence was related to distal facies, whereas the increase of detrital sediments indicates more proximal facies, as pointed by Burchette and Wright (1992). Some relict microfossil skeletal grains are preserved, such as gastropods, foraminifera, and bivalve (Figure 7A), which occur mostly marked as vuggy and moldic porosity. Some levels are composed of marl rocks characterized by the mixing of clay minerals and dolomite in relatively similar proportions (Figure 7B). Allochemical grains such as peloids (Figure 7C) were also found, which are ellipsoidal form, and composed of microcrystalline dolomite without internal structure and interpreted as the result of faecal pellets produced by microorganisms. Two types of dolomite texture were also recognized: (i) the planar-e dolomite has euedric crystals, some of them with zonation (Figure 7D) and (ii) the planar-s dolomite occurs as subhedral crystals with lobate contact (Figure 7E). Microbial mats are well-laminated and reveal that it is an intercalation of dark layers of organic-rich clay and bright layers of spathic dolomite with levels of sulfides (Figure 7F). Therefore, it is probably formed by action of benthic microbes as a result of agglutination of sedimentary particles or by biomineralization process (Riding, 2011).

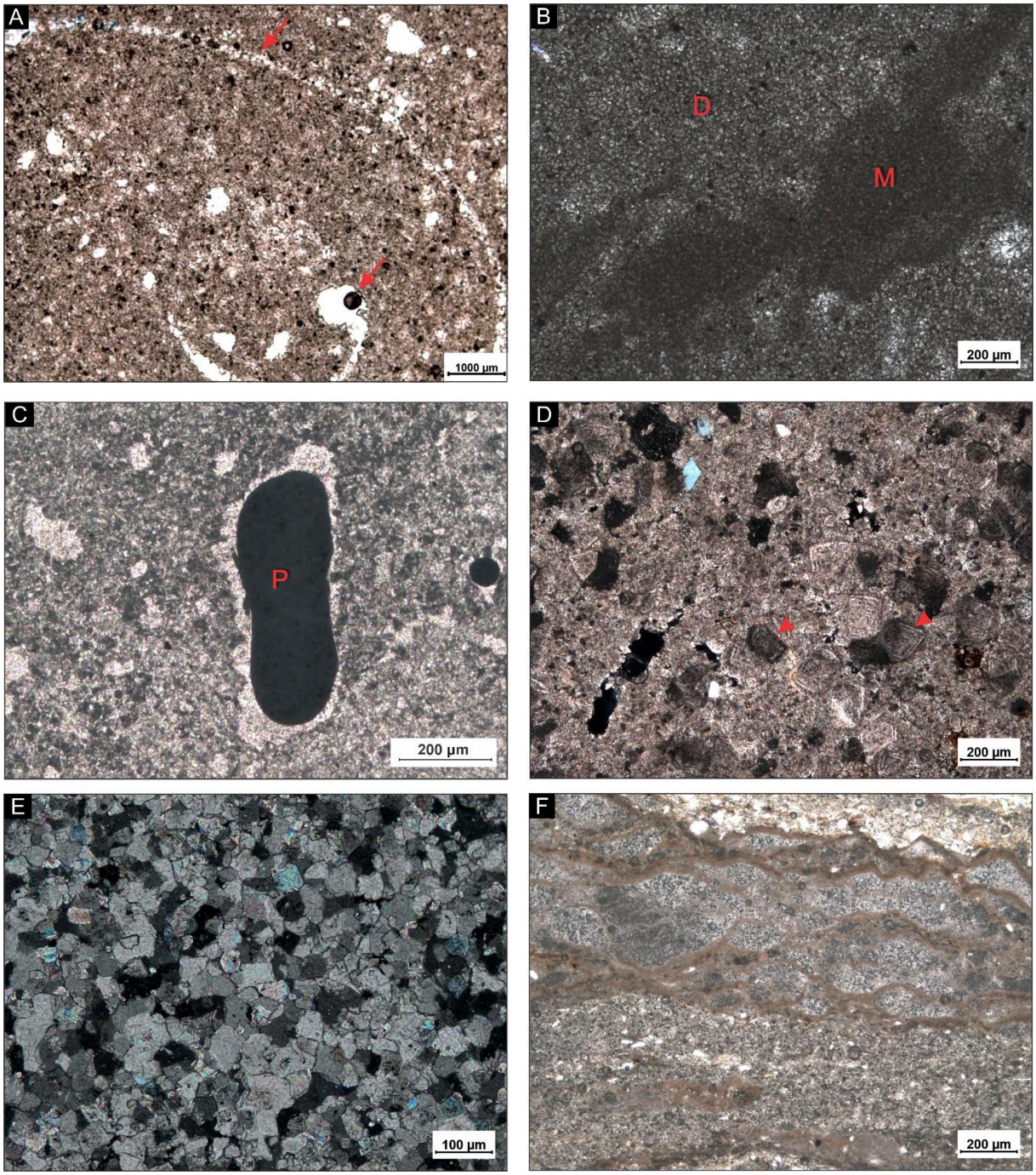

Figure 7. Photomicrographs showing the main aspects of dolostone interval from Estiva Formation. (A) Disarticulated shell of bivalve mold (red arrows) in a dolowackestone sample (plane-polarized light); (B) Preserved micrite matrix rich in dolomite sample (crossed polarized light). (C) Ellipsoidal and elongate peloids, black to brownish color of a peloidal dolowackestone sample (plane polarized light); (D) Planar-e dolomite in a dolostone sample; (E) General aspect of marl sample; (F) Detail of a well-laminated microbialite.

4.3 Geochemistry

The geochemical data obtained in the drill cores shows values of TOC ranging from 0.09 to 3.60% and TS from 0.20 to 1.29%. The $\delta^{13}C_{org}$ is between -24.65 and -18.89‰. The TN is from 0.02 to 0.08 % and the bulk $\delta^{15}N$ is from +0.93 to +5.44‰ (Table 2). The TOC/TN ratio measured in the studied profile exhibits lower to higher values 6.3 to 55. The TOC values are suggestive of an organic accumulation in the basin during the deposition of Estiva Formation, as well as the high TS content is in accordance with the pyrite content observed in the thin section. The $\delta^{13}C_{org}$, and TOC/TN ratio measured is suggestive of marine algae deposition, as well as the high values indicates an ^{13}C enrichment in some stratigraphic levels.

Table 2. Geochemical data of Estiva Formation in the 1 LABIO PE 1 well.

Sample	TN (%)	TOC (%)	TS (%)	$\delta^{13}C$ (‰)	TOC/TN	$\delta^{15}N$ (‰)	Depth
CP1	0.03	1.61		-24.58	53.7	2.39	46.2
CP2	0.02	0.95		-24.65	47.5	1.32	46.5
CP3		0.34	0.62				48.0
CP4		0.30	0.23				48.2
CP5		0.25	0.4				48.4
CP6	0.03	0.39	0.56	-21.66	13.0		49.2
CP7		0.42	1.2				49.5
CP8		0.35	0.4				49.6
CP9	0.03	0.47	0.35	-21.01	15.7		50.0
CP10	0.07	2.09	1.19	-20.55	29.9		51.9
CP11		0.26	0.76				53.1
CP12		2.26	1.32				53.2
CP13	0.08	3.60		-23.53	45.0	3.97	53.3
CP14	0.03	0.71	0.13	-21.60	23.7		53.7
CP15		0.82	0.6				54.1
CP16		0.98	0.18				54.2
CP17	0.03	0.36	0.46	-20.88	12.0		54.8
CP18	0.03	0.19	0.52	-21.27	6.3		55.3
CP19	0.06	1.24		-22.63	20.7	3.18	56.1
CP20		0.28	0.62				56.7
CP21		0.23	0.38				56.8
CP22		0.24	0.37				57.1
CP23		0.28	0.42				57.2
CP24		0.26	0.5				57.5

CP25		0.24	0.3				57.6
CP26	0.04	0.87		-22.27	21.8	2.43	58.7
CP27	0.04	0.91		-22.36	22.8	5.34	60.4
CP28		0.79		-23.34			62.8
CP 29	0.08	0.88		-21.82	11.0	5.27	63.4
CP30	0.03	0.33	1.11	-21.33	11.0		64.3
CP31	0.04	0.78		-23.57	19.5	5.44	66.1
CP32	0.05	1.39	1.29	-21.09	27.8		68.0
CP33	0.02	0.14	0.02	-20.12	7.0		69.2
CP34		0.32		-18.89			70.9
CP35		0.41		-21.57			72.6
CP36	0.01	0.55		-21.08	55.0	0.93	74.4

5 DISCUSSION

5.1 Geochemical signatures

The isotopic data of $\delta^{13}C_{org}$ of the samples from 1 LABIO PE 1 well indicates a mixing of the organic matter type of the investigated samples and a trend to marine contributions (Figure 8A). The data obtained plotted in the TOC *vs.* TS diagram (*cf.* Kelley et al., 1994) is suggestive that the samples from the Estiva Formation were deposited under freshwater to a normal marine condition (Figure 8B). In addition, it corroborates with the constraints established by Moura et al. (2020), who also proposed suboxic-anoxic conditions during the Cenomanian-Turonian ages in the Pernambuco Basin.

The $\delta^{13}C_{org}$ *vs.* TOC/TN diagram, the organic matter of the investigated samples was classified predominantly as marine algae (Figure 8C). However, the high TOC/TN ratio in the samples indicates a mixing source by C3 land plants (continental source) and marine algae (*cf.* Meyers, 1994). Furthermore, the relatively depleted $\delta^{13}C_{org}$ (*ca.* -22 to -20‰) and the TOC/TN ratio (near 6-10) suggest that the main marine algae contribution was from phytoplankton (Meyers, 1994). According to Calvert (2004) and Zhang et al. (2019), the significant correlation between TOC with TN data (r^2 = 0.7) further support that the main source of N content is the organic matter, and thus the inorganic N may be negligible (Figure 8D), as well as represent the depositional signal.

On the other hand, Araújo (2014) studied the same stratigraphical interval in the northern border of the Pernambuco Basin (1 LABIO PE 3 well) and found the

$\delta^{13}C_{org}$ varies from -23.79 to -22.93‰, which are similar to the values obtained in this contribution and also indicates a mixing of terrestrial and marine algae.

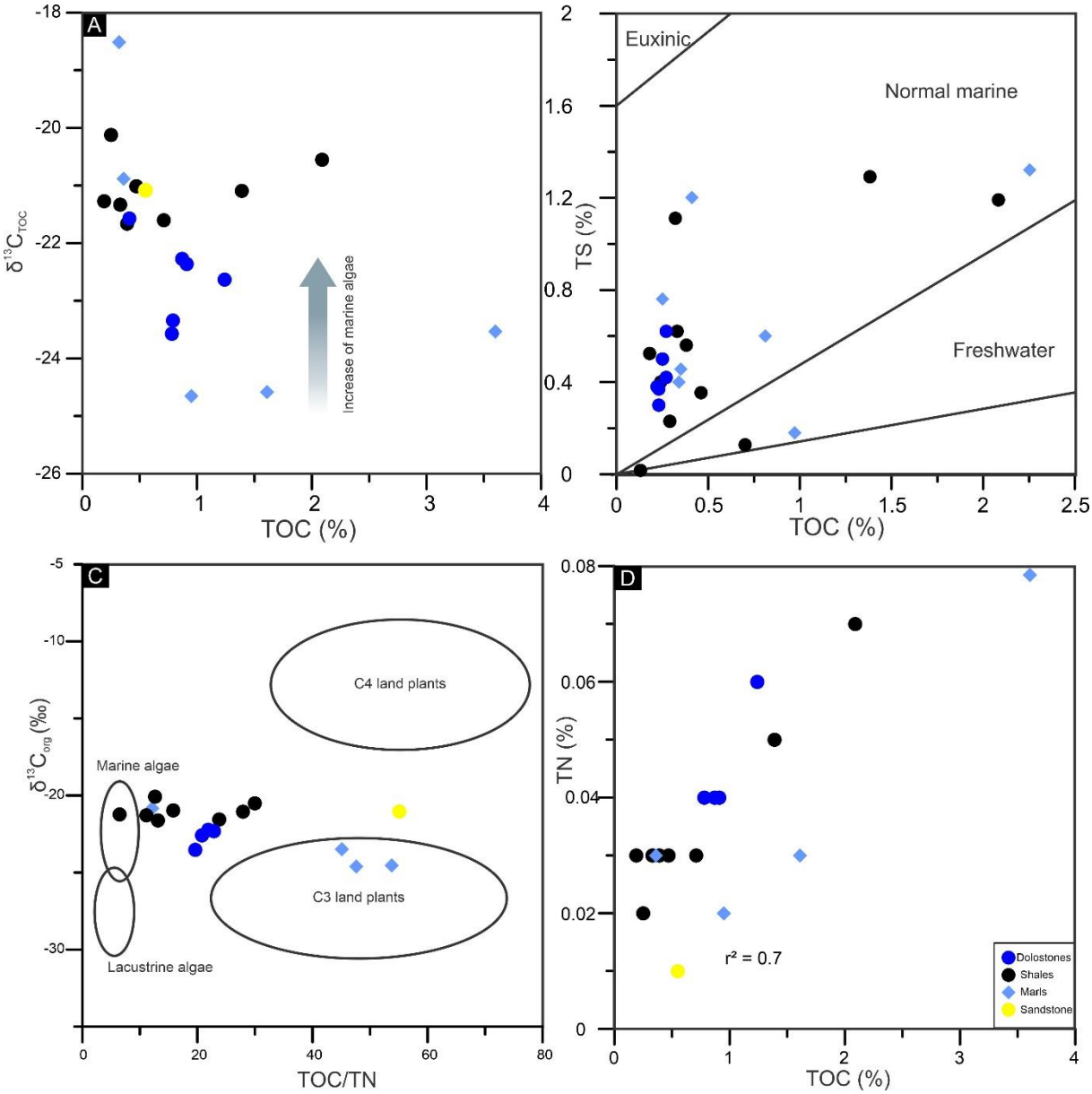

Figure 8. Geochemical diagrams for samples from 1 LABIO PE 1 well. (A) $\delta^{13}C_{org}$ *vs.* TOC content; (B) TOC *vs.* TS (proposed by Kelley et al., 1994); (C) $\delta^{13}C_{org}$ *vs.* TOC/TN ratio (as proposed Meyers, 1994); (D) TN *vs.* TOC (proposed by Calvert, 2004)

In general, it was recognized three positive peaks through the $\delta^{13}C_{org}$ profile, which suggest a perturbation in the carbon cycle. In the lower part of studied section (69.0 to 71.0 m depth) shows a slight positive $\delta^{13}C_{org}$ incursion with a value of *ca*. -18.5‰. This first peak in the lower part (70.9 m depth) was interpreted by the

influence of OAE 1d (?) (Figure 9). This event has been demonstrated in some locals of the earth and shows positive incursions between *ca.* +0.5 to 2‰ in the carbon cycle (*e.g*. Bornemann et al., 2005; Scott et al., 2013) and associated with pelagic marls. These characteristics has a lithological, and isotopic behavior similar to the studied profile and therefore allow us to supported this interpretation.

In the middle part of the studied section (63.0 to 64.0 m depth) the second positive incursion in the $\delta^{13}C_{org}$ was observed with a value of *ca*. -21.3‰. Furthermore, this slight increase of $\delta^{13}C_{org}$ is followed by low values of the TOC/TN ratio, which may suggest a prominent marine contribution in this section of studied profile. This peak was related to the isotope signature of the Middle Cenomanian Event (MCE) (?) proposed by Coccioni and Galeotti (2003). The MCE have been related to precedes the OAE 2 (Coccioni and Galeotti, 2003, Andrieu et al., 2015). This anoxic event is marked by a positive shift of *ca.* +1‰ and an association with the carbonate production (Andrieu et al., 2015).

In the upper part of the studied section (50.0 to 52.0 depth), the $\delta^{13}C_{org}$ reached a value on the order of *ca.* -20.5‰ which also reflects the enhanced burial of ^{13}C-enrichment isotope in the organic matter (*cf.* Jenkyns et al., 1994; Hayes et al., 1999; Jarvis et al, 2011). In addition, low values of TOC/TN ratio, is accomplished, and support a higher marine algae contribution (Figure 9) being interpreted as the OAE 2 expression.

The nitrogen cycle is biologically influenced by the oxygenation state of both the water column and the sediments (Mouro et al., 2017; Danzelle et al., 2020). Under anoxic conditions and stratified waters occurs a segregation into NH_3^- reservoirs in oxygenated part of the water column, and NH_4^+ accumulation in the anoxic part of the water column (Danzelle et al., 2020). The loss of nitrogen and slight bulk $\delta^{15}N$ positive incursion is interpreted as bacterial denitrification process, which converting NO_3^- to N_2 and N_2O (Ruvalcaba-Baroni et al., 2015; Danzelle et al., 2020).

The bulk $\delta^{15}N$ values obtained in the studied section ranging from *ca.* +3 to +4‰, make it possible to infer a denitrification process. Such reduction can be considered carried out by photosynthetic organisms triggered by the increase of oxygen-minimum zones resulting from the expansion of the anoxic conditions (Figure 9; Hoefs, 2018; Zhang et al., 2019; Danzelle et al., 2020). According to Junium et al. (2018) during the Cenomanian-Turonian boundary the values reported of bulk $\delta^{15}N$ is

ranging from *ca.* -4 to +2‰, which is different of the values observed in the studied section. However, the fact of the Pernambuco Basin was a restricted basin during the Cenomanian-Turonian ages suggest that the nitrogen source was not exclusively from the atmosphere and leading to infer a contribution of outside sources, such as rivers nutrient input, and may reflect the bulk $\delta^{15}N$ values observed.

In addition, the reported values of bulk $\delta^{15}N$ (from +0.90 to +2.00‰) in the lower and upper sections of the studied profile (Figure 9) may indicate nitrogen fixation process, which converts atmospheric N_2 into NH_4^+ by the action of bacteria (Hoefs, 2018). This process is assumed here to have caused the increase of denitrification, which is possible due to depletion of the oxygen-free water in the ocean (Ruvalcaba-Baroni et al., 2015).

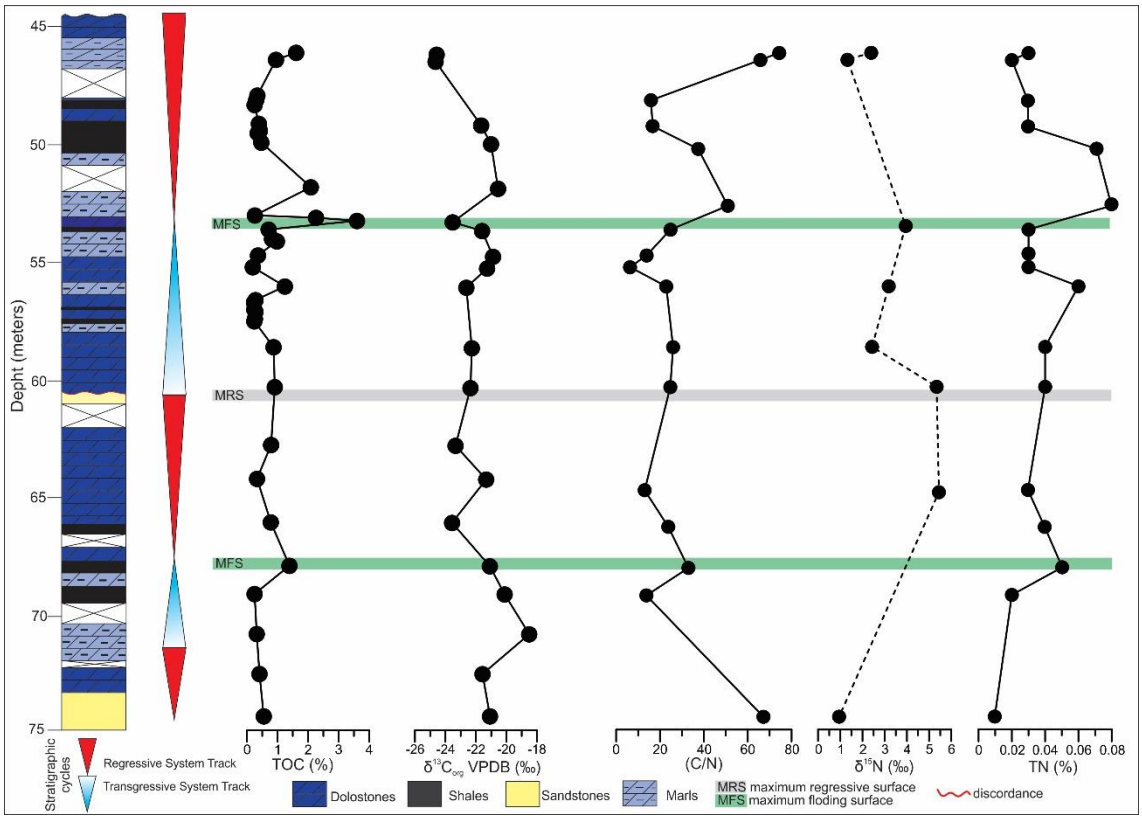

Figure 9. Stratigraphic profile and geochemical logs of organic carbon, and nitrogen concentrations and their respective isotopes, through the Estiva Formation.

5.3 The Oceanic Anoxic Event (OAE 2) in the Pernambuco Basin and a global correlation

The geochemical features of 1 LABIO PE 1 well are suggestive that the upper part (50 to 52 m depth) of the stratigraphic profile represents the OAE 2 record in the

Pernambuco Basin. The OAE 2 or Bonarelli event (Schlanger and Jenkys, 1976; Schlanger et al., 1981; Jenkyns, 2010), which occurred during a greenhouse interval due to oceanic crust formation and volcanism associated that also promoted the rise of relative sea level and a positive carbon excursion (Mort, 2007; Jarvis et al., 2011).

Those isotopic behaviors observed in the Estiva Formation were correlated with other sections worldwide, such as the Furlo section (Italy; Keller et al., 2004), Eastbourne section (England; Paul et al., 1999) and Demerara rise section (IODP site 1258 Central Atlantic; Erbacher et al., 2005) (Figure 10). In general, a positive incursion of 1-4‰ in the $\delta^{13}C_{org}$ values has been recorded during the Cenomanian-Turonian boundary, leading to an increase in the primary productivity (Erbacher et al., 2005; Jarvis et al., 2011). Similar isotopic features of OAE 2 have been shown by means of the average in the $\delta^{13}C_{org}$ values, ranging from -25 to -21‰ (*e.g.* Ulicny et al.,1997; Paul et al., 1999; Keller et al., 2004; Tsikos et al., 2004; Erbacher et al., 2005; Mort et al., 2007; Hetzel et al., 2009).

The OAE 2 expression were also observed by Takaki and Rodrigues (1993); Rodrigues et al. (2019), and Valle et al. (2019) in the Sergipe-Alagoas Basin (south of Pernambuco Basin) with TOC values ranging from 0.1 to 2.0% and a positive $\delta^{13}C_{carb}$ 3-5‰ incursion. Therefore, the values reported in the studied profile are close to those recorded during the OAE 2 event in other sections worldwide (Figure 10).

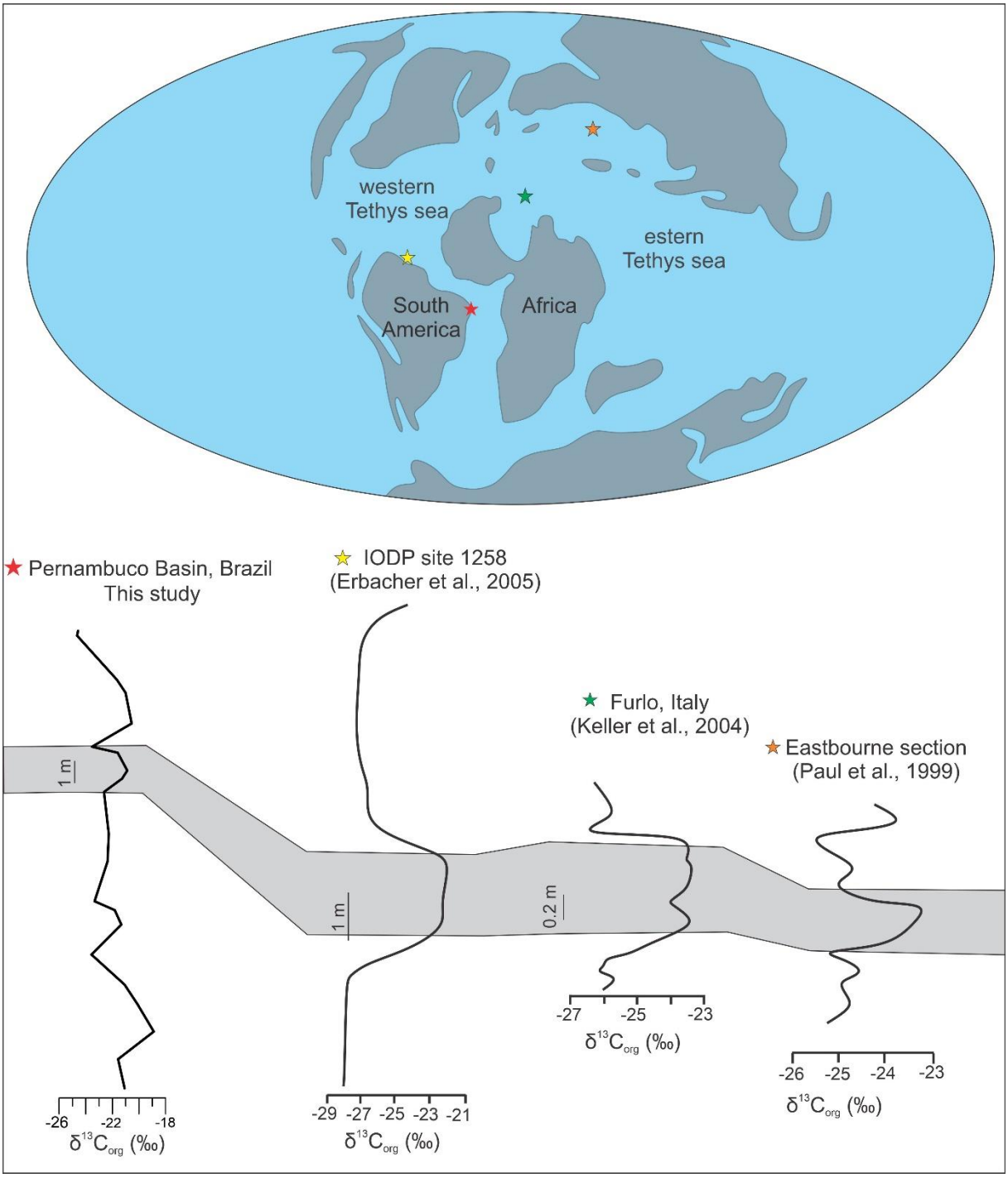

Figure 10. Global correlation across the main $\delta^{13}C$ profile of OAE 2 event. The map reconstruction is from the Cenomanian-Turonian boundary (~94 Ma) adapted from Scotese (2014).

In addition, Riedel et al. (2019), studying the organic-phosphorus accumulation, in a Cenomanian-Turonian interval, in the 1 LABIO PE 3 well, reported values between 0.08 and 8.15 µmol/g, and associated the low values with OAE 2, which were related

to increase of anoxic conditions that remobilized the phosphorus content in the sediments to the photic zone.

The deposition of the late Albian to Turonian interval in the Pernambuco Basin (Estiva Formation) probably occurred during a greenhouse period thought to be caused by oceanic crust formation and volcanism activities by Large Igneous Province (LIPs) (Schlanger et al., 1981; Mort et al., 2007). The hypothesis that the OAE 2 was influenced by volcanic activities has been proposed by some authors in others regions worldwide, such as Turgeon and Creaser (2008), Adams et al. (2010) and Jenkyns et al. (2017). In the Pernambuco Basin, the volcanic activity occurred during the middle to late Albian, which formed the rocks of the Ipojuca Magmatic Suite (*ca.* 104-100 Ma) related to the Santa Helena hot-spot in northeastern Brazil (Nascimento, 2003). This volcanism may be the thermal mechanism, which enhanced the primary organic carbon productivity and probably influenced the perturbation of carbon and nitrogen cycle due to release of CO_2 in the oceans (*cf.* Jenkyns, 2010). In addition, the effect of volcanism may have led to a high rate of bacterial sulfate reduction, which increased the sulfur content in the oceans and could promoted a large pyritization observed in the studied samples as textural pyritized levels of organic matter in thin sections and by the sulfur content up to 1.29%, in a similar way to what occurred worldwide pointed by Poulton et al. (2015) and Danzelle et al. (2020).

On the other hand, global oceanic paleoenvironment models during the Cenomanian-Turonian boundary have been reported (Scotese and Moore, 2014a, b; Ladant et al., 2020). According to Scotese and Moore (2014b) during the Cenomanian-Turonian boundary, anoxic waters were dominant in northeast Brazil (Figure 11A). Those models also infer high-salinity (34-36 PSU) and moderated to hot (28-30 °C) waters in this Brazilian portion (Figure 11B; Ladant et al., 2020). Those reconstructions are in accordance with the $\delta^{13}C_{org}$ and bulk $\delta^{15}N$ positive anomalies recorded in the Estiva Formation, and may be caused by the expression of the OAE 2 in this Earth portion.

In addition, the significant siliciclastic input observed in the thin section (Figures 7D, 7E) may be explained by the perturbation of carbon cycle during anoxic events that promotes a rise of fluvial nutrients input in the oceans due to warm climates (Jenkyns, 2010; Jarvis et al., 2011). The expression of OAE 2 in the Pernambuco

Basin was possibly due to entrance of western Tethys seawaters that reached the Brazilian northeast portion as restricted to narrow channels (Figure 11C; Ladant et al., 2020).

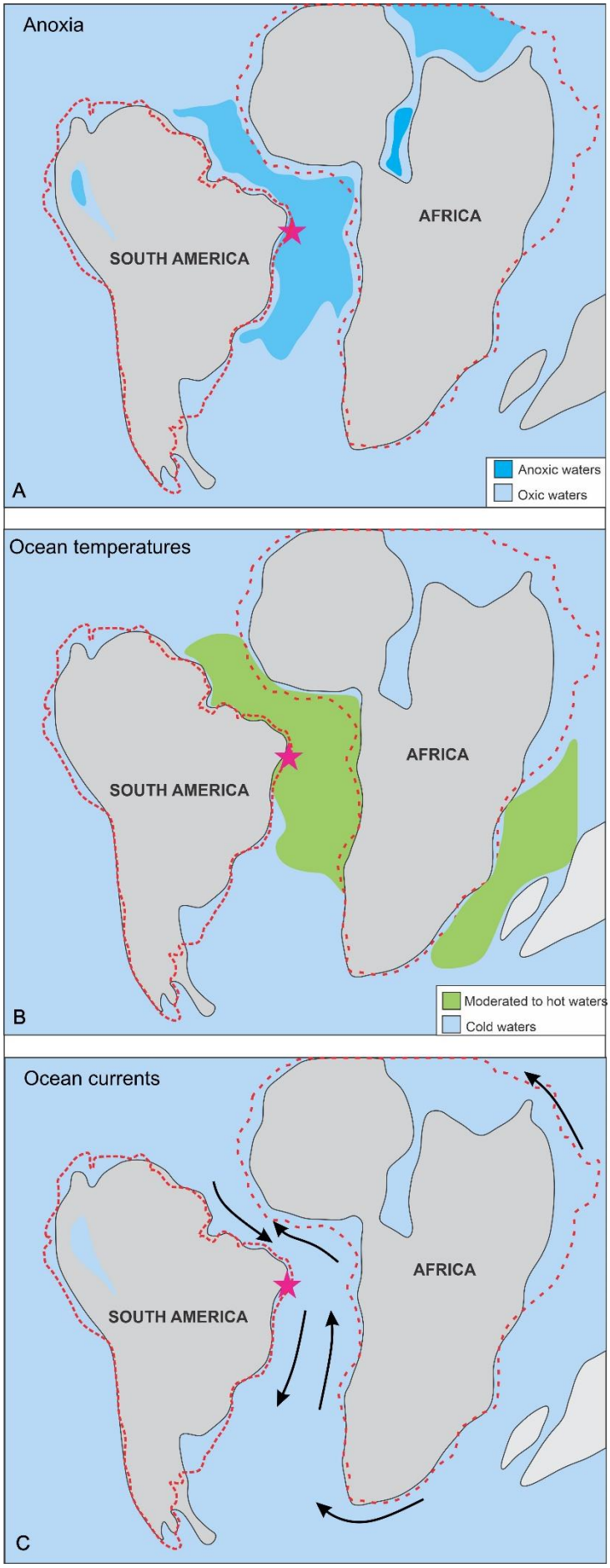
Anoxia
AFRICA
SOUTH AMERICA
Anoxic waters
Oxic waters
A
Ocean temperatures
AFRICA
SOUTH AMERICA
Moderated to hot waters
Cold waters
B
Ocean currents
AFRICA
SOUTH AMERICA
C

Figure 11. Paleoenvironmental models for the Cenomanian age. (A) Anoxia; (B) ocean temperature and (C) ocean currents circulation; (A, is adapted by Scotese and Moore, 2014a, b); (B, C, are adapted from Ladant et al., 2020). The pink star is the location of Pernambuco Basin.

5.4 Stratigraphic and Paleogeographic Implications

Based on palynological content, Lima-Filho and Santos Silva (2001) established a biostratigraphic zonation of Estiva Formation as P-350 (superzone) related to late Albian to Santonian ages. However, a marine influence is just evidenced by dinoflagellates from the top of P-300 (superzone) related to middle to late Albian ages (Maia, 2012). Araújo (2014) also using the palynological content in the 1 LABIO PE 3 well, determined late Albian to early Cenomanian ages in the lower of Estiva Formation, based on both the presence of *Gnetaceapollenites undalutus* and *Psilatricolporites papilianiformis* and a marine contribution due to the presence of palynoforaminifers. However, the most abundant specimens are exclusively from Cenomanian-Santonian ages, such as *Psilatricolpites papiloniformis* (Regali et al., 1974) and *Hexaporotricolpites coronatus* (Lima-Filho and Santos-Silva, 2001; Ferreira, 2009). Furthermore, the gastropod content is similar to that of the Riachuelo Formation of the Sergipe-Alagoas Basin (Beurlen and Cobra, 1960) due to the presence of *Lima Fazenda Estivica* (Maury, 1930) and *Graginia ariquindai* (Muniz and Almeida, 1988).

According to Ferreira (2009) in the lower part of Estiva Formation is marked by reworking of Devonian phytoclasts and dinocysts. This biostratigraphic inferences also corroborate the Estiva sedimentation starting in an epicontinental sea (Lima-Filho, 1998) during the late Albian age in the Pernambuco Basin, with seawater supply possibly coming from earlier than the Sergipe Alagoas Basin.

Since the Albian age, an effective rupture of continental crust and generation of oceanic crust in the northeast, Brazil, were influenced by the action of Santa Helena mantellic plume (Long et al., 1986; Lima-Filho, 1998; Szatmari and Milani, 1999; Nascimento, 2003). However, the oceanic crust spreading in the Pernambuco basin may have occurred later than the Camamu-Almada and Sergipe-Alagoas basins, it is probably due to the short time of the plate separation, as demonstrated by Perez-

Dias and Eagles (2017). The oceanic crust formation in the Pernambuco Basin is related in the Albian-Cenomanian boundary (Nascimento, 2003).

After the oceanic crust formation, and the total disruption of Pernambuco High, the seawater establishment processes began to suffer the entrance of the western Tethys seawaters (Dias-Brito, 1994; and Perez-Dias and Eagles, 2017; Silva-Jr. et al., 2020). Based on new stratigraphic, petrographic, and geochemical data presented here, we suggest that the ingression of western Tethys seawater occurred due to the effective rupture of Pernambuco High, which acted as a geographical barrier until the Albian-Cenomanian boundary. In addition, the consequent increase in relative sea level also contributed to expansion of the western Tethys seawaters at northeast sedimentary basins.

Regarding the stratigraphic discussion of the post-rift to drift phase formations (Lima-Filho, 1998; Maia, 2012; Correia-Filho, 2017; Lima-Filho et al., 2019), our proposal is that the Paraíso Formation (Maia, 2012; Correia-Filho, 2017) comprises a lateral variation of the Estiva Formation, associated with decrease of accommodation space and consequently increase of siliciclastic input, making the basin dominantly siliciclastic. Furthermore, the carbonate rocks were deposited during an increase of high accommodation space and a decrease of siliciclastic supply, and consequently retrogradation of coastline. Besides that, the greater siliciclastic contribution in some carbonate levels suggests proximal conditions and a restricted basin (Lima-Filho, 1998; Tomé et al., 2006; Moura et al., 2020).

6 CONCLUSIONS

During the late Albian-Turonian ages in the Pernambuco Basin, the carbonate sedimentation recorded by the Estiva Formation was developed with a greater continental influence. Moreover, the primary features (microbialites) observed in the thin sections point to a microbial contribution to the carbonate sedimentation from Estiva Formation. The studied profile has low to high TOC content (0.19 to 3.60%), indicating a primary productivity and organic matter accumulation. The $\delta^{13}C_{org}$ data (-24.65 to -18.89‰) suggests a mixing of organic matter contribution from transitional (C3 land plants) to marine algae. The bulk $\delta^{15}N$ (+0.93 to +5.44‰) indicates both the N_2 fixation related to reduction of nitrogen (N_2) to ammonium (NH_4^+), and denitrification process associated with a reduction of nitrate (NH_3^-) to nitrogen (N_2)

respectively, by photosynthetic organisms, such as microbial bacteria. A positive incursion in the $\delta^{13}C_{org}$ followed by denitrification process by the $\delta^{15}N$ values, and low values of TOC/TN ratio, in the upper studied section marks the expression of the OAE 2 in the Pernambuco Basin. Furthermore, the effective rupture of Pernambuco High and oceanic crust formation during the late Albian to early Cenomanian probably promoted a narrow connection with the western Tethys, which permits the OAE 2 record in the Pernambuco Basin and other sedimentary basins of northeast Brazil.

ACKNOWLEDGEMENTS

We would like to thank the PETROBRAS S.A. for the LABIO drilling project (401812/2010-3) executed in the Pernambuco Basin. W.A.L.M. thanks the National Council for Scientific and Technological Development (CNPq) for post-degree scholarships. J.A.S.N. is also grateful to CNPq for his research grant (process number 312.275/2017-0). We are thankful to Dr. Rysoaurya Keyla Travassos and Dr. Bruno Costa (LOQUIM-UFPE) for carbon and nitrogen isotopes and C-N elemental analyses.

REFERENCES

Adams, D. D., Hurtgen, M. T., Sageman, B. B. 2010. Volcanic triggering of a biogeochemical cascade during Oceanic Anoxic Event 2, Nature Geoscience, 3, 201–204.

Araújo. I.G., 2014. Litoestratigrafia. Palinologia. Geofísica e Geoquímica do Furo 1-LABIO-PE3. Borda Norte da Bacia de Pernambuco: Implicações estratigráficas. MSc. Dissertation, Federal University of Pernambuco.

Barbosa. J.A., Maia. M.F.B., Lima Filho. M.F., Magalhães. J. R., Correia Filho. O.J., 2014. Seismic stratigraphy of onshore portion of Pernambuco Basin. Evidence of break-up during Albian for the South Atlantic rift in Northeast Brazil. In: AAPG Annual Metting and Exhibition. Houston. Abstracts, 1-5.

Beurlen, K., Cobra, R.Q., 1960. Novas localidades fossilíferas no litoral sul de Pernambuco, Anais da Academia Brasileira de Ciências, 32, 1-2.

Buarque, B.V., Barbosa, J.A., Magalhães, J.R.G., Oliveira, J.T.C., Correia Filho, J.O., 2016. Post-rift volcanic structures of the Pernambuco Plateau, northeastern Brazil. Journal of South American Earth Science, 70, 251-267.

Buarque, B.V., Barbosa, J.A., Oliveira, J.T.C., Magalhães, J.R.G., Correia Filho, O.J., 2017. Carbonate Build-ups in the Pernambuco Basin, NE Brazil. Anais da Academia Brasileira de Ciências, 89, 841-857.

Burchette, T.P., Wright, V.P., 1992. Carbonate ramp depositional systems. Sedimentary Geology, 79, 3-57

Burne, R.V., Moore, L.S., 1987. Microbialites: Organossedimentary deposits of Benthic Microbial Communities. The Society of Economic Paleontologists and Mineralogists (PALAIOS), 2, 241-257.

Calvert, S.E. 2004. Beware intercepts: interpreting compositional ratios in multi-component sediments and sedimentary rocks. Organic Geochemistry, 35, 981-987.

Campos Neto, O.P.A., Souza Lima. W., Cruz. F.E.G., 2007. Bacia de Sergipe Alagoas. Boletim de Geociências da Petrobras, 15, 405-415.

Correia Filho, O.J., 2017. Análise de estruturas compressionais na região onshore da Bacia Pernambuco, NE do Brasil-Possíveis influências no potencial petrolífero. MSc. Dissertation. Federal University of Pernambuco.

Dantas, M.V.S., Holz, M., 2020. High-resolution sequence stratigraphy of a cretaceous mixed siliciclastic-carbonate platform sucession of the Sergipe-Alagoas basin, NE Brazil. Facies, 66, 1-17.

Danzelle, J., Riquier, L., Baudin, F., Thomazo, C., Pucéat, E. 2020. Nitrogen and carbon cycle perturbations through the Cenomanian-Turonian oceanic anoxic event 2 (~94 Ma) in the Vocontian Basin (SE France). Palaeogeography, Palaeoclimatology, Palaeoecology,538, 109443.

Dias Brito, D., 1994. Comparação dos carbonatos pelágicos do Cretáceo médio da margem Atlântica brasileira com os do Golfo do México: Novas evidências do Tétis sul-atlantiano. In: Boletim do 3º Simpósio sobre o Cretáceo do Brasil, Abstract, 11-18.

Dunham, R.J., 1962. Classification of Carbonate Rocks According to Depositional Textures. In: Ham, W. E. (Ed.), Classification of Carbonate Rocks. Memoir 1. American Association of Petroleum Geologists, 1-14.

Embry, A.F., Klovan, J.E., 1971. A late Devonian reef tract on Northeastern Banks Island. NWT, Canadian Petroleum Geology Bulletin, 19, 730-781.

Ferreira, J.A., 2009. Variação Organofaciológica da Sequência Cenomaniano-Turoniana da Bacia Pernambuco. MSc. Dissertation, Federal University of Pernambuco.

Grabau, A.W., 1904. On the classification of sedimentary rocks. American Geologist, 33, 228-247.

Haq, B.U., 2014. Cretaceous eustasy revisited. Global and Planetary Change, 113, 44-58.

Hay, W.W., De Conto, R., Wold, C.N., Wilson, K.M., Voigt, S., Schulz, M., Wold-Rossby, A., Dullo, W.C., Ronov, A.B., Balukhovsky, A.N., Soding, E. 1999. Alternative Global Cretaceous Paleogeography. In: Barrera, E. and Johnson, C. (Eds.), The Evolution of Cretaceous Ocean/Climate Systems, Geological Society of America Special Paper, 332, 1-47.

Hazin, P., Taati. F., Van Buchem, F.S.P., 2010. Sequence Stratigraphy of Cenomanian-Turonian carbonate plataforms margins (Sarvak Formation) in the High Zagros. SW Iran: an outcrop reference model for the Arabian Plate. Geological Society of London, Special Publications, 329, 187-218.

Hoefs, J. 2018. Stable Isotope Geochemistry. Springer-Verlag, 8, 460p.

Huber, B., Norris, R.D., MacLeod, K.G., 2002. Deep-sea paleotemperature record of extreme warmth during the Cretaceous, Geology, 30, 123-126.

Jarvis, I., Lignum, J.S., Grocke, D.R., Jenkyns, H.C., Pearce, M.A. 2011. Black shale deposition, atmospheric CO2 drawdown, and cooling during the Cenomanian-Turonian Oceanic Anoxic Event. Paleooceanography, 26, 1-17

Jenkyns, H.C., 1980. Cretaceous anoxic events. from continents to oceans. Journal of the Geological Society of London, 137, 171-188.

Jenkyns, H.C., Dickson, A.J., Ruhl, M., van den Boorn, S.H.J.M. 2017. Basalt-seawater interaction, the plenus cold event, enhanced weathering and geochemical change: deconstructing oceanic anoxic event 2 (Cenomanian–Turonian, late cretaceous). Sedimentology, 64, 16-43

Jenkyns, H. C. 2010. Geochemistry of oceanic anoxic events. Geochemistry, Geophysics, Geosystems, 11, 1-30

Keller, G., Stueben, D., Berner, Z., Adatte, T., 2004. Cenomanian Turonian $\delta^{13}C$, $\delta^{18}O$, sea level and salinity variations at Pueblo, Colorado. Palaeogeography, Palaeoclimatology, Palaeoecology, 211, 19-43.

Kelley, P.A., Mertani, B., Williams, H.H. 1994. Brown shale formation: Paleogene lacustrine source rocks of central Sumatra. In: Katz, B. (ed.). Petroleum Source Rocks. Springer-Verlag, 283-308

Ladant, J-B., Poulsen, C., Fluteau, F., Tabor, C.R., MacLeod, K.G., Martin, E.E., Haynes, S.J., Rostami, M.A. 2020. Paleogeographic controls on the evolution of Late Cretaceous ocean circulation. Climate of the Past, 16, 973-1006.

Lima Filho, M.F., 1998. Análise Estrutural e Estratigráfica da Bacia Pernambuco. PhD. Thesis, University of São Paulo.

Lima Filho, M.F., Pedrosa, F.A, Araújo. I.G., 2019. Reativação cretácica na Zona de Cisalhamento Pernambuco resultados iniciais em dados bioestratigráficos. In: 28 Simpósio de Geologia do Nordeste. Abstract, 1p.

Lima Filho. M.F., Silva Santos. P.R., 2001. Biocronoestratigrafia da Bacia Pernambuco: Implicações paleoambientais e paleogeográficas, Revista Brasileira de Paleontologia, 2, 1-16.

Long, L. E., Sial, A. N., Nekvasil, H., Borba, G. S. 1986. Origin of granite at Cabo de Santo Agostinho, northeast Brazil. Contributions to mineralogy and petrology, 92, 341-350.

Maia, M.F.B., 2012. Revisão da estratigrafia do intervalo Aptiano-Albiano da Bacia de Pernambuco. Nordeste do Brasil. MSc. Dissertation, Federal University of Pernambuco.

Matos, R.M.D. 1999. History of the Northeast Brazilian rift system: Kinematic implications of the break-up between Brazil and West Africa. Geological Society of London, Special Publications, 153, 55-73.

Maury, C.J.O., 1930. Cretáceo da Paraíba do norte. BSc. Monograph, Serviço geológico e mineralógico do Brasil.1-95.

Meyers, P.A., 1994. Preservation of elemental and isotopic source identification of sedimentary organic matter. Chemical Geology, 114, 289-302.

Milani, E.J., Rangel, H.D., Bueno, G.V., Stica. J.M., Winter. W.R., Caixeta. J.M., Pessoa Neto. O.C.P., 2007. Bacias Sedimentares Brasileiras-Cartas Estratigráficas. Boletim de Geociências da Petrobras, 15, 183-205.

Mohriak, W.U., Leroy. S., 2012. Architecture of rifted continental margins and break-up evolution: insights from the South Atlantic. North Atlantic and Red Sea-gulf of Aden conjugate margins. Geological Society of London, 369, 497-535.

Mort, H.P. Jacquat, O., Adatte, T., Steinmann, P., Follmi, K., Mareta. V., Berner, Z., Stuben, Z., 2007. The Cenomanian/Turonian anoxic event at the Bonarelli level in Italy and Spain: enhanced productivity or better preservation ?. Cretaceous Research, 28, 597-612.

Moura, W.A.L., Araújo, I.G. Lúcio, T., Paiva, A.C., Souza Neto, J.A. Lima Filho, M.F. 2020. Folhelhos Negros da Formação Estiva (Cenomaniano Superior-Turoniano) da Bacia Pernambuco: implicações no potencial petrolífero. Anuário do Instituto de Geociências, 43, 35-46.

Mouro, L.D., Rakociński, M., Marynowski, L., Pisarzowska, A., Musabelliu, S., Zatoń, M., Carvalho, M.A., Fernandes, A.C.S., Waichel, B.L. 2017. Benthic anoxia, intermittent photic zone euxinia and elevated productivity during deposition of the Lower Permian, post-glacial fossiliferous black shales of the Paraná Basin, Brazil. Global and Planetary Change, 158, 155-172.

Muniz, G.C.B., Almeida, J.A.C., 1988. Contribuição ao reconhecimento da idade do calcário Ipojuca, Formação Estiva, Bacia do Cabo. In: 35 Congresso Brasileiro de Geologia. Anais, 2371-2374.

Nascimento, G.H. 2018. Estudo geoquímico e geocronológico de novas ocorrências das rochas vulcânicas Albianas e Maastrichtinias da Suite Magmática Ipojuca, bacia Pernambuco. Ph.D. Thesis, Federal University of Pernambuco.

Nascimento, M.A.L. 2003. Geologia. Geoquímica Geocronologia e Petrogênese das Rochas Ígneas Cretácicas da Província Magmática do Cabo e as suas Relações com as Unidades Sedimentares da Bacia de Pernambuco (NE do Brasil). PhD. Thesis, Federal University of Rio Grande do Norte.

Norris, R. D. K. L., Bice, E. A., Magno., Wilson, P. A., 2002. Jiggling the tropical thermostatic the Cretaceous hothouse. Geology, 30, 299-302

Okubo, J., lykawka, R., Warren, L.V., Favoreto, J., Dias-Brito, D., 2015. Depositional, diagenetic, and stratigraphic aspects of Macaé group carbonates (Albian): example from an oilfield from Campos Basin. Brazilian Journal of Geology, 45, 243-258.

Paul, C.R.C., Larnolda, M.A., Mitchell, S.F., Vaziri, M.R., Gorostidi, A., 1999. The CenomanianeTuronian boundary at Eastbourne (Sussex, UK): a proposed European reference section. Palaeogeography, Palaeoclimatology, Palaeoecology, 150, 83-121.

Pérez-Dias, L., Eagles, G., 2017. South Altlantic paleobathimetry since early Cretaceous. Scientific Reports, 7, 1-16.

Poulton, S.W., Henkel, S., März, C., Urquhart, H., Flögel, S., Kasten, S., Damsté, J.S.S., Wagner, T. 2015. A continental-weathering control on orbitally driven redox-nutrient cycling during Cretaceous Oceanic Anoxic Event 2. Geology, 43, 963-966.

Ramírez, J.D.V. 2017. Inferências Paleoambientais na Bacia Pernambuco (Furo IATE 1 LABIO-PE3. Albiano-Maastrichtiano) com base em análise de Palinofácies. MSc. Dissertation, Federal University of Pernambuco.

Regali, M.S.P., Uesugui, N., Santos. A.S., 1974. Palinologia dos sedimentos meso-cenozoicos do Brasil. Boletim Técnico da Petrobras, 17, 263-301.

Riding, R., 2011. Microbialites, stromatolites, and thrombolites. In: Reitner, J. and Thiel V. (Eds.), Encyclopedia of Geobiology. Springer, 635-654.

Riedel, P.R., Lima Filho, M.F., Mort, H.P., 2019. Quimioestratigrafia de Fósforo do testemunho de sondagem 1-LABIO-PE-3 (Furo Iate): Investigação do evento de anoxia oceânica na Bacia Pernambuco. Estudos Geológicos, 29, 120-134.

Ruvalcaba-Baroni, I., Van Helmand, N.A.G.M., Tsandev, I., Middleburg, J.J., Slomp, C.P., 2015. The nitrogen isotope composition of sediments from the proto-North Atlantic during Oceanic Anoxic Event 2. Paleoceanography, 30, 923-937.

Sibley, D.F., Gregg, J.M. 1987. Classification of dolomite rock textures. Journal of Sedimentary Petrology, 57, 967-975.

Schalanger, S.O., Jenkys, H.G., Premoli-Silva, I., 1981. Volcanism and vertical tectonics in the pacific basin related to global cretaceous transgression. Earth and Planetary Science Letters, 52, 435-449.

Schlanger, S.O., Jenkyns, H.C., 1976. Cretaceous oceanic anoxic events: causes and consequences. Geologie en Mijnbouw, 55, 179-184.

Scotese, C.R., and Moore, T.L., 2014a. Atlas of Phanerozoic Ocean Currents and Salinity (Mollweide Projection), Volumes 1-6, PALEOMAP Project PaleoAtlas for ArcGIS, PALEOMAP Project, Evanston, IL.

Scotese, C.R., and Moore, T.L., 2014b. Atlas of Phanerozoic Oceanic Anoxia (Mollweide Projection), Volumes 1-6, PALEOMAP Project PaleoAtlas for ArcGIS, PALEOMAP Project, Evanston, IL.

Sherata, A.A., Fawal, F.M.E., Ito, M., Abdel-Aal, M.H., Sarhan, M.A., 2019. Cenomanian-Turonian depositional history of a post-Gondwana rift sucession in the West Beni Suef Basin, Egypt. Journal of African Earth Science, 150, 783-798.

Sigman, D.M., Granger, J., Fiore, P.J., Lehmann, M.M., Ho, R., Cane, G., van Geen, A. 2005. Coupled nitrogen and oxygen isotope measurements of nitrate along the eastern North Pacific margin: N and O isotopes of nitrate along the North Pacific margin. Global Biogeochemistry Cycles, 19, 1-14.

Silva Filho, A.F., Guimarães, I.P., Ferreira, V.P., Armstrong, R., Sial, A.N., 2010. The Águas Belas pluton, Northeastern Brazil: Evidence on age, emplacement, and magma sources during Gondwana amalgamation. Precambrian Research, 17, 676-687.

Silva Jr., R., Rios-Netto, A. M., Silva, S.C., Valle, B., Borghi, L., Abbots-Queiroz, F., 2020. Middle Cretaceous calcareous nannofossils from the cored well UFRJ-2-LRJ-01-SE, Sergipe-Alagoas Basin, Brazil: New biostratigraphy and paleobiogeographical inferences. Cretaceous Research, 106, 1-12.

Szatmari, P., Milani, E.J., 1999. Microplate rotation in the northeast Brazil during the South Atlantic rifting: analogies with the Sinai microplate. Geology, 27, 1115-1118.

Tesdal, J.E., Galbraith, E.D., Kienast, M. 2013. Nitrogen isotopes in bulk marine sediment: linking seafloor observations with subseafloor records. Biogeosciences, 10,101-118.

Tomé, M.E.T.R., Lima Filho, M.F., Neumann, V.H.M.L., 2006. Análise Estratigráfica do Albiano Turoniano da Bacia Pernambuco: Considerações sobre a Paleogeografia e Geração de Hidrocarbonetos. Geociências, 25, 1-10.

Tsikos, H., Jenkys, H.C., Walsworth-Bell, B., Petrizzo, M.R., Forster, A., Kolonic, S., Erba, E., Premoli-Silva, I., Baas, M., Wagner, T., Sinninghe da msté, J.S., 2004. Carbon-isotope stratigraphic recorded by the Cenomanian-Turonian Oceanic Anoxic Event: correlation and implications based on three localities. Journal of the Geological Society of London, 161, 711-719.

Turgeon, S.C., and Creaser, R.A. (2008), Cretaceous oceanic anoxic event 2 triggered by a massive magmatic episode. Nature, 454, 323–326,

Ulicny, D., Hladikova, J., Attrep Jr., M.J., Stanislav, C., Hradecka, L., Svobodova, M., 1997. Sea level changes and geochemical anomalies across the Cenomanian-Turonian boundary: Pecínov quarry. Bohemia. Palaeogeography, Palaeogeography and Palaeoecology, 132, 265-285.

Valle, B., Dal' Bó, P.F., Mendes, M., Favoreto, J., Rigueti, A.L., Borghi, L., Mendonça, J.O., Silva, M., 2019. The expression of the Oceanic Anoxic Event (OAE-2) in the northeastern of Brazil (Sergipe-Alagoas Basin). Palaeogeography, Palaeoclimatology and Palaeoecology, 529, 12-23.

Zhang, X., Gao, Y., Chen, X., Hu, D., Li, M., Wang, C., Shen, Y. 2019. Nitrogen isotopic composition of sediments from the eastern Tethys during Oceanic Anoxic Event 2. Paleogeography, Paleoclimatology, Paleoecology, 515,123-133.

3.2 Artigo 2

Applying spectral tools in a mixed siliciclastic-carbonate environment: an integrative case study from the Estiva Formation, northeast Brazil

Willian Alexandre Lima de Moura[1,2]*

ORCID: http://orcid.org/0000-0002-1471-3752

Thais Andressa Carrino[1,3]

ORCID: http://orcid.org/0000-0001-8528-5225

Rosa Elvira Correa Pabón[4]

ORCID: https://orcid.org/0000-0002-0635-9095

Mário Ferreira de Lima Filho[1,2,3]

ORCID: https://orcid.org/0000-0002-8523-3457

João Adauto de Souza Neto[1,2,3]

ORCID: http://orcid.org/0000-0002-9870-7113

1 Programa de Pós Graduação em Geociências, PPGEOC, Universidade Federal de Pernambuco: Avenida da Arquitetura s/n, 50740-550, Recife, Brazil.

2 Laboratório de Geologia Sedimentar e Ambiental, LAGESE, Instituto de Petróleo e Energia, LITPEG: Avenida da Arquitetura s/n, 50740-550, Recife, Brazil.

3 Departamento de Geologia, Centro de Tecnologia e Geociências, Universidade Federal de Pernambuco: Avenida da Arquitetura s/n, 50740-550, Recife, Brazil.

4 Instituto Tecnológico Vale: Rua Prof. Paulo Magalhães s/n, 35400-000 Ouro Preto-MG, Brazil.

Corresponding author*: Willian Alexandre Lima de Moura - Email: willian.moura@ufpe.br

HIGHLIGHTS

Reflectance spectral library in the SWIR of Estiva Formation, Pernambuco Basin

Point spectral characterization of dolostones, shales, marl, sandstones and calcite vein

Use of imaging spectroscopy for compositional and textural analysis

ABSTRACT

The aim of this work is to present a case study of the application of reflectance and imaging spectroscopy, integrated with petrographic data from core samples of the late Albian-Turonian carbonate environment from the Pernambuco Basin, northeast Brazil. In order to discuss the main useful application of this technique and their respective limitations in sedimentological and stratigraphical descriptions. Four lithofacies were described, namely: dolostones, shales, marls, and sandstones, as well as late calcite veins, filling the dolostone lithofacies. The point spectral characterization (ASD-FieldSpec), in the SWIR range, allowed the individualization of some lithologies based on the main absorption features, such as dolostones (~2318-2320 nm), shales (~2210 nm), marls (doublet absorption features at ~2210 and 2318-2336 nm) and the calcite vein (2340 nm). The sandstone lithofacies show an absorption feature at 2319 nm due to dolomite cement and at 2209-2220 nm (terrigenous input). The hyperspectral imaging (HySpex data – SWIR-384 camera) corroborated the textural and mineral classification of core samples, including the recognition of late clay filling and microbial mats and the compositional variety among dolomite and marl. The geological, petrographic, and spectral data integration made it possible to determine with a better accuracy a high-resolution description of the studied core samples. The innovative use of reflectance and imaging spectroscopy thus represent a useful tool for sedimentology studies and mineral prospecting.

Keywords: Reflectance spectroscopy; HySpex (SWIR-384) camera, drill core samples, Estiva Formation.

1 INTRODUCTION

Nowadays, carbonate rocks provide 60% of oil production and 40% of gas production in the world (Schulumberger, 2019). Additionally, they can host many mineral deposit types (*e.g.* Mississippi Valley Type; SEDEX, Irish, Volcanogenic Massive Sulfide) (Pirajno 2009; Dill et al., 2010; Gregg et al., 2015), making their study relevant to exploration and industry activities.

In the Brazilian marginal platform, the carbonate rocks host the most important petroleum reservoirs in some sedimentary basins (*e.g.* Santos, Campos, Espírito Santo basins), being also related to the recently discovered Brazilian “pre-salt” reservoir (Mohriak, 2015; Wright and Rodrigues, 2018; Lima and De Ros, 2019). Thus, the study of carbonate rocks has gained increasing economic importance, guiding new detailed geological data acquisition and new and innovative investigation approaches (Ramsey et al., 2002; Landis and Keane, 2010; Kurz et al., 2011; Machado et al., 2015).

Traditional approaches (*e.g.,* petrography, isotopic geochemistry, major and trace element determination) have been used for characterizing carbonate environments, as observed in case studies of Brazilian carbonate deposits (*e.g.* Okubo et al., 2015; Cabral et al., 2019; Lima and De Ros, 2019). On the other hand, examples of unconventional methodology that can be applied to study carbonate environments involve the employment of remote sensing techniques, such as reflectance and imaging spectroscopy, which are already standard and rapid tools used in mineral exploration (*e.g.* Prado et al. 2016; Mathieu et al. 2017; Cloutier et al., 2017; Naleto et al., 2019; Ross et al., 2019; Lypaczewski et al., 2019).

Reflectance spectroscopy is a technique based on the absorption spectroscopic properties due to specific chemical compositions and structural ordering of atoms and molecules (Hunt, 1977; Hunt and Ashley, 1979; Clark, 1999), measuring the reflected light intensity as a function of wavelength in the visible to near-infrared range (VNIR: 350 to 1,000 nm) and shortwave infrared (SWIR: 1,001 to 2,500 nm). Specifically, the absorption features related to minerals are due to transition metals and molecular groups (*e.g.* Fe2+, Fe3+, OH, metal-OH, C-O, S-O), with specific wavelength position, shape, and intensity of the absorptions, which provide a standard spectrum for each mineral (Clark,1999).

Following the evolution of mineral data acquisition technologies, imaging spectroscopy has been arising as a complementary approach to the point spectral analysis provided by reflectance spectroscopy (Coulter et al., 2017). In this case, hyperspectral images obtained from rock samples or outcrops are a reliable and rapid tool for detailed studies of both compositional and textural properties of sedimentary rocks (Greenberger et al. 2015; Martini et al. 2017). For supporting the stratigraphic and sedimentological studies, the application of reflectance and imaging spectroscopy has been poorly exploited, and the studies of Koptíková et al. (2010), Kurz et al. (2011), Zaini et al. (2014), and Jacq et al. (2019) stand out.

Concerning the potential use of spectral analysis for sedimentary environment characterization and with possible economic applications, this work aims at an integrated study of mineralogy, sedimentology and stratigraphy from core samples of Estiva Formation, Pernambuco Basin, northeast Brazil. It introduces a systematic approach of combined use of reflectance and imaging spectroscopy to characterizing the stratigraphy and sedimentology of a carbonate environment in a Brazilian marginal basin, as a case study.

2 GEOLOGICAL SETTING

The Pernambuco Basin, located in northeast Brazil, comprises a Cretaceous basin formed due to the Gondwana break-up (Matos 1999; Bueno 2003). The earliest rifting stages occurred during the late Barremian(?)-Aptian ages (Lima-Filho, 1998; Lima-Filho and Silva-Santos, 2001; Maia, 2012 Figure 1A). The Pernambuco Basin is bounded on the south by the Sergipe-Alagoas basin and on the north by the Paraíba basin, and on the west by the Precambrian Borborema Province (Figure 1). The structural framework is controlled by the Pernambuco Shear Zone, on the north, and the Maragogi-Barreiros High, on the south (Lima-Filho, 1998; Figure 1B).

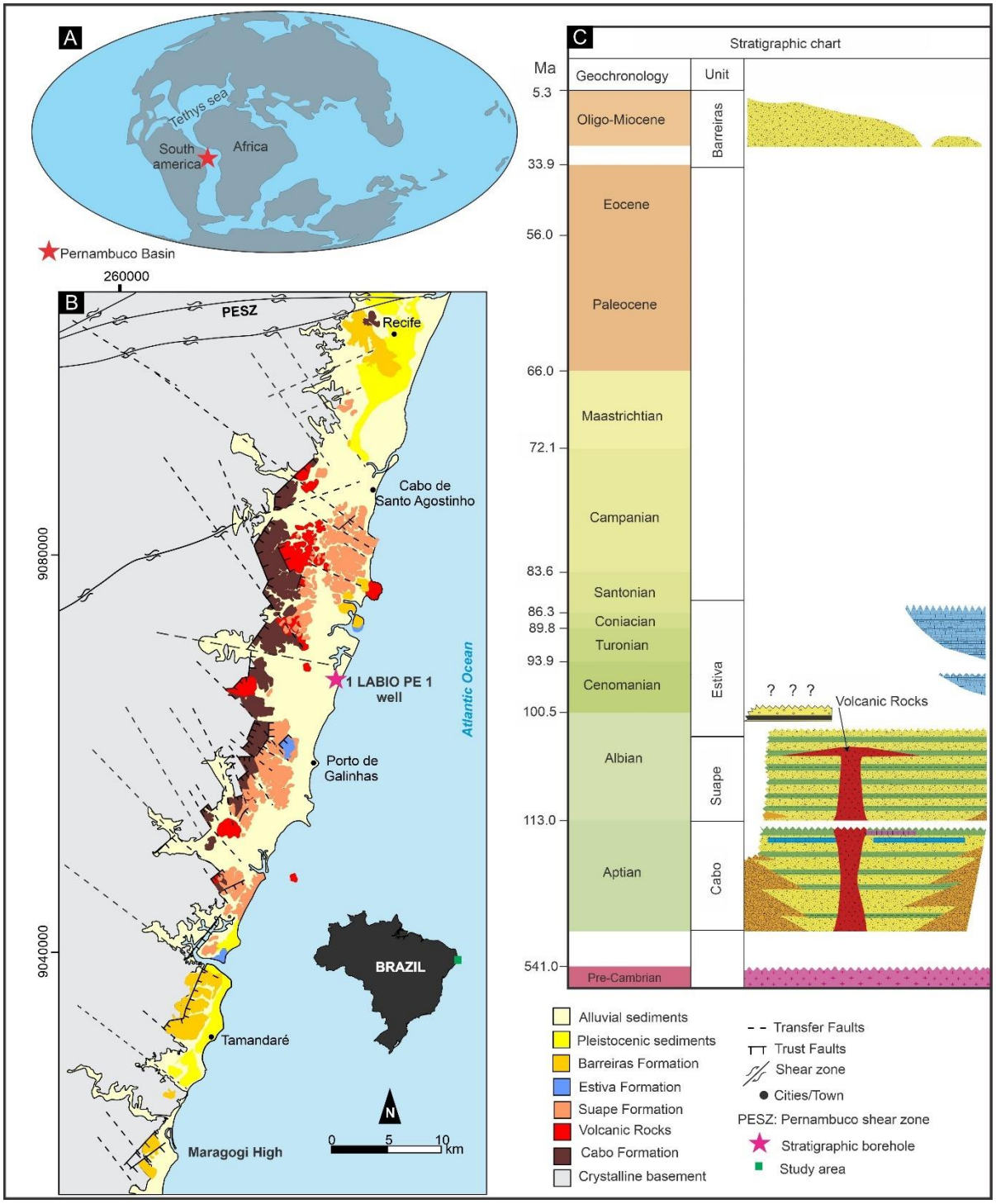

Figure 1. (A) Paleogeographic map reconstruction during the late Albian to Cenomanian ages (http://www.odsn.de/odsn/services/paleomap/paleomap.html). (B) Simplified geological map of Pernambuco Basin (Adapted from Correia Filho, 2017). (C) Stratigraphic chart of the Pernambuco Basin (Compiled from Maia, 2012; Correia Filho, 2017).

2.1 Crystalline basement

The crystalline basement corresponds to supracrustal and granitic rocks from the Pernambuco-Alagoas domain from Borborema Province (Figure 1B, 1C) (Van Schmus et al., 2011; Neves et al., 2015; Silva-Filho et al., 2016). In the Pernambuco-Alagoas domain, Paleoproterozoic orthogneiss occurs related to Belém de São Francisco Complex (Silva-Filho et al., 2016). The paragneisses, quartzites, and schists from Cabrobó Complex were deposited during the Neoproterozoic (maximum depositional age of 650 Ma – U/Pb SHRIMP zircons; Neves 2015), and the metamorphic event occurred during the Gondwana amalgamation (Neves et al., 2015). Alkali-K syenites with shoshonitic affinity related to Ipojuca-Atalaia Batholith, associated with arc-magmatic and collisional events in the Gondwana context, were also recorded (Silva-Filho et al., 2016).

2.2 Pernambuco Basin

The basal sedimentation (Barremian (?) – Aptian ages) of the Pernambuco Basin is represented by the Cabo Formation, composed of orthoconglomerates, sandstones, and mudstones deposited from alluvial fans that migrate to fan delta systems. This unit represents a stage I rift deposited during the Aptian age (123-113 Ma; Maia 2012).

The Suape Formation comprises a stage II rift II, characterized mainly by sandstones and mudstones that record braided-type fluvial deposits during the Albian age (113-102 Ma; Maia, 2012; Barbosa et al., 2014). A contemporaneous volcanic pulse (Ipojuca Magmatic Suite) is dated at 104.4±0.8 to 100.3± 0.6 Ma ($^{40}Ar/^{39}Ar$ sanidine; Nascimento, 2003; Nascimento et al., 2004) and comprises basalts, trachytes, trachybasalts, rhyolites, pyroclastic flows and the youngest granite of Brazil (Cabo Granite, 102 Ma; Long et al., 1986; Nascimento, 2003; Nascimento et al., 2004).

The carbonate-siliciclastic rocks of the Estiva Formation were deposited from late Albian to Turonian ages (Figure 1C; Lima Filho et al., 1998; Tomé et al., 2006; Moura et al. in preparation), during the drift stage and, consequently, indicating the sea opening in the Pernambuco Basin. The Estiva Formation is predominantly composed of dolostones, dolomitized limestones mostly pyritized during diagenesis, marls, sandstones, and black shales marked by Total Organic Carbon (TOC) content with

an average of 2% (Moura et al., 2020). This unit records a transition from an estuarine environment to shallow water conditions (ramp) (Tomé et al., 2006), with sediments deposited into a restricted basin with an intense siliciclastic input (Moura et al. in preparation).

The Oligocene-Miocene sandstones and mudstones represent the Barreiras Formation. The sedimentary deposition is associated with structural highs and, consequently, with tectonic reactivation (Rossetti et al., 2013; Bezerra et al., 2014)

3 MATERIAL AND METHODS

The study was conducted using a drill core (1-LABIO-PE-1) from the Biostratigraphy Project of the Pernambuco Basin (LABIO) collection. The core location is near the centre of the Pernambuco Basin at the Cupe Beach central region (281523E, 9064610N, UTM zone 25S; Figure 1B), and it was drilled in 2014. 1-LABIO-PE- 1 well comprises a complete sequence of the Estiva Formation of about 30 m thickness.

Detailed geological logging was performed, observing the macroscopic aspects, such as colour, texture, lithofacies, and sedimentary structures. In this stage, the classification of Grabau (1904) for carbonate rocks was used. Nineteen thin sections were produced for microscopic analysis using a Zeiss Axio Scope-A1 polarizing microscope from the Laboratory of Sedimentary Petrology of the Federal University of Pernambuco (UFPE), Brazil. The classification of Dunham (1962) and Enbry and Klovan (1979) for carbonate rocks, together with the textural classification of dolostones from Sibbley and Gregg (1987), was used.

Sixty-five representative core samples of all lithofacies were collected for reflectance analyses using the point-measuring ASD-FieldSpec®-4 Standard Resolution spectroradiometer from the Institute of Geosciences of the University of Campinas (UNICAMP), Brazil. The spectroradiometer records spectra in 2,151 channels with wavelengths ranging from the visible to near-infrared region (VNIR: 350 – 1,000 nm) and the shortwave infrared (SWIR: 1,001 – 2,500 nm). The continuum removal (hull quotient) technique was applied for enhancing absorption features and, consequently, improving mineral identification (Clark and Roush, 1984). All reflectance spectra obtained were qualitatively analyzed using the USGS digital spectral library (Kokaly et al., 2017) as a reference, as well as libraries from Hunt

(1977, 1979), Gaffey (1986) and Pontual et al. (2008). Specifically for this case study, the research was driven to the investigation of the reflectance signature of lithofacies using the SWIR data (~1,400-2,500 nm) due to the presence of the main absorption features of clay and carbonate minerals (Hunt 1977, 1979; Gaffey, 1986).

The hyperspectral imaging was obtained in four representative samples using the HySpex (SWIR-384) camera, operating in 930-2500 nm and covering 288 channels. The imaging was performed considering a distance of 30 cm between the sensor and the sample, and a field of view of 16º-17º, resulting in a pixel size of about 1 mm. Data were also acquired on a white standard (Spectralon® plate) for the empirical transformation of the raw data (radiance, L) to the reflectance measures ($\rho = L_{image}/L_{Spectralon}$). The imaging was taken at the Brazilian Institute of Robotics (SENAI-CIMATEC). All data processing was performed using Envi® 5.5, whose license was provided by the Instituto Tecnológico Vale, Brazil.

The Savtizky-Golay filter was applied to reduce the noise typical of hyperspectral images. It is a lowpass filter based on a polynomial least-squares fit that reduces noise and, at the same time, maintains the shape of the reflectance spectra for each pixel (Schafer, 2011). Empirical tests were applied to the HySpex images, with the best results associated with parameters such as the window size of 6 or 8 and the degree of the smoothing polynomial of 2.

After the continuum removal processing was applied to the HySpex bands, a qualitative inspection of pixel spectra was performed for choosing the endmembers (reference spectra) of each lithofacies (*e.g.,* dolostones, marls, clay-rich veinlets). Finally, the Spectral Angle Mapper (SAM) classifier was applied for mineralogical mapping. SAM is based on the comparison of each pixel reflectance spectrum of the image (transformed to vector in a D-dimensional space, where D is the number of bands) with the spectra of the endmembers (also transformed to vectors). The output image shows the similarity of the pixel spectrum with the endmember spectra assigned by angles in radians (Kruse et al. 1993); the smaller the angle is, the more similar a pixel will be to a specific endmember. For the Estiva Formation case study, the use of HySpex bands 212 (2101.82 nm) to 276 (2450.92 nm) showed the best SAM results due to the fact that the most diagnostic spectral absorptions for the target minerals are contained in this wavelength range.

4 RESULTS

Herein, we describe all results obtained.

4.1 Macroscopic aspects

The drill core 1 LABIO PE 1 well intersects around a 45-m-thick layer of recent sediments followed by a 30 m thick layer of the Estiva Formation. Concerning this unit, four lithofacies were identified: dolostones, marls, shales, and sandstones (Figure 2). The dolomite unit shows massive structures, some vuggy-rich levels, and bioturbation structures. The marl unit shows a similar amount of siliciclastic and carbonate fractions, whilst the shale unit is composed of clay minerals and a significant amount of organic matter. The sandstone unit is mainly composed of quartz and feldspar grains, plus dolomite cement.

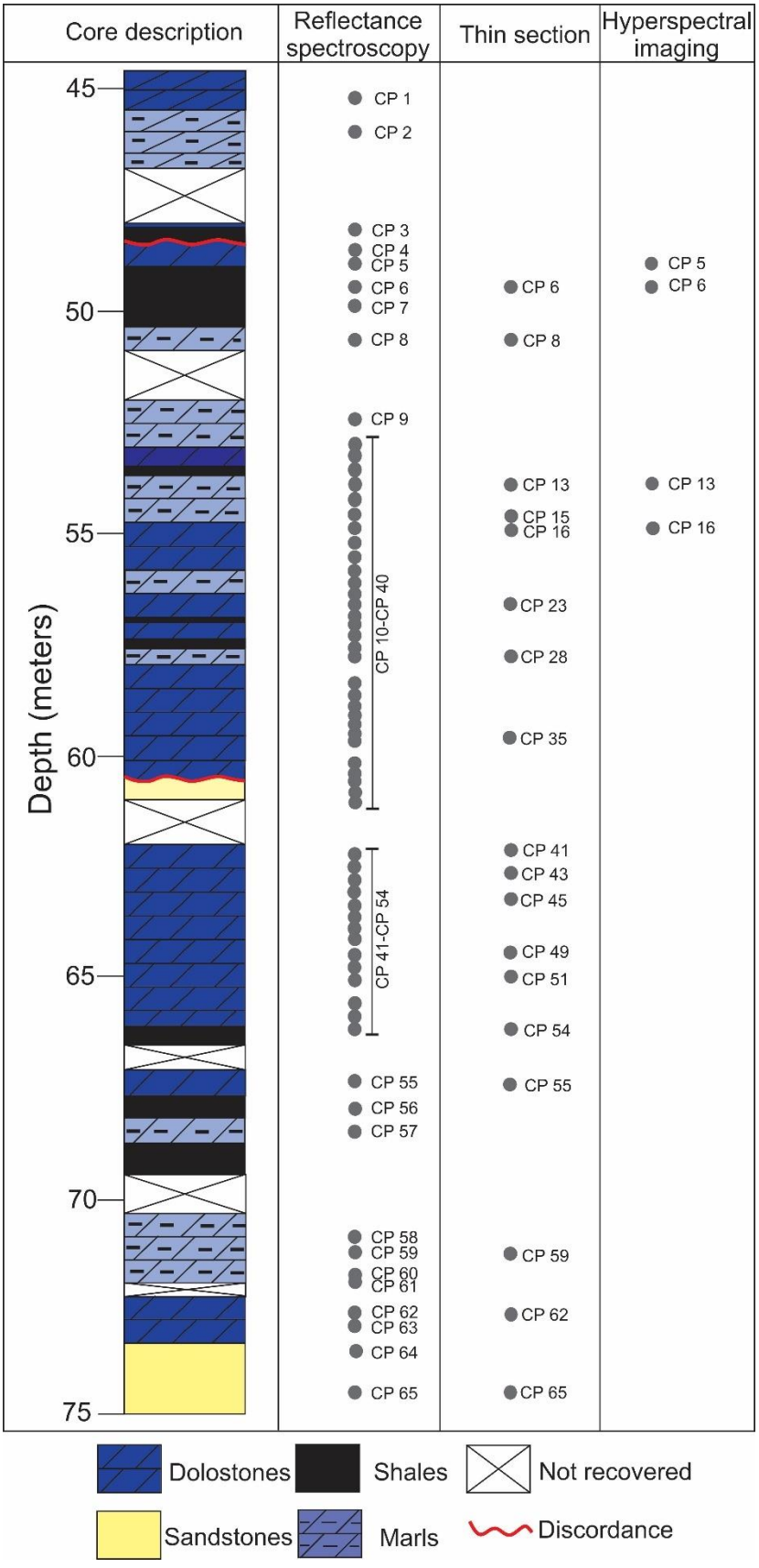
Core description
Reflectance spectroscopy
Thin section
Hyperspectral imaging
Depth (meters)
45
50
55
60
65
70
75
CP 1
CP 2
CP 3
CP 4
CP 5
CP 6
CP 7
CP 8
CP 9
CP 10-CP 40
CP 41-CP 54
CP 55
CP 56
CP 57
CP 58
CP 59
CP 60
CP 61
CP 62
CP 63
CP 64
CP 65
CP 6
CP 8
CP 13
CP 15
CP 16
CP 23
CP 28
CP 35
CP 41
CP 43
CP 45
CP 49
CP 51
CP 54
CP 55
CP 59
CP 62
CP 65
CP 5
CP 6
CP 13
CP 16
Dolostones
Shales
Not recovered
Sandstones
Marls
Discordance

Figure 2. Lithological section of the drill core 1 LABIO PE 1 well (Estiva Formation), and indication of samples analyzed by reflectance spectroscopy, thin sections and hyperspectral imaging.

4.1.1 Dolostones

The dolostones are the most abundant rocks, characterized by microbial mats with horizontally stratified biofilm with wave-like structures with low amplitude of layers (Figure 3A), massive and fluidized dolostone with minor vuggy associated with moldic porosity (Figure 3B), veins filled by clay minerals in massive dolostone (Figure 3C), decimeter-sized karsts (Figure 3D), as well as intense bioturbation recorded by fossil molds. It results in a moldic porosity at the samples (Figures 3E, 3F).

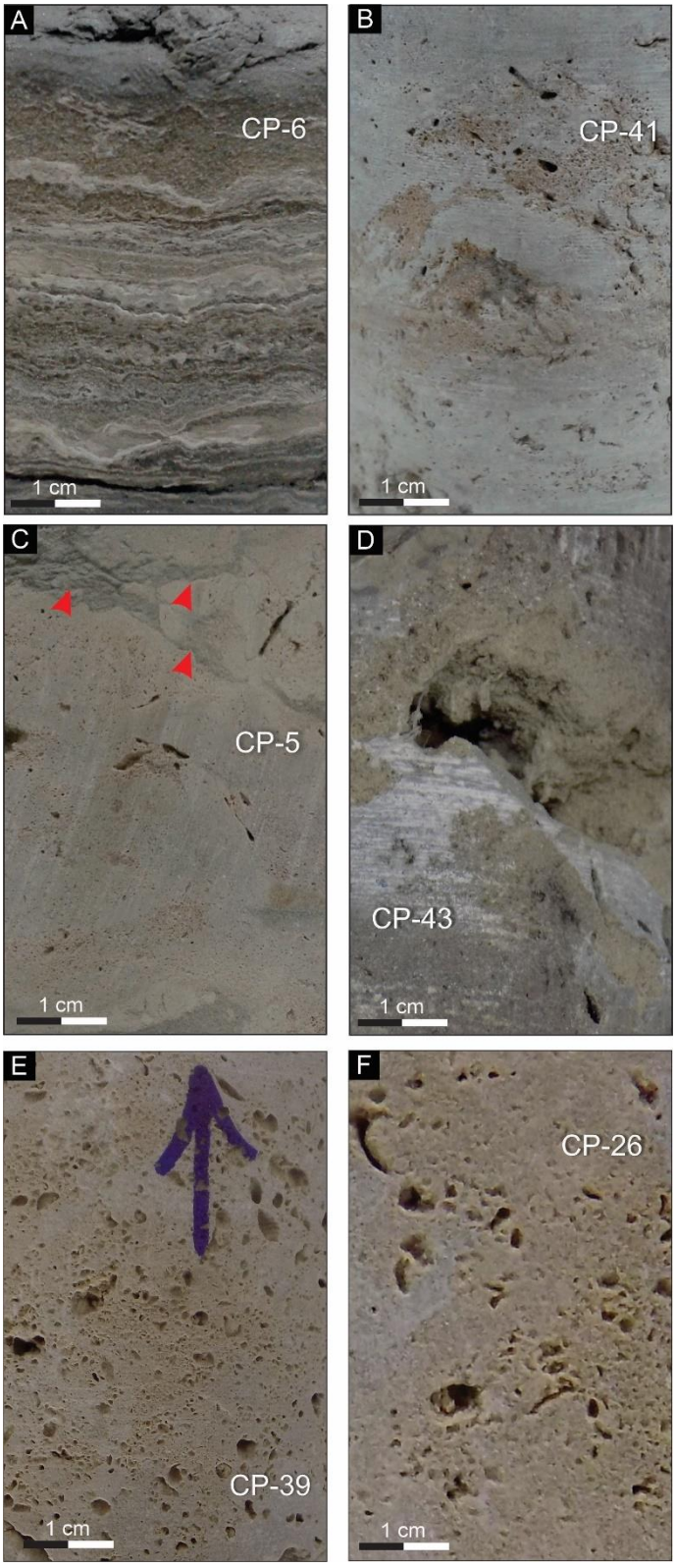

Figure 3. Core samples of 1 LABIO PE 1 well. (A) Microbialite with brown organic-rich layers and microbial mats indicated by white layers. (B) Massive dolostone with moldic porosity and fluidized structures. (C) Clay-rich fracture (red arrows) in a

dolostone. (D) Detail of vuggy in a massive dolostone sample. (E, F) Intense moldic porosity in a dolostone sample.

4.1.2 Shales

Shales are characterized by gray to black clay, quartz, muscovite, and TOC amount varying from 0.2 to 1.8%. Fissility and oxidation surfaces are also observed, as well as wavy-flaser structures marked by asymmetrical intercalations of clay and sand (Figure 4A).

4.1.3 Marls

The representative samples of the marl unit are characterized by a mix of dolomite and clays. There are convolute structures indicating fluidization conditions probably related to post-rift tectonic stresses (Figure 4B) and reworking of dolostones by the high-energy process. In addition, dissolution structures with irregular behavior are observed (Figure 4C). An amount of organic matter is also recorded by TOC data with values ranging from 0.2 to 3.6%.

4.1.4 Sandstones

The representative samples of the sandstone unit are characterized by a framework of quartz grains and dolomite cement. Cross bedding stratification and massive structures are also observed, as well as wood fragments (Figures 4D, 4E). Also, an erosional discordance was also recorded (Figure 4D).

4.1.5 Calcite veins

Calcite veins are poorly represented in the drill core. They are millimeter- to decimeter-sized and fill late fractures in dolostone lithofacies (Figure 4F).

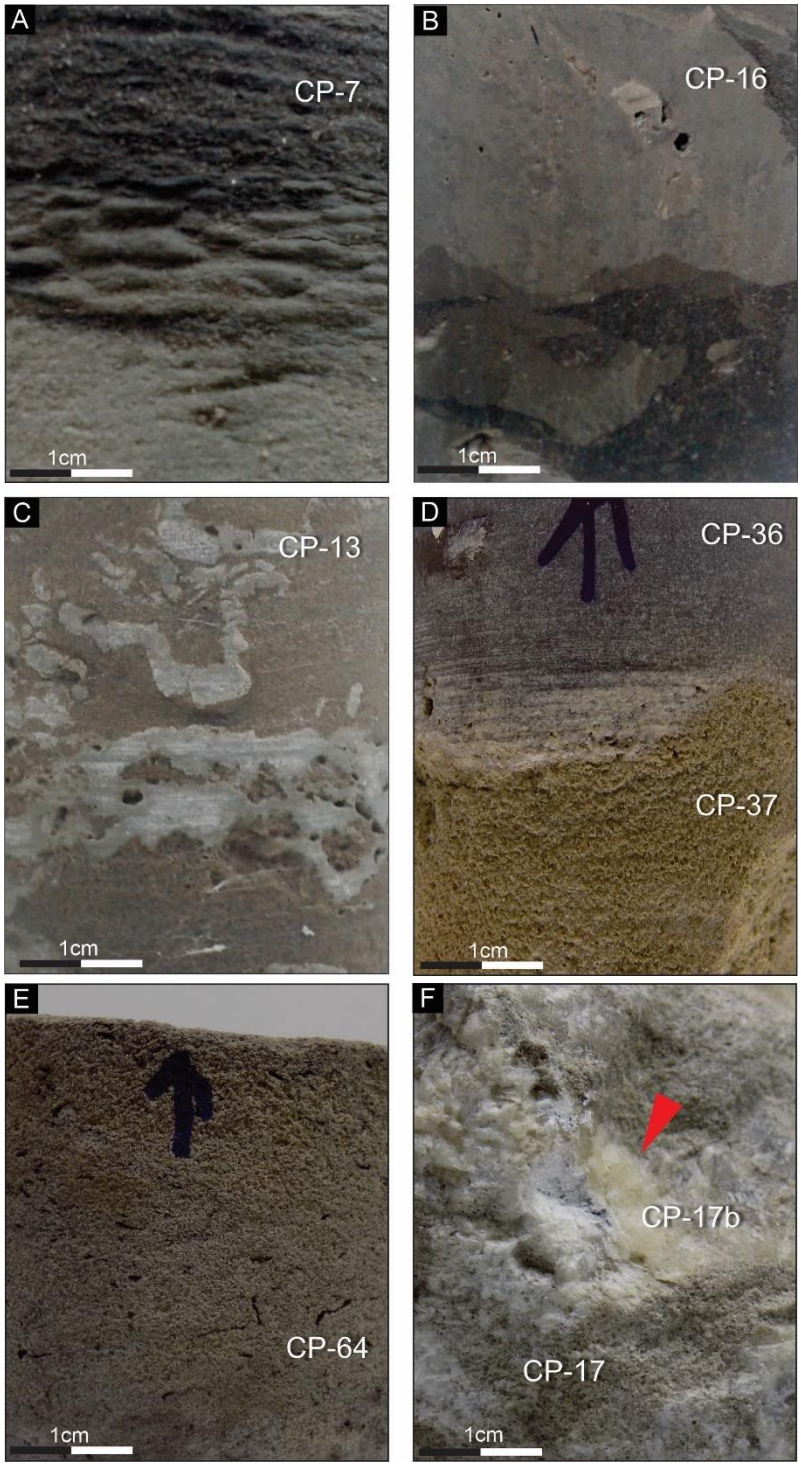

Figure 4. Core samples from 1 LABIO PE 1 well. (A) Grey to black shale. (B) Marl sample with convolute structure. (C) Dissolution structures in a marl sample. (D) Erosional discordance between dolomite-sandstone and dolostone. (E) Fine- to medium-grained sandstone with wood fragments. (F) Detail of a calcite vein (red arrow).

4.2 Petrographic aspects

4.2.1 Dolostones

The dolostones are mainly massive with some decametric-wide karsts and show a siliciclastic input varying between 10 and 40%. In thin sections, samples are intensely dolomitized. Few depositional structures have been preserved, such as peloids, microbial mats, and bioclasts. The peloids are brown to black colored, with an ellipsoidal form constituted by micrite dolomite (Figure 5A). In contrast, the bioclasts occur as molds of bivalves disarticulated shells and gastropods forming karsts (Figure 5B). Microbialites, classified as dolobindstones, were also recognized by wave sheet-like laminae with intercalation of organic matter-rich layers and dolomite-rich layers (Figure 5C). Some siliciclastic grains are well preserved, such as quartz and feldspars (Figure 5D). Furthermore, depositional textures, such as dolowackstones with peloids and siliciclasts, and dolobindstones, are recognized (Figure 5) using the classification of Enbry and Klovan (1979).

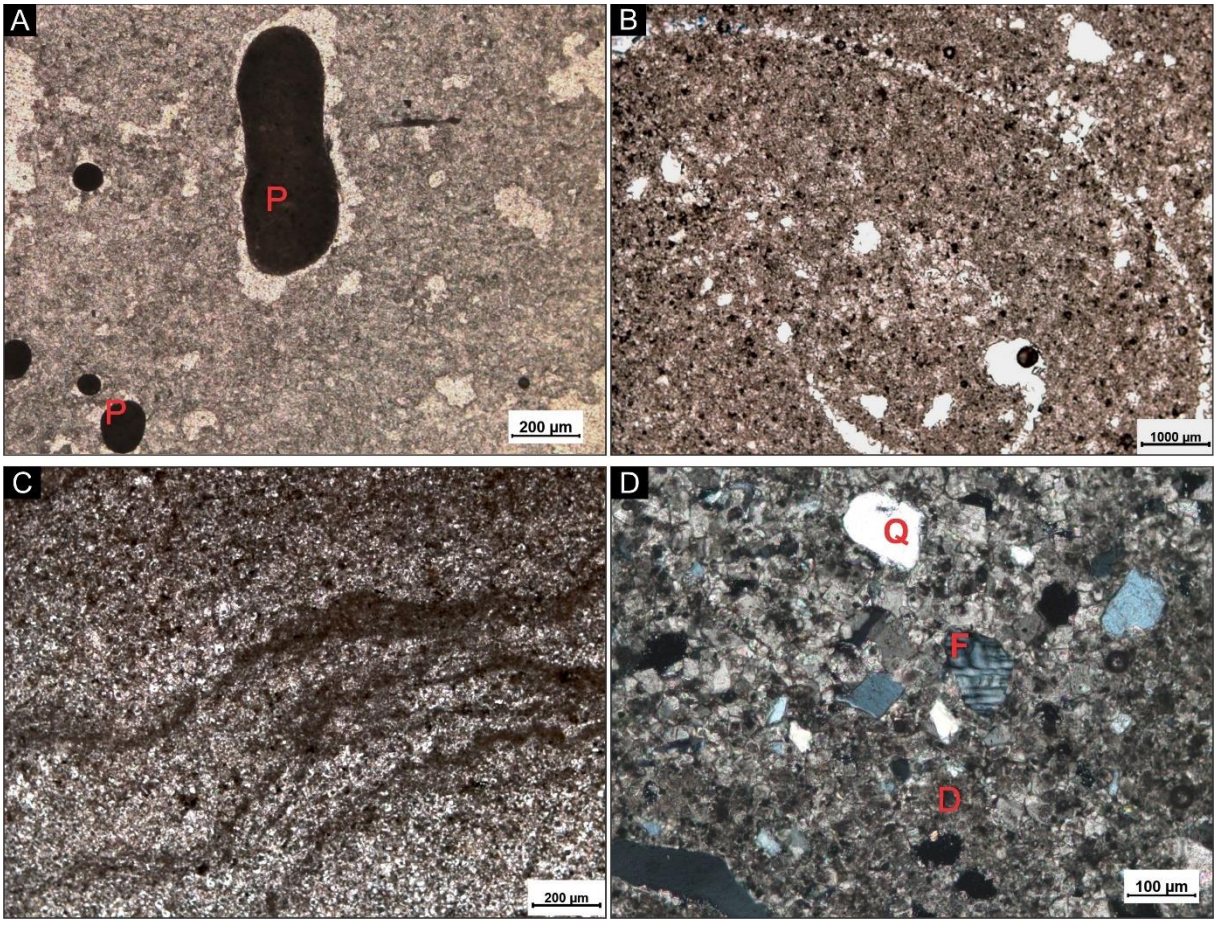

Figure 5. Microphotographs of dolostone samples from the Estiva Formation. (A) Detail of peloid grain in a dolowackstone with peloids sample. (B) Detail of disarticulated bioclastic shells, of bivalve forming moldic porosity in a dolowackstone

sample. (C) Microbial mats in a dolobindstone sample. (D) The occurrence of quartz feldspar grains in the sample of dolowackstone with siliciclasts. P = peloids; F = feldspars; Q = quartz; D = dolomite. Transmitted plane-polarized light images: (A), (B), and (C). Transmitted crossed-polarized light image: (D).

Diagenetic features, such as dolomitization, sulfidation, stylolitization and karstification, constitute the studied samples' main diagenetic aspects (Figure 6). The dolomite morphology has around 10 to 20 μm-width. The crystals are classified as idiomorphic and subidiomorphic, as well as planar-e and planar-s dolomites (Figures 6A, 6B; Sibley and Gregg, 1987). The sulfidation occurs mainly associated with organic matter or cement replacement, stylolites, and calcite veins. Two sulfide generations are recognized: I) xenomorphic crystals (up to 20 μm thickness) with organic matter relicts, as well as cement filling (Figure 6C); II) idiomorphic crystals of pyrite (up to 200 μm width) associated with late calcite vein (Figure 6E) occurring linked (Figure 6F). The stylolitization is recognized by small amplitudes of sutured seams. Vertical and horizontal stylolites are observed, indicating two generations of pressure (Figure 6D).

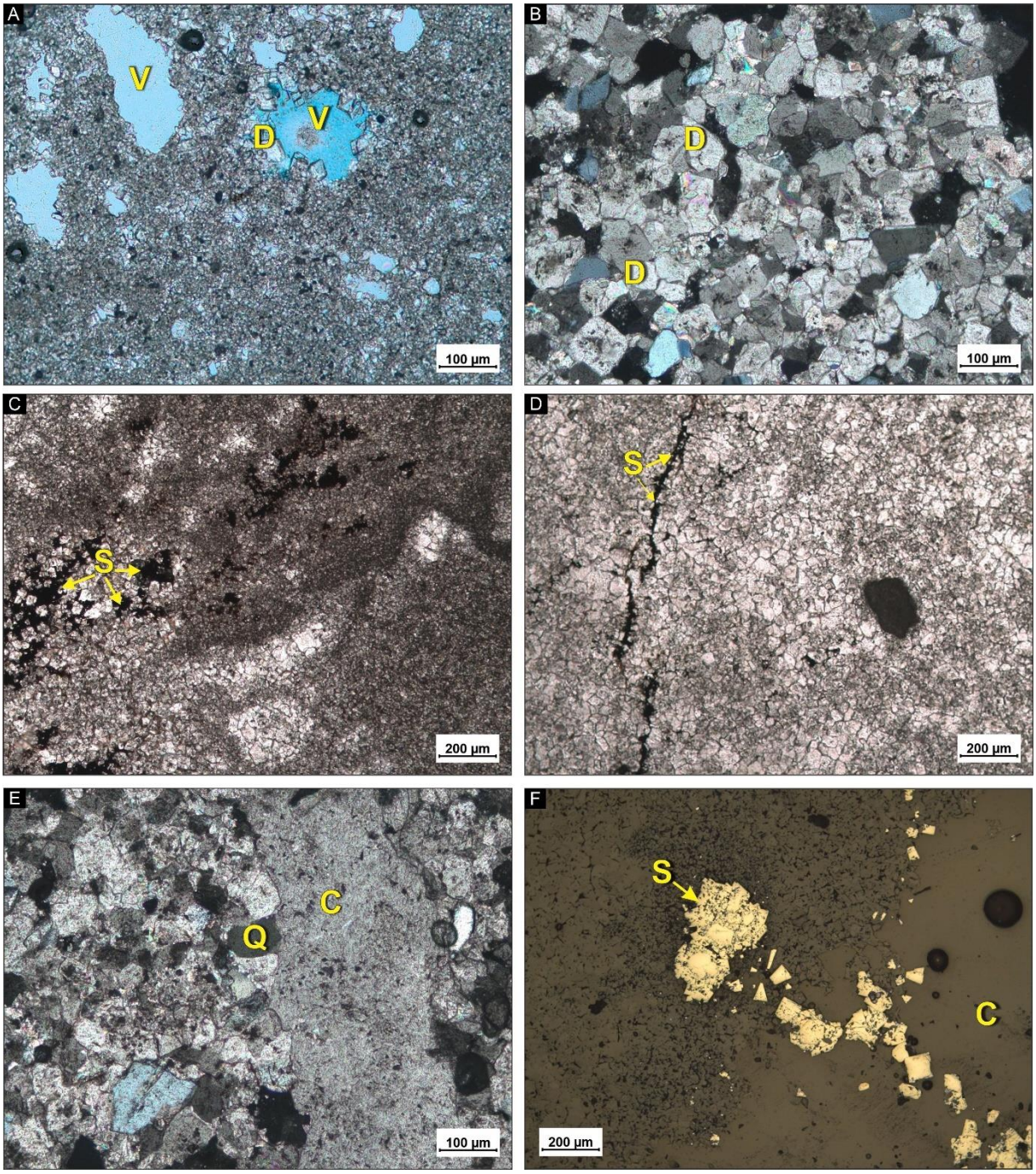

Figure 6. Diagenetic features of Estiva Formation (dolostones). (A) Example of planar-e dolomite associated with karstification. (B) Detail of planar-s dolomite. (C) The occurrence of sulfide cement replacing the organic matter. (D) Detail of vertical small-amplitude stylolite. (E) The occurrence of calcite vein. (F) Idiomorphic to subidiomorphic sulfides associated with late calcite vein. V = vuggy; D = dolomite; C = calcite; S = sulfide; Q = quartz. Transmitted plane-polarized light images: (A), (B), (E). Transmitted crossed-polarized light images: (C), (D). Reflected plane-polarized light image: (F).

4.2.2 Marls

The marl unit is formed by a mixture of clay and dolomite in similar proportions (Figure 7). In the thin section it was not observed depositional structures preseverd at this lithofacies. However, fluidized structures are present due to plastic rheology of the clays (Figure 7).

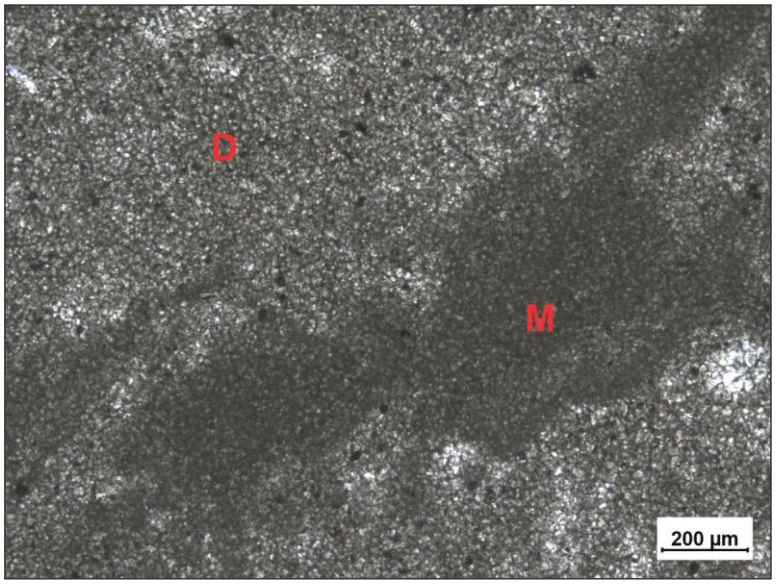

Figure 7. Microphotograph (transmitted plane-polarized light) of marl, showing the detail of brown clay matrix mixed with dolomite. D = dolomite; M = matrix.

4.2.3 Sandstones

The sandstone samples are constituted by quartz (~70%) and feldspar (~20%), as well as dolomite cement (~10%) (Figure 8). Quartz grains are monocrystalline and polycrystalline, poorly to moderate sorted, have subangular morphology, and 70-200 µm width. Feldspar grains is also observed as subangular morphology and it is composed of plagioclase and potassium feldspar (Figure 8).

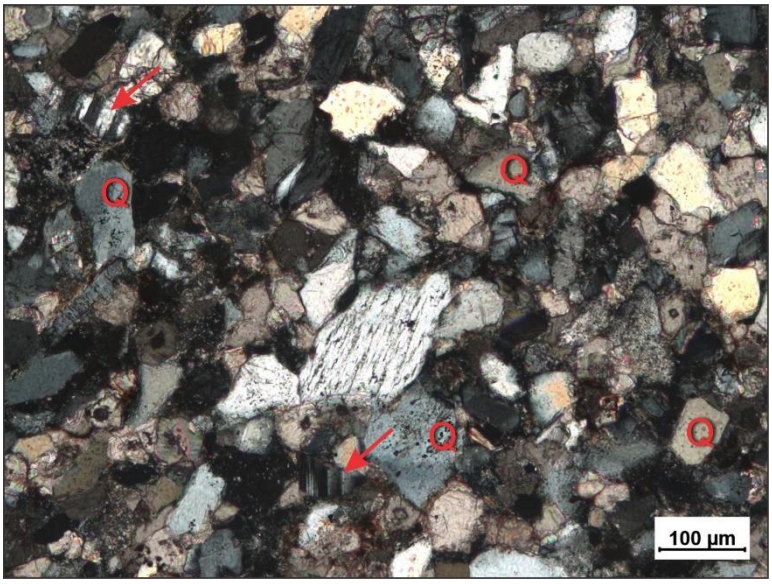

Figure 8. Microphotograph (transmitted crossed-polarized light) of sandstone lithofacies showing sub-angular quartz morphologies and preserved feldspar grains (red arrows). Q = quartz.

4.3 Spectral characterization

4.3.1 Dolostones

This unit is marked by a deep and asymmetrical absorption feature of dolomite at 2318-2320 nm associated with C-O vibrational processes. A secondary absorption at ~2275 nm is also due to C-O bonds (Gaffey, 1986; Pontual et al., 2008). Besides, the reflectance spectra exhibit other absorption features, such as that associated with OH^- and water at ~1410 nm, a subtle absorption at ~2200 nm (Al-OH) (possibly, related to minor content of clay minerals in the samples; Hunt, 1977), and another water absorption at ~1900 nm (Figure 9).

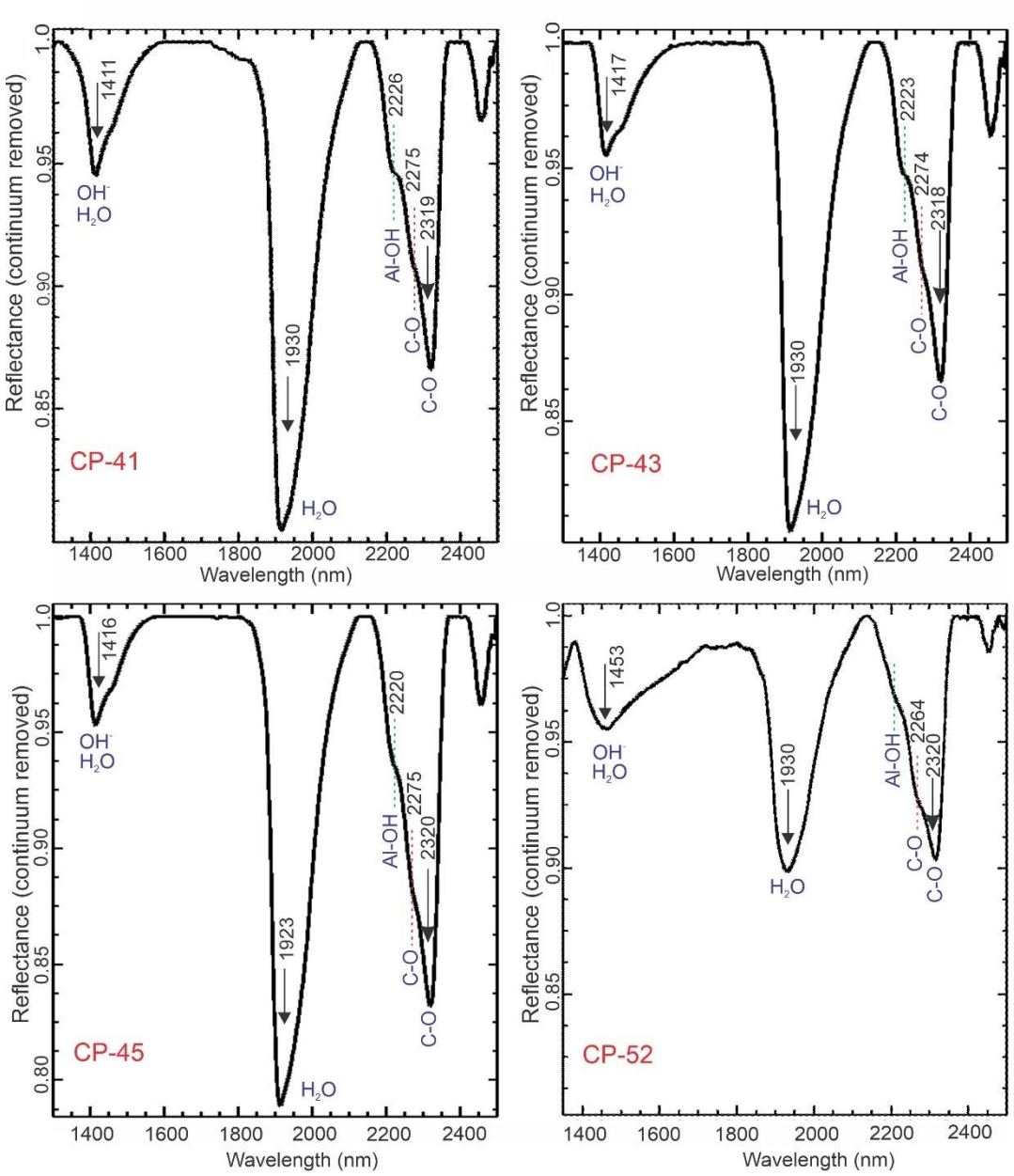

Figure 9. Normalized reflectance spectra of dolostone samples in the SWIR region. Note the deep and asymmetrical absorption feature at ~2320 related to dolomite.

Calcite veins in the dolostone unit show an asymmetrical and deep absorption at 2340 nm, including a subtle feature at 2296 nm, both due to C-O vibration processes (Gaffey, 1986). Moreover, absorption features also occur at 1460 nm (possibly associated with some clay mineral in minor proportion; OH^-), and at 1875, 1990, and 2162 nm, both related to C-O bonds (Gaffey, 1986) (Figure 10).

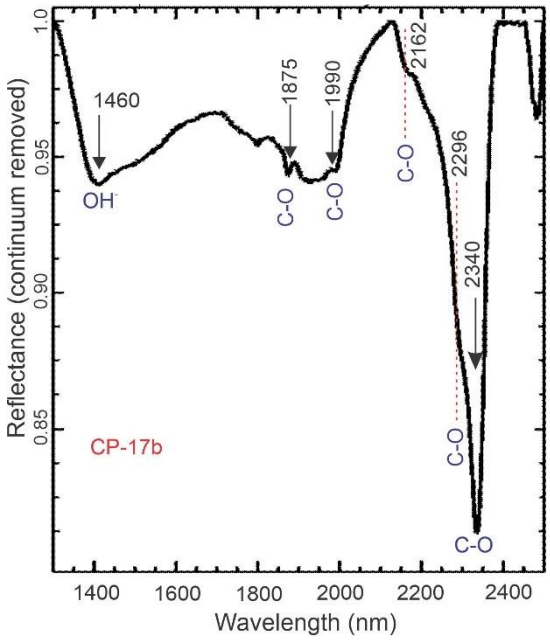

Figure 10. The normalized reflectance spectrum of a calcite vein sample in the SWIR region. Note the deep and asymmetrical absorption feature at 2340 related to calcite.

4.3.2 Shales

This unit exhibits absorption features at 2210 nm arising from Al-OH bonds (Hunt, 1977; Pontual et al., 2008), 1410 nm (OH^- and water), and 1930 nm, the latter derived from the water molecules. This spectral pattern characterizes the presence of the illite and/or smectite mineral group as the main clay minerals associated with low carbonate mineral contribution. Most data (except sample CP-09) show a subtle absorption feature centered at 2326-2340 nm, related to C-O bonds (Figure 11).

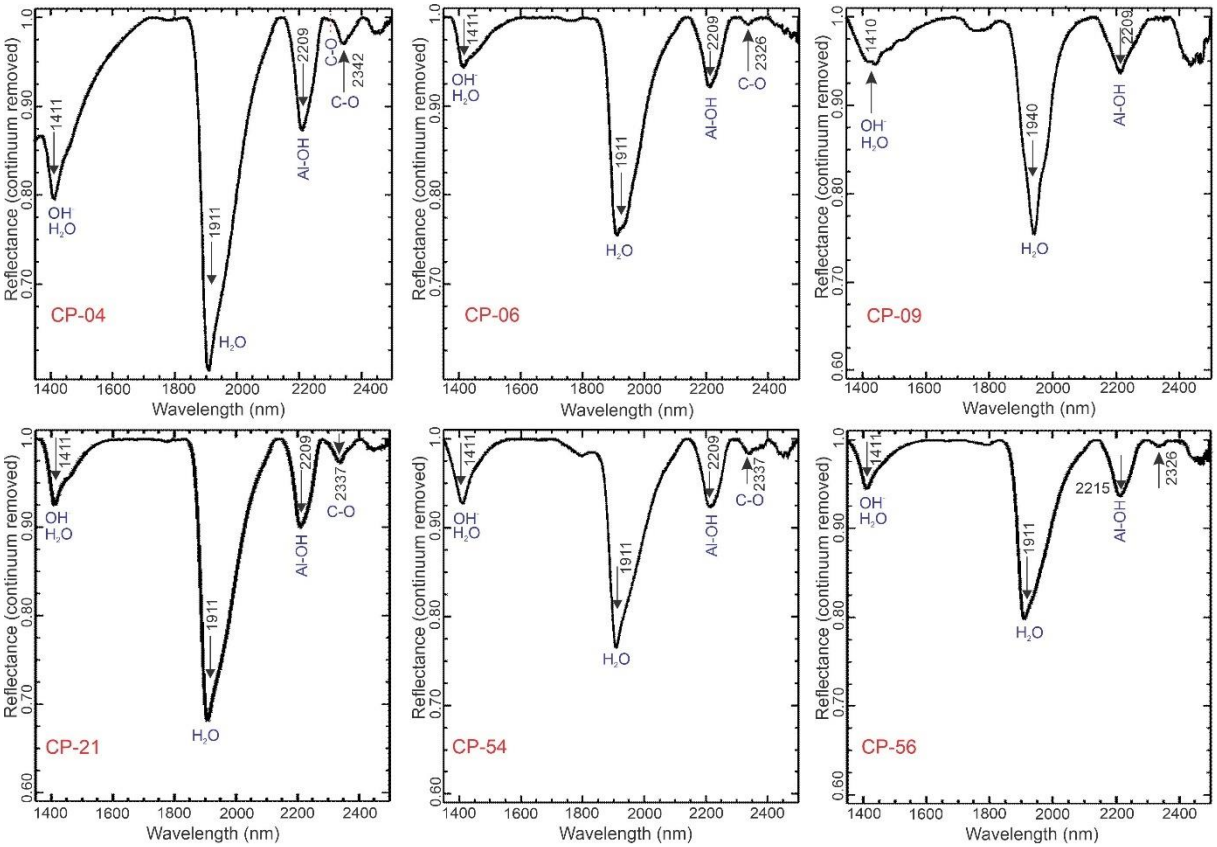

Figure 11. Normalized reflectance spectra of shale samples. Note the main and in-depth absorption feature arising from Al-OH (~2210 nm) in the SWIR region.

4.3.3 Marls

This unit is marked by absorption features of Al-OH (~2210 nm) and C-O bonds (~2318-2336 nm) (Hunt, 1977; Gaffey et al., 1986; Pontual et al., 2008). Some samples show the domain of carbonates related to calcite (*e.g.,* samples CP-14, CP-25, CP-60, characterized by absorptions centered at 2335-2336 nm), whereas samples CP-28, CP-31, and CP-59 are dominated by dolomite, marked by an absorption feature centered at 2318-2326 nm (Figure 12). Absorption features at ~1410 nm (OH^- and water) and at ~1900 nm (water) indicate illite and/or smectite as the main clay mineral phases.

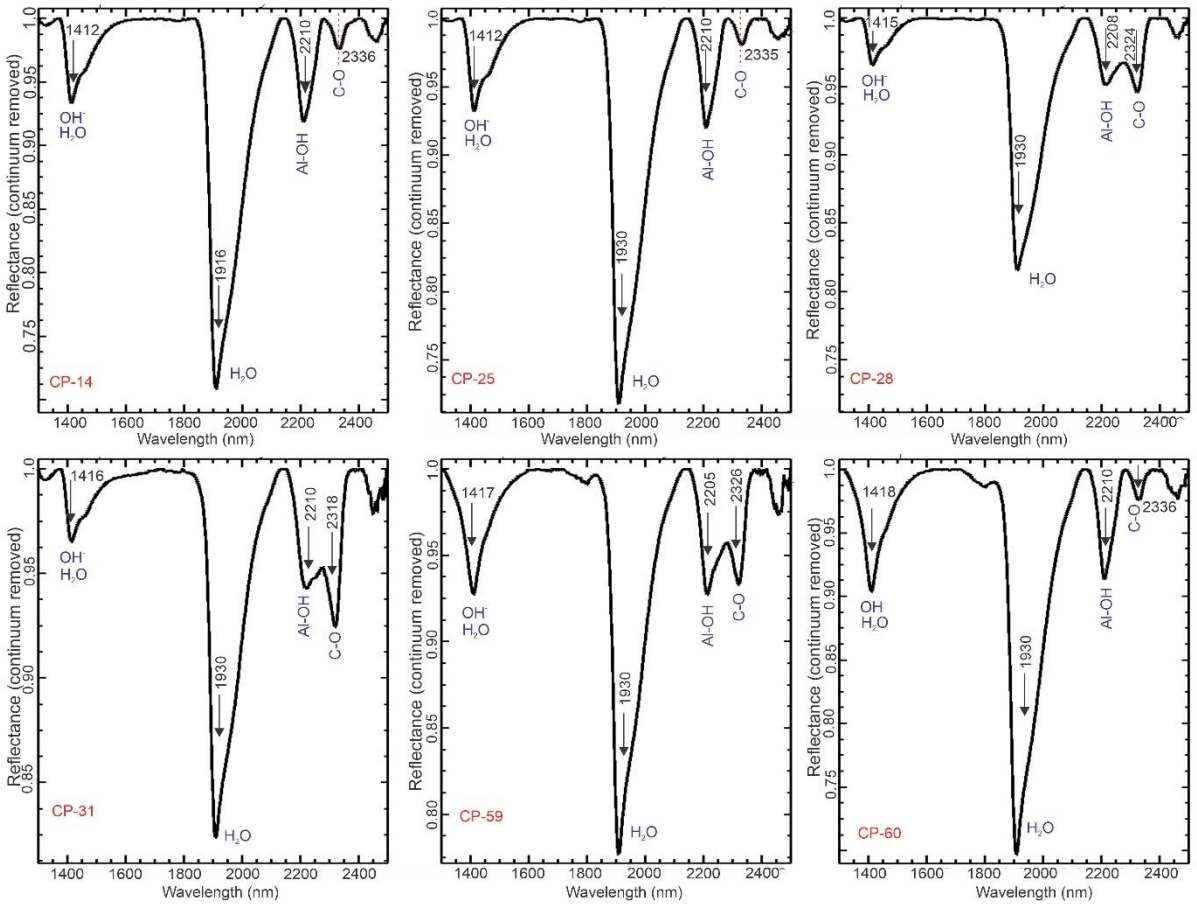

Figure 12. Normalized reflectance spectra of marl samples, showing the main absorption features arising from Al-OH and C-O bonds.

4.3.4 Sandstones

The sandstone samples show main absorption features at ~2209-2220 nm related to clay minerals (terrigenous input), and at 2319 nm associated with dolomite cement. This unit is not spectrally discriminated in relation to the other units here described, due to the presence of diagnostic absorption features of clays and carbonate, and the absence of diagnostic quartz absorption features in the SWIR. (*e.g.,* Rockwell and Hofstra, 2008) (Figure 13).

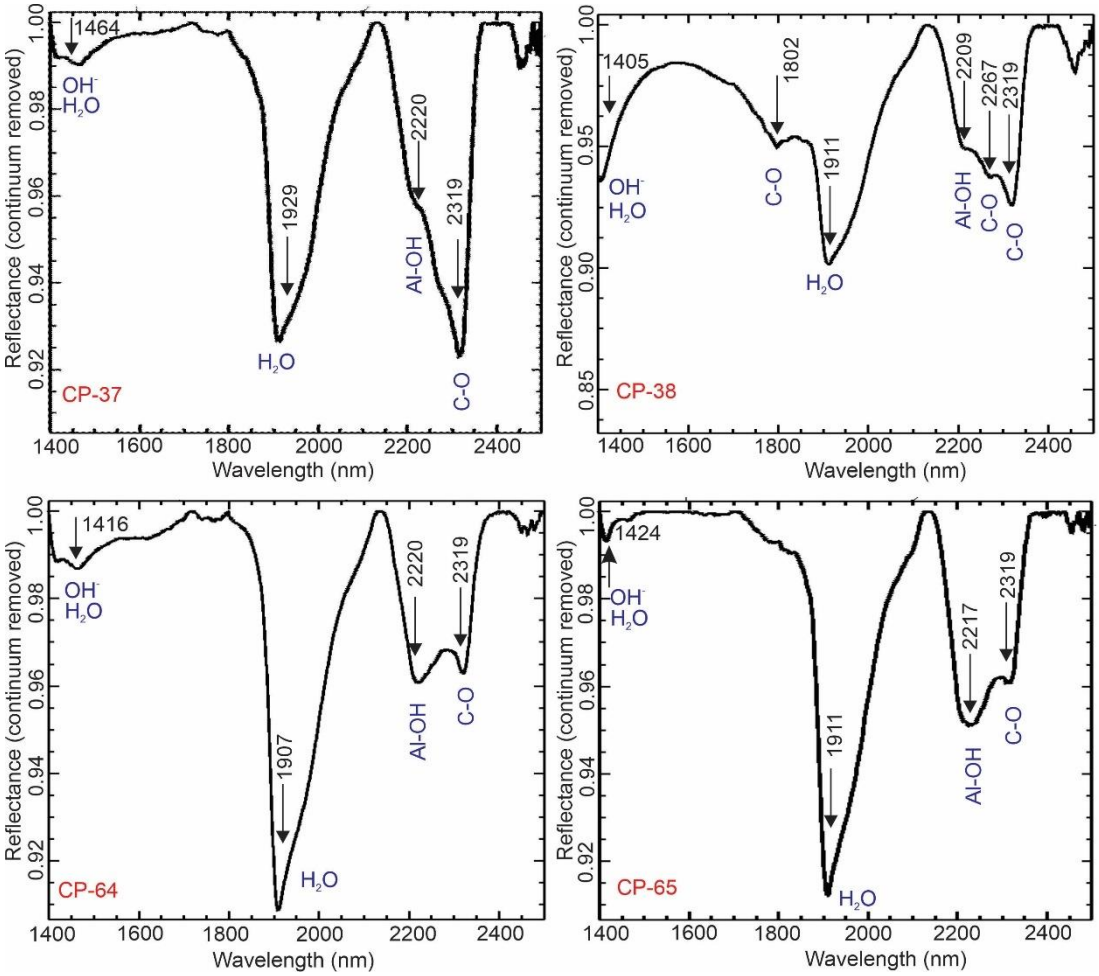

Figure 13. Normalized reflectance spectra of sandstone samples. Note the main absorption features of clay minerals (~2209-2220 nm) and dolomite cement (2319 nm).

4.4 Hyperspectral imaging

Compositional and textural features were also investigated using HySpex SWIR images in four representative samples of the drill core 1 LABIO PE 1 well.

The sample of microbialite (CP-6) is characterized by lighter layers related to microbial mats (Figure 14A), mainly constituted by dolostone, which is marked by deep and asymmetrical absorption feature of dolomite at 2320 nm (Figures 14B, 14C). These microbial mats have a wave-like structure with low amplitude, a texture well mapped by the SAM technique (Figure 14B). The dark layers comprise the substrate of the microbial mats, and they are mainly composed of clay minerals with minor dolomite, forming a marl level. The main absorption features of the marl level are centered at 2212 nm (Al-OH) and 2315 nm (C-O; dolomite) (Figure 14C).

Sample CP-16 is characterized as marl, marked by sub-angular and sub-rounded intraclasts of dolostone (Figure 14D). These intraclasts have the main absorption feature at 2320 nm (C-O), related to dolomite, as shown in the mineral map (Figure 14E) and pixel spectrum (Figure 14F). The dark layers are related to marl levels (Figures 14D, 14E), spectrally marked by absorption features at 2210 nm (Al-OH) and 2336 nm (C-O), which correspond to clay minerals and dolomite-calcite, respectively (Figure 14F). The sample investigated is related to a higher energy environment that ripped up and transported the lithified carbonate.

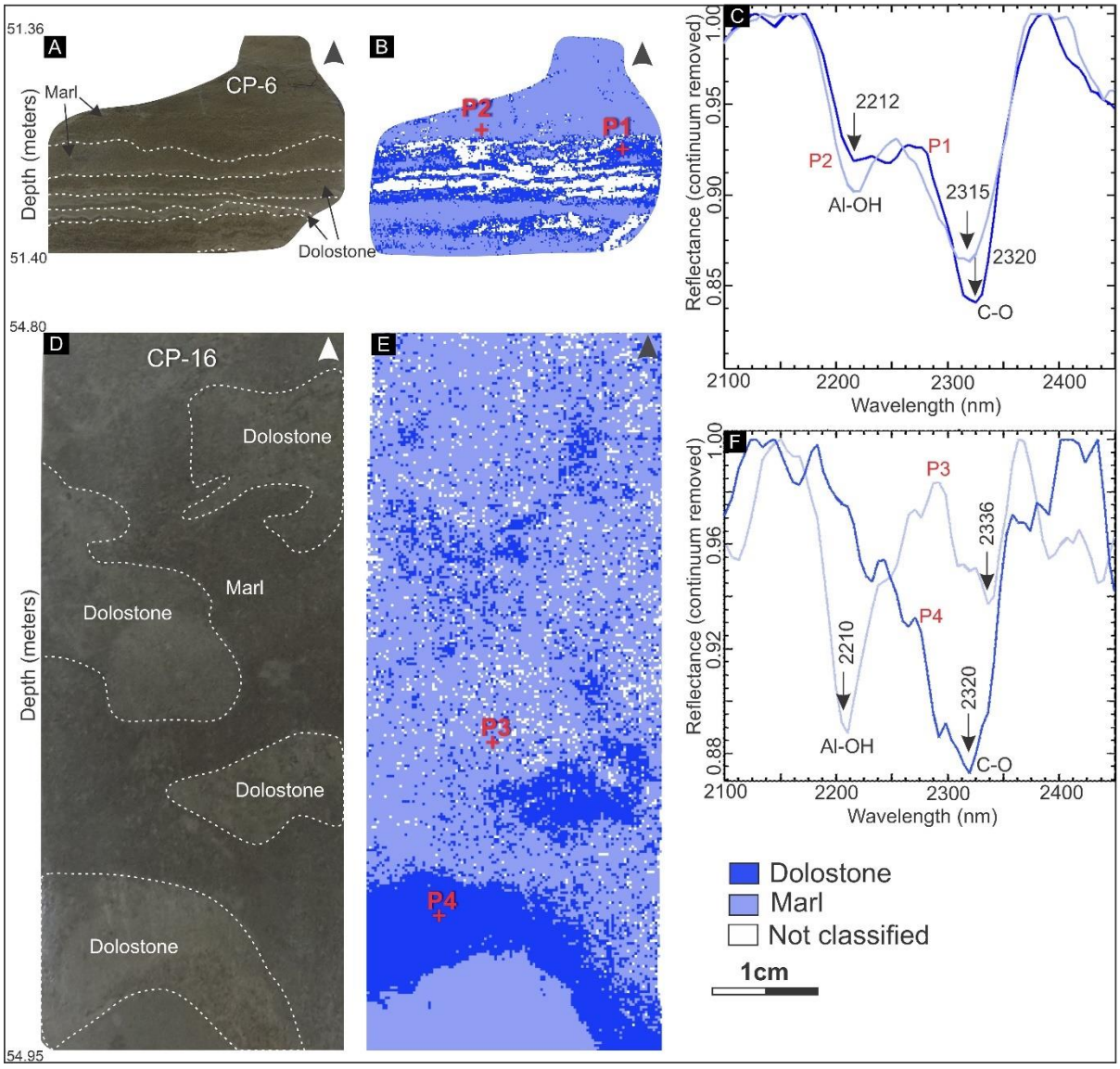

Figure 14. Imaging spectroscopy results. (A) The core of microbialite, (B) its compositional map, and (C) the pixel spectra showing the dolostone and marl responses as the main mineral phases of microbial mats. (D) The core of dolostone

and marl, (E) its compositional map, and (F) the pixel spectra extracted showing dolomite as the dolostone intraclasts' main mineral phase.

Sample CP-5 is composed essentially of beige-colored dolostone (Figure 15A), fractured at the top (~1 mm-sized) and at the base (~2 cm-sized). These fractures are filled by clay minerals, represented by dark levels (Figure 15A), and characterized by a deep absorption feature at 2210 nm (Al-OH), opposite to the dolostone levels that are dominant in the sample (Figure 15B) and marked by an absorption feature at 2325 nm (C-O) (Figure 15C).

Sample CP-13 comprises marl with a tube-like chemical dissolution structure (grayish levels; *cf.* Figure 15D). The chemical dissolution, with up to 1 cm-width (Figure 15D), is associated with diagenetic features and composed of dolostone, as shown in the compositional and textural map (Figure 15E), and in the pixel spectrum, marked by diagnostic absorption feature at 2314 nm (C-O; dolomite) (Figure 15F). This spectral response differs from the spectral signature of marl, which is characterized by absorption features at 2221 (Al-OH) and 2320 nm (C-O) (Figures 15E, 15F).

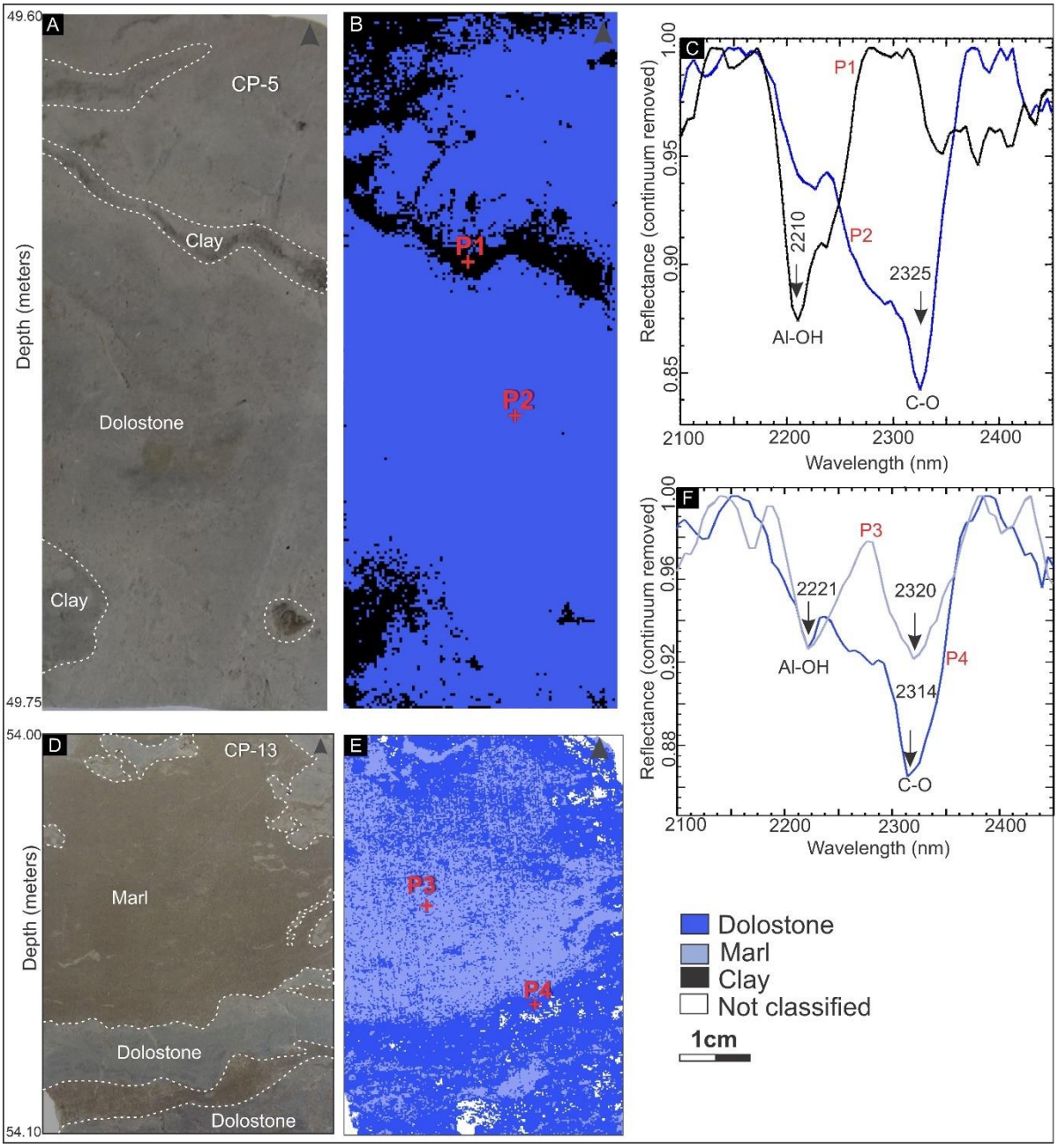

Figure 15. Imaging spectroscopy results. (A) The core of dolostone filled by clay veinlets, (B) its compositional map, and (C) the pixel spectra extracted showing clay minerals mainly in fractures and dolostone dominating the sample. (D) The core of marl with chemical dissolutions, (E) its compositional map, and (F) the pixel spectra indicating the signatures of marl and dolostone, this latter related to the dissolution features.

5 DISCUSSION

5.1 Contribution to lithological and sedimentological studies of the Estiva Formation

The application of reflectance spectroscopy in a mixed siliciclastic-carbonate environment allowed differentiating and individualizing lithological units from a drill core of the Estiva Formation based on its spectral behaviour. In this case study, dolostones (with calcite veins associated), marls, shales, and sandstones were the main lithofacies recognized based on the integrated analysis of reflectance, macroscopic description and petrographic data.

The main spectral range to discriminate different lithofacies comprises the interval between 1400 and 2500 nm due to the occurrence of SWIR-active minerals, such as dolomite, calcite, and clay minerals, such as illite and/or smectite (Hunt, 1977, 1979; Gaffey, 1986; Van der Meer, 1996; Clark, 1999; Pontual et al., 2008). Dolostones are marked mainly by a deep and asymmetrical absorption feature at ~2320 nm (C-O; Figure 9), whilst calcite veins are diagnosed by an absorption feature at ~2340 nm (C-O; Figure 10), shales by a deep absorption feature at ~2210 nm (Al-OH; Figure 11), and marls by two absorptions at ~2210 nm (Al-OH) and ~2320 nm (C-O) (Figure 12). Only the sandstone was not discriminated from the other lithologies (Figure 13) due to the fact that it is not a SWIR-active mineral. For discriminating quartz, a different approach would be necessary, as silica-bearing minerals are spectrally active in the thermal infrared only.

In relation to the use of HySpex (SWIR-384) camera, the imaging spectroscopy also corroborated the point spectral data, introducing the production of compositional and textural maps of core samples for highlighting features such as chemical dissolution, clay veinlets, microbial mats, dolomite intraclasts, and diagenetic features (Figures 14, 15). These aspects can support sedimentological studies involving the systematic analysis of drill cores or outcrops using this spectral-based methodology (Kurz et al., 2011; Kurz et al., 2012; Zaini et al., 2014; Ruitenbeek et al., 2019).

5.2 Contribution to sedimentary studies

The main lithofacies of the Estiva Formation (*e.g.,* dolostone, shales, marls) were discriminated using reflectance and imaging spectroscopy data, generating

direct implications for sedimentological and stratigraphic studies, such as a faster identification of the clay levels and carbonate minerals, as well as mineral association, diagenetic features, dolomitized levels, and textural maps and in macroscale, for example. In addition, the integrative application of spectral characterization may provide a useful approach to field mapping interpretations, detailing of outcrops as well as contributes to a useful and accurate approach in the identification of rock-cutting samples.

In this study, we applied the calculation of the wavelength of the minimum reflectance in all the point spectral data normalized by the continuum removal technique (Clark and Roush, 1984) as a strategy for a rapid determination of the main lithofacies in the drill core 1 LABIO PE 1 (Figure 16). The integrative approach of spectral characterization and stratigraphic features of studied drill-core aiming to improve the lithological characterization of the main lithofacies existing at the 1 LABIO PE 1 well. In addition, some geological inferences may be applied based on the application of the wavelength of the minimum reflectance.

I) The increase of argillosity (a spectral metric related to the normalized reflectance data marked by the wavelength of minimum reflectance at ~2210 nm – Al-OH) could be associated with the variation of continental input inside the basin and low energy conditions during the deposition (Figure 16).

II) The carbonate interval can be identified in the core by samples with a minimum reflectance at ~2320 nm and ~2340 nm (C-O). It may facilitate the identification of dolomitized levels through the adsorption at ~2320 nm and no dolomitized levels through the absorption at 2340 nm. In addition, the deposition of carbonate rocks is related to the retrogradation of the coastline due to an increase of accommodation space and low siliciclastic input (Catuneanu, 2006), being associated with regressive and transgressive conditions (Figure 16). Furthermore, the presence of some siliciclastic grains in the carbonate framework (Figure 5D) also suggests that the Estiva deposition occurred under restricted basin conditions.

III) The presence of sulfide-rich in calcite veins (Figure 6E, F) mainly associated with calcite veins also corroborates the delimitation of transgressive levels (*cf*. Ruffell and Parnell, 1998) as well as may be applied to mining prospecting in carbonate-hosted deposits.

IV) The sandstone and shale levels are related to the decrease of the accommodation space and the increase of siliciclastic input on the basin, which promoted the progradation of coastline during regressive conditions (Catuneanu, 2006). The absence of spectral signature related to quartz in the SWIR range and the domain of spectral responses of dolomite cement or terrigenous input (Figure 13) create an ambiguous spectral response of the sandstone in comparison with marls, shales, and dolostones, and limiting the application of this technique (Figure 16).

V) The wavelength of minimum reflectance of marls oscillates between ~2210 nm (Al-OH) for samples marked by high clay mineral content and ~2320 nm (C-O, for samples with more dolomite content (Figure 16). This oscillation in this lithofacies' spectral signature allows accurate mapping of clay-rich marls (the domain of minimum reflectance at ~2210 nm) and carbonate-rich marls (the domain of minimum reflectance at ~2320 nm).

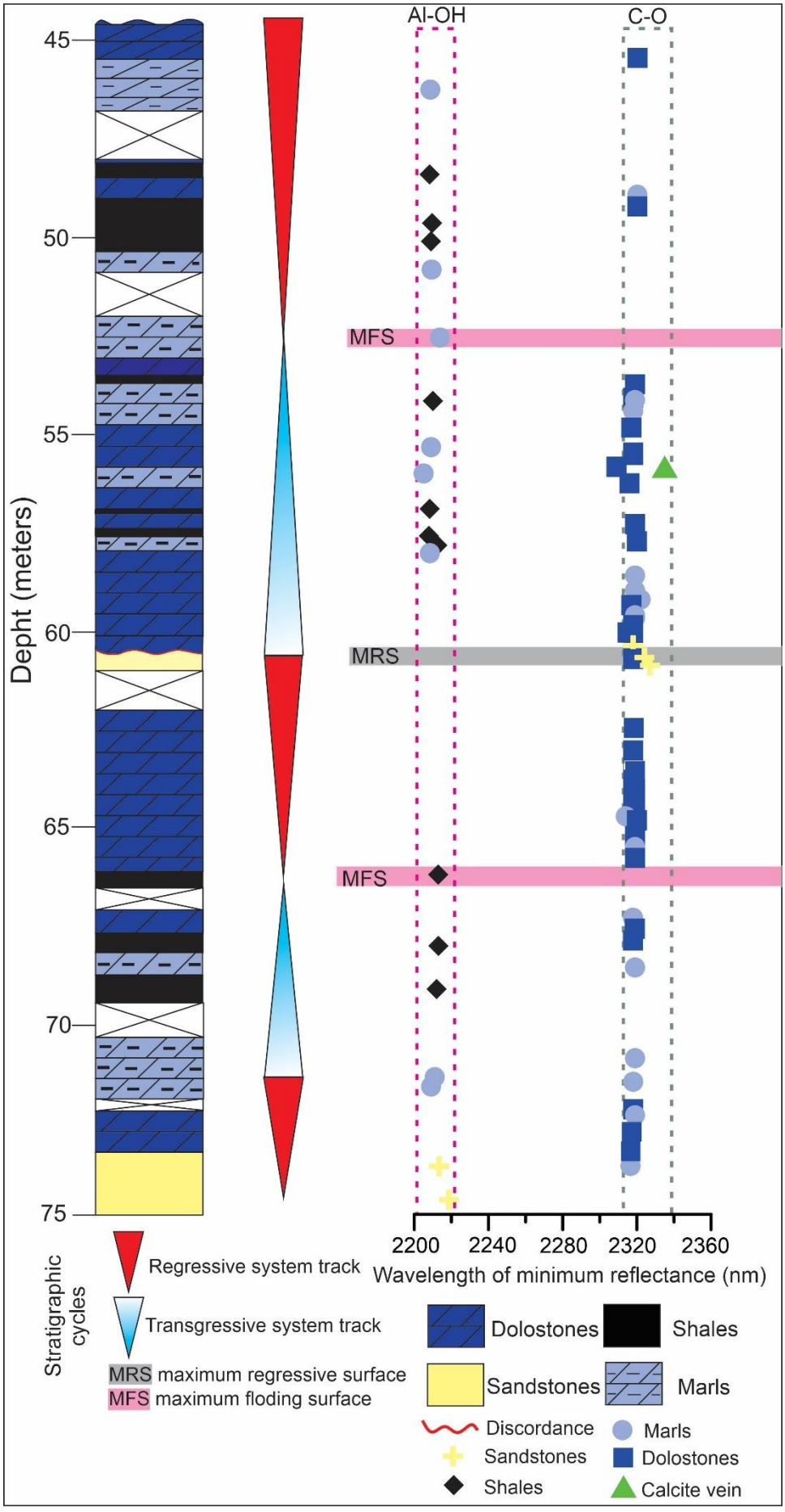
Al-OH
C-O
45
50
55
60
65
70
75
Depht (meters)
MFS
MRS
MFS
2200
2240
2280
2320
2360
Wavelength of minimum reflectance (nm)
Stratigraphic cycles
Regressive system track
Transgressive system track
MRS maximum regressive surface
MFS maximum floding surface
Dolostones
Shales
Sandstones
Marls
Discordance
Sandstones
Shales
Marls
Dolostones
Calcite vein

Figure 16. Lithological section, sequence stratigraphic interpretation and point spectral data integration from the Estiva Formation in the drill core 1 LABIO PE 1.

6 CONCLUSION

The investigation of the Estiva Formation, Pernambuco Basin, by application of spectral technologies combined with conventional geological methodologies (macroscopic description of core samples and petrography), allowed differentiating the lithological composition of dolostone, shales, marls, and calcite using a systematic data acquisition by reflectance spectroscopy. The method employed also includes the wavelength of minimum reflectance (in normalized spectral data) for a rapid determination of lithofacies and argillosity, and this latter is a spectral metric associated with responses of clay minerals linked to the wavelength of minimum reflectance at ~2210 nm (Al-OH).

Besides lithological characterization, the textural analysis, mainly related to diagenetic processes (*e.g.,* chemical dissolution, fracturing), can be detailed by the use of hyperspectral imaging. This increases the potential of spectral analysis for sedimentological studies, as shown with the high accuracy attained in this study by the identification of compositional zonation of marl and dolomite, microbial mats, and clay veinlets.

Concerning mixed siliciclastic-carbonate environments, such as the Estiva Formation, spectral technologies have not been properly exploited to understand sedimentological and stratigraphic aspects in sedimentary basins. However, this study shows that reflectance and imaging spectroscopy could be used in conjunction with conventional methodologies in an innovative approach that will reduce time and/or cost factors, mainly for detailed studies of the carbonate industry.

ACKNOWLEDGMENTS

We would like to thank Petrobras S.A for the LABIO drilling project (401812/2010-3) executed in the Pernambuco Basin. W.A.L.M would like to thank the Conselho Nacional de Desenvolvimento Científico e Tecnológico (CNPq) for his master's scholarship, and J.A.S.N. also thanks the CNPq for his research grant (process number 312.275/2017). We would like to thank the Institute of Geosciences (UNICAMP), especially Prof. Carlos Roberto de Souza Filho and Dr. Rebecca

Scafutto for the assistance in the ASD-FieldSpec data acquisition. We thank the Instituto Brasileiro de Robótica (SENAI-CIMATEC) for the facilities in the use of the HySpex SWIR-384 camera.

REFERENCES

Almeida, F.F.M., Hasui, Y., Brito Neves, B.B., Fuck, R.A. 1981. Brazilian structural provinces: an introduction. Earth Science Reviews, 17, 1-29.

Araújo. I.G., 2014. Litoestratigrafia. Palinologia. Geofísica e Geoquímica do Furo 1-LABIO-PE3. Borda Norte da Bacia de Pernambuco: Implicações estratigráficas. MSc. Dissertation, Federal University of Pernambuco.

Barbosa. J.A., Maia. M.F.B., Lima Filho. M.F., Magalhães. J. R., Correia Filho. O.J., 2014. Seismic stratigraphy of onshore portion of Pernambuco Basin. Evidence of break-up during Albian for the South Atlantic rift in Northeast Brazil. In: AAPG Annual Metting and Exhibition. Houston. Abstracts, 1-5.

Bezerra, F.H.R., Rosseti, D.F., Oliveira, R.G.; Medeiros, W.E., Neves, B.B.B; Balsamo, F. Nogueira, F.C.C., Dantas, E.L.; Andrades, C., Góes, A.M. 2014. Neotectonic reactivation of shear zones and implications for faulting style and geometry in the continental margin of NE Brazil. Tectonophysics, 614, 78-90.

Bueno, G.V. 2003. Diacronismo de Eventos no Rifte Sul-Atlântico. Boletim de Geociências da Petrobrás, 12, 1-28.

Cabral, F.A.A., Silveira, A.C., Ramos, G.M.S., Miranda, T.S., Barbosa, J.A., Neumann, V.H.L.M. 2019. Microfacies and diagenetic evolution of the limestones of the upper part of the Crato Formation, Araripe Basin, northeastern Brazil. Brazilian Journal of Geology, 49, 1-13.

Cainelli, C., Mohriak, W.U. 1999. General evolution of the eastern Brazilian continental margin. The Leading Edge, 18, 800-804

Catuneanu, O. 2006. Principles of sequence stratigraphy. Elsevier. V.1,369p.

Clark, R. N. 1999. Spectroscopy of Rocks and Minerals, and Principles of Spectroscopy, in Manual of Remote Sensing, Remote Sensing for the Earth Sciences, (A.N. Rencz, ed.). John Wiley and Sons, New York, V.3, 3- 58.

Clark, R.N., Roush, T.L., 1984. Reflectance spectroscopy: quantitative analysis techniques for remote sensing applications. Journal of Geophysical Research, 89, 6329–6340.

Cloutier J, Piercey S.J., Lode S., Vande G.M., Copeland, D.A, 2017. Lithostratigraphic and structural reconstruction 1 of the Zn-Pb-Cu-Ag-Au Lemarchant volcanogenic massive sulphide (VMS) deposit, Tally Pond group, central Newfoundland, Canada. Ore Geology Reviews, 84, 154-173

Correia Filho, O.J., 2017. Análise de estruturas compressionais na região onshore da Bacia Pernambuco, NE do Brasil-Possíveis influências no potencial petrolífero. MSc. Dissertation. Federal University of Pernambuco.

Coulter, D.W., Harris, P.D., Wickert, L.M., Zhou, X. 2017. Advances in Spectral Geology and remote sensing: 2008-2017. “Proceedings of Exploration: Sixth Decennial International Conference on Mineral Exploration, 17, 23-50.

Dill, H. 2010. The “chessboard” classification scheme of mineral deposits: Mineralogy and geology from aluminum to zirconium. Ore Geology Reviews, 100, 1-420.

Dunham, R.J., 1962. Classification of Carbonate Rocks According to Depositional Textures. In: Ham, W. E. (Ed.), Classification of Carbonate Rocks. Memoir 1. American Association of Petroleum Geologists, 1-14.

Embry, A.F., Klovan, J.E., 1971. A late Devonian reef tract on Northeastern Banks Island. NWT, Canadian Petroleum Geology Bulletin, **19**, 730-781.

Gaffey, S. J. 1986. Spectral reflectance of carbonate minerals in the visible and near infrared (0.35-2.55 microns); calcite, aragonite, and dolomite. American Mineralogist, 71, 151-162.

Galloway, W.E., 1989. Genetic stratigraphic sequences in basin analysis, I. Architecture and genesis of flooding-surface bounded depositional units. Bulletim of American Association of Petroleum Geologists, 73, 125–142.

Grabau, A.W., 1904. On the classification of sedimentary rocks. American Geologist, 33, 228-247.

Greenberger, R.N., Mustard, J.F., Ehlmann, B.L., Blaney, D.L., Cloutis, E.A., Wilson, J.H., Green, R.O., Fraeman, A.A. 2015. Imaging spectroscopy of geological samples and outcrops: novel insights from microns to meters. GSA Today, 25, 4-10.

Gregg, J.M., Bish, D.L., Kaczmarek, S.E., Machel, H. 2015. Mineralogy, nucleation and growth of dolomite in the laboratory and sedimentary environment: A review. Sedimentology, 62: 1749-1769.

Hecker, C., van Ruitenbeek, F,J.A., van der Werff, H.M.A., Bakker, W.H.,Hewson, R.D., van der Meer, F.D. 2019. Spectral Absorption Feature Analyses for Finding Ore. IEE Geoscience and Remote Sensing Magazine, 19, 51-71.

Hockwell, B.W., Hofstra, A.H. 2008. Identification of quartz and carbonate minerals across northern Nevada using ASTER thermal infrared emissivity data – Implications for geological mapping and mineral resource investigations in well-studied and frontiers areas. Geosphere, 4, 218-246.

Hunt, G.R. 1979. Near infrared (1.3 – 2.4 μm) spectra of alteration minerals – Potential for use in remote sensing. Geophysics, 44, 1974-1986.

Hunt, G.R., 1977. Spectral signatures of particulate minerals in the visible and near infrared. Geophysics, 42, 501-513.

Hunt, G.R., Ashley, R.P. 1979. Spectra of Altered Rocks in the Visible and Near Infrared. Economic Geology, 74, 1613-1629.

Jacq, K., Giguet-Covex, C., Sabatier, P., Perrette, Y., Fanget, B., Coquin, D., Debret, M., Arnaud, F. 2019. High-resolution grain size distribution of sediment core with hyperspectral imaging. Sedimentary Geology, 393, 105536.

Johnson, J.G., Murphy, M.A. 1984. Time-rock model for Siluro-Devonian continental shelf, western United States. Geological Society of America Bulletin, 95, 1349-1359.

Kokaly, R.F., Clark, R.N., Swayze, G.A., Livo, K.E., Hoefen, T.M., Pearson, N.C., Wise, R.A., Benzel, W.M., Lowers, H.A., Driscoll, R.L., and Klein, A.J. 2017. USGS Spectral Library Version 7: U.S. Geological Survey Data Series 1035, 61 p.

Koptíková, L., Bábek, O., Hladil, J., Kalvoda, J., Slavík, L. 2010. Stratigraphic significance and resolution of spectral reflectance logs in Lower Devonian carbonates

of the Barrandian area, Czech Republic; a correlation with magnetic susceptibility and gamma-ray logs. Sedimentary Geology, 225, 83-98.

Kruse, F.A., Lefkoff, A.B., Boardman, J.W., Heidebrecht, K.B., Shapiro, A.T., Barloon, P.J., Goetz, A.F.H. 1993. The Spectral Image Processing System (SIPS) – Interactive Visualization and Analyses of Imaging Spectrometer Data. Remote Sensing Environment, 44, 145-163.

Kurz, T. H., Buckley, S. J., Howell, J. A., Schneider, D. 2011. Integration of panoramic hyperspectral imaging with terrestrial lidar data. The Photogrammetric Record, 26, 212-228.

Kurz, T. H., Dewit, J., Buckley, S. J., Thurmond, J. B., Hunt, D. W., Swennen, R. 2012. Hyperspectral image analysis of different carbonate lithologies (limestone, karst and hydrothermal dolomites): the Pozalagua Quarry case study (Cantabria, North-west Spain). Sedimentology, 59, 623-645.

Landis, E.N., Keane, D.T. 2010. X-ray microtomography. Materials. Characterization, 61, 1305-1316.

Lima Filho, M.F., 1998. Análise Estrutural e Estratigráfica da Bacia Pernambuco. PhD. Thesis, University of São Paulo.

Lima Filho. M.F., Silva Santos. P.R., 2001. Biocronoestratigrafia da Bacia Pernambuco: Implicações paleoambientais e paleogeográficas, Revista Brasileira de Paleontologia, 2, 1-16.

Lima, B. E. M., De Ros, L. F. 2019. Deposition, diagenetic and hydrothermal processes in the Aptian Pre-Salt lacustrine carbonate reservoirs of the northern Campos Basin, offshore Brazil. Sedimentary Geology, 383, 55-81.

Long, L.E., Sial, A.N., Nekvasil, H., Borba, G.S., 1986. Origin of granite at Cabo de Santo Agostinho, Northeast Brazil. Contribution to Mineralogy and Petrology, 92, 341-350.

Lypaczewski, P., Rivard, B., Gaillard, N., Perrouty, S., Piette-Lauzière, N., Bérubé, C. L., Linnen, R. L. 2019. Using hyperspectral imaging to vector towards mineralization at the Canadian Malartic gold deposit, Québec, Canada. Ore Geology Reviews, 111, 102945.

Machado, A.S., Dal Bó, P.F.F., Lima, I., Borghi, L., Lopes, R. 2015. X-ray microtomography characterization of carbonate microbialites from a hypersaline coastal lagoon in the Rio de Janeiro State—Brazil. Nuclear Instruments and Methods in Physics Research Section A: Accelerators, Spectrometers, Detectors and Associated Equipment, 784, 574-580.

Maia, M.F.B., 2012. Revisão da estratigrafia do intervalo Aptiano-Albiano da Bacia de Pernambuco. Nordeste do Brasil. MSc. Dissertation, Federal University of Pernambuco.

Martini, B. A., Harris, A.C., Carey, R., Goodey, N., Honey, F., Tufilli, N., Thomas, M. D. 2017. Automated Hyperspectral Core Imaging–A Revolutionary New Tool for Exploration, Mining and Research. In Proceedings of Exploration, 17, 911-922.

Mathieu, M., Roy, R., Launeau, P., Cathelineau, M., Quirt, D. 2017. Alteration mapping on drill cores using a HySpex SWIR-320m hyperspectral camera:

Application to the exploration of an unconformity-related uranium deposit (Saskatchewan, Canada). Journal of Geochemical Exploration, 172, 71-88.

Matos, R.M.D., 1999. History of the Northeast Brazilian rift system: Kinematic implications of the break-up between Brazil and West Africa. Geological Society of London, Special Publications, 153, 55-73.

Mohriak, W. 2015. Carbonate reservoir plays in the South Atlantic and worldwide analogs. EGUGA, 12825.

Moore, C. H., Wade, W. J. 2013. Carbonate reservoirs: Porosity and diagenesis in a sequence stratigraphic framework. Developments in Sedimentology, V.2, 361p.

Moura, W.A.L., Araújo, I.G. Lúcio, T., Paiva, A.C., Souza Neto, J.A. Lima Filho, M.F. 2020. Folhelhos Negros da Formação Estiva (Cenomaniano Superior-Turoniano) da Bacia Pernambuco: implicações no potencial petrolífero. Anuário do Instituto de Geociências, 43, 35-46.

Naleto, J. L. C., Perrotta, M. M., da Costa, F. G., Souza Filho, C. R. 2019. Point and imaging spectroscopy investigations on the Pedra Branca orogenic gold deposit, Troia Massif, Northeast Brazil: Implications for mineral exploration in amphibolite metamorphic-grade terrains. Ore Geology Reviews, 107, 283-309.

Nascimento, M.A.L., Vasconcelos, P.M., Souza, Z.C., Jardim de Sá, E.F., Carmo, I.O., Thiede, D. 2004. $^{40}Ar/^{39}Ar$ Geochronology of Cabo Magmatic Province, Pernambuco Basin, NE Brazil. Short Papers – IV South American Symposium on Isotope Geology, 624-627.

Nascimento, G.H. 2018. Estudo geoquímico e geocronológico de novas ocorrências das rochas vulcânicas Albianas e Maastrichtinias da Suite Magmática Ipojuca, bacia Pernambuco. Ph.D. Thesis, Federal University of Pernambuco.

Nascimento, M.A.L. 2003. Geologia. Geoquímica Geocronologia e Petrogênese das Rochas Ígneas Cretácicas da Província Magmática do Cabo e as suas Relações com as Unidades Sedimentares da Bacia de Pernambuco (NE do Brasil). PhD. Thesis, Federal University of Rio Grande do Norte.

Neves, S.P., Bruguier, O., Silva, M.R., Mariano, G., Silva Filho, A.J., Teixeira, C.M.L., 2015. From extension to shortening: Dating the onset of the Basiliano orogeny in eastern Borborema Province (NE Brazil). Journal of South American Earth Science, 58, 238-256.

Okubo, J., lykawka, R., Warren, L.V., Favoreto, J., Dias-Brito, D., 2015. Depositional, diagenetic, and stratigraphic aspects of Macaé group carbonates (Albian): example from an oilfield from Campos Basin. Brazilian Journal of Geology, 45, 243-258.

Pirajno, F., 2009. Hydrothermal Processes and Mineral Systems. Springer, Berlin, 1291p.

Pontual, S., Merry, N., and Gamson, P., 2008. Spectral interpretation - field manual. GMEX. Spectral analysis guides for mineral exploration: Victoria, AusSpec International Pty. Ltd., 189 p.

Prado, E. M. G., Silva, A. M., Ducart, D. F., Toledo, C. L. B., de Assis, L. M. 2016. Reflectance spectroradiometry applied to a semi-quantitative analysis of the mineralogy of the News deposit, Carajás Mineral Province, Pará, Brazil. Ore Geology Reviews, 78, 101-119.

Ross, P. S., Bourke, A., Schnitzler, N., Conly, A. 2019. Exploration Vectors from Near Infrared Spectrometry near the McLeod Volcanogenic Massive Sulfide Deposit, Matagami District, Québec. Economic Geology, 114, 613-638.

Rossetti, D.F., Bezerra, F.H.R., Dominguez, J.M.L., 2013. Late Oligocene-Miocene transgressions along the equatorial and eastern margins of Brazil. Earth-Science Reviews, 132, 87-112.

Schafer, R.W. 2011. What is a savitzky-Golay Filter?. IEE Signal Processing Magazine, 11, 111-117

Schulumberger 2019. Carbonate Reservoirs: Overcoming challenging heterogeneity. https://www.slb.com/technical-challenges/carbonates. acessed 09/28/2020

Sibley, D.F., Gregg, J.M. 1987. Classification of dolomite rock textures. Journal of Sedimentary Petrology, 57, 967-975.

Silva Filho, A. F., de Pinho Guimarães, I., Santos, L., Armstrong, R., Van Schmus, W. R., 2016. Geochemistry, U–Pb geochronology, Sm–Nd and O isotopes of ca. 50 Ma long Ediacaran High-K Syn-Collisional Magmatism in the Pernambuco Alagoas Domain, Borborema Province, NE Brazil. Journal of South American Earth Sciences, 68, 134-154.

Tomé, M.E.T.R., Lima Filho, M.F., Neumann, V.H.M.L., 2006. Análise Estratigráfica do Albiano Turoniano da Bacia Pernambuco: Considerações sobre a Paleogeografia e Geração de Hidrocarbonetos. Geociências, 25, 1-10.

Tós, C., Gwózdz, R., Ochtyra, A., 2015. An assessment of remote sensing for the classification of sedimentary rocks-a case study of Tauron Group Quarry, Poland. Environment Enginnering symposium, Srodowisko, 1-10p.

van der Meer, F. 1996. Spectral mixture modelling and spectral stratigraphy in carbonate lithofacies mapping. ISPRS journal of photogrammetry and remote sensing, 51, 150-162.

van Ruitenbeek, F. J. A., van der Werff, H. M. A., Bakker, W. H., van der Meer, F. D., Hein, K. A. A. 2019. Measuring rock microstructure in hyperspectral mineral maps. Remote sensing of environment, 220, 94-109.

van Schmus, W.R., Kozuch, M., Brito Neves, B.B., 2011. Precambrian History of the Zona Transversal of the Borborema Province. Journal of South America Earth Sciences 31, 227-252.

Warren, J. 2000. Dolomite: occurrence, evolution and economically important associations. Earth-science Reviews, 52, 1-81.

Wright, P., Rodriguez, K. 2018. Reinterpreting the South Atlantic pre-salt ‘microbialite’reservoirs: Petrographic, isotopic and seismic evidence for a shallow evaporitic lake depositional model. First Break, 36, 71-77.

Zaini, N., van der Meer, F., van der Werff. 2014. Determination of Carbonate Rock Geochemistry Using Loboratory-Based Hyperspectral Imagery. Remote Sensing, 6, 4149-4172.

5 CONCLUSÕES E RECOMENDAÇÕES

A partir das interpretações apresentadas nesta presente dissertação pode se concluir que: A Formação Estiva foi depositada durante o Albiano superior ao Turoniano (100-88 Ma). Esta unidade compreende calcários intensamente dolomitizados, folhelhos, margas e arenitos calcíferos. São reconhecidos desde fácies predominantemente siliciclásticas (associadas a condições de alta taxa de acumulação) à fácies carbonáticas (relacionadas às condições de baixa taxa de acumulação de sedimentos).

A presença de grãos siliciclásticos em rochas carbonáticas sugere que durante o aporte de terrígenos foi intenso durante a deposição carbonática sugerindo condições de uma bacia faminta. A Formação Estiva foi depositada em ambiente marinho raso, com intenso aporte de sedimentos continentais. Durante a deposição desta unidade estratigráfica foi registrado o evento de anoxia global, ocorrido durante a passagem do Cenomaniano-Turoniano evidenciada pelos valores de isótopos de carbono e nitrogênio. Adicionalmente foram reconhecidas três sequências estratigráficas, limitadas pela SIM (*sensu* Galloway, 1989).

A utilização sistemática de técnicas espectrais permitiu uma melhor resolução e acurácia na identificação de litologias existentes na sondagem estratigráfica utilizada. A aplicação de imageamento hiperspectral em amostras representativas da Formação Estiva, também permitiu uma caracterização textural (estruturas sedimentares) e composicional (mineralogia).

Adicionalmente, sugere-se a aplicação de outras técnicas geoquímicas como isótopos de estrôncio (Sr) cálcio (Ca) e magnésio (Mg) para um melhor aprofundamento sobre o processo de dolomitização ocorrido nesta unidade. Dados isotópicos obtidos por U-Pb em calcita e/ou dolomita podem corroborar com um melhor posicionamento geocronológico. Também se sugere uma investigação acerca de possíveis mineralizações de Pb, Zn e Ag. Uma melhor acurácia das interpretações aqui indicadas pode ser obtida a partir de novas sondagens estratigráficas, principalmente na região offshore da Bacia Pernambuco.

REFERÊNCIAS

(Apenas as referências citadas nos capítulos 1 e 2)

ALHEIROS, M.M.; FERREIRA, M.G.V.X. Considerações Sedimentológicas e Estratigráficas sobre a Formação Cabo, PE. **Revista Brasileira de Geociências**, v. 191, p. 17-24. 1989.

ARAÚJO. I.G. **Litoestratigrafia. Palinologia. Geofísica e Geoquímica do Furo 1-LABIO-PE3. Borda Norte da Bacia de Pernambuco: Implicações estratigráficas**. 2014. Dissertação (Mestrado) – Universidade Federal de Pernambuco, Recife. 2014. 74p.

BARBOSA, J. A., & LIMA FILHO, M. Os domínios da Bacia da Paraíba. *In*: CONGRESSO BRASILEIRO DE P&D EM PETRÓLEO E GÁS. **Anais** […] ABPG: Salvador. V.3, p. 287-306. 2005

BARBOSA, J.A., MAIA. M.F.B., LIMA FILHO, M.F., MAGALHÃES. J. R., CORREIA FILHO. O.J., Seismic stratigraphy of onshore portion of Pernambuco Basin. Evidence of break-up during Albian for the South Atlantic rift in Northeast Brazil. *In:* AAPG ANNUAL MEETING AND EXHIBITION. **Anais** [...] AAPG: Houston. V. 5 p. 1-16. 2014.

BARBOSA, J.A., NEUMANN, V.H., LIMA FILHO, M., SOUZA, E.D., MORAES, M.D. Estratigrafia da faixa costeira Recife-Natal (Bacia da Paraíba e Plataforma de Natal), NE Brasil. **Estudos geológicos,** v.17(2), p. 3-30. 2007

BUARQUE, B.V., BARBOSA, J.A., OLIVEIRA, J.T.C., MAGALHÃES, J.R.G., CORREIA FILHO, O.J. Carbonate Build-ups in the Pernambuco Basin, NE Brazil. **Anais da Academia Brasileira de Ciências**, v.89, p. 841-857. 2017

CAPUTO, M.V., LIMA, E.C. Estratigrafia, idade e correlação do Grupo Serra Grande–bacia do Parnaíba. In: CONGRESSO BRASILEIRO DE GEOLOGIA. **ANAIS** [...] SBG: Belo Horizonte v. 33, p. 740-753. 1984.

CÓRDOBA, V.C., JARDIM DE SÁ, E.F., SOUZA, D., ANTUNES, A.F., CRUZ, L.R. Bacia de Pernambuco-Paraíba. **Boletim de geociências da Petrobrás**, v.*15*(2), p.391-403. 2007.

CORREIA FILHO, O.J. **Análise de estruturas compressionais na região onshore da Bacia Pernambuco, NE do Brasil-Possíveis influências no potencial petrolífero**. 2017. Dissertação (Mestrado) – Universidade Federal de Pernambuco, Recife. 2017. 161p.

COULTER, D.W., HARRIS, P.D., WICKERT, L.M., ZHOU, X. 2017. Advances in Spectral Geology and remote sensing: 2008-2017. *In:* PROCEEDINGS OF EXPLORATION: SIXTH DECENNIAL INTERNATIONAL CONFERENCE ON MINERAL EXPLORATION. **Anais** […] BEG: Toronto, V. 17, p. 23-50.

DUNHAM, R.J., 1962. Classification of Carbonate Rocks According to Depositional Textures. *In*: HAM, W. E. (Ed.), Classification of Carbonate Rocks. Memoir 1. American Association of Petroleum Geologists, 1-14.

EMBRY, A.F., KLOVAN, J.E., A late Devonian reef tract on Northeastern Banks Island. NWT, **Canadian Petroleum Geology Bulletin,** v.19, p. 730-781. 1971.

FERREIRA, J.A., **Variação Organofaciológica da Sequência Cenomaniano-Turoniana da Bacia Pernambuco.** 2009. Dissertação (Mestrado) – Universidade Federal de Pernambuco, Recife, 2009. 172p.

GRABAU, A.W., On the classification of sedimentary rocks. **American Geologist**, v.33, p. 228-247. 1904.

GREGG, J.M., BISH, D.L., KACZMAREK, S.E., MACHEL, H. Mineralogy, nucleation and growth of dolomite in the laboratory and sedimentary environment: A review. **Sedimentology**, v. 62. p.1749-1769. 2015

HARDIE, L.A. Dolomitization; a critical view of some current views. **Journal of Sedimentary Petrology**, v. 57, p. 166-183. 1987

HUNT, G.R., SALISBURY, J.W. Visible and Near Infrared spectra of minerals and rocks: II Carbonates. **Modern Geology**, v.2, p. 23-30. 1971.

JARDIM DE SÁ, E.F., SILVA, F.C.A., FILHO, M. F. L., ANTUNES, A.F., CRUZ, L. R., & ALMEIDA, C.B. (2003). As Relações de Borda da Sequência Rifte na Sub-Bacia de Pernambuco, NE do Brasil. *In:* CONGRESSO BRASILEIRO DE P&D EM PETRÓLEO E GÁS. **Anais** […] ABPG: Rio de Janeiro, V. 2, p. 1-5.

KURZ, T. H., BUCKLEY, S. J., HOWELL, J. A., SCHNEIDER, D. Integration of panoramic hyperspectral imaging with terrestrial lidar data. **The Photogrammetric Record**, v. 26, p. 212-228. 2011.

KURZ, T.H., DEWIT, J., BUCKLEY, S.J., THURMOND, J.B., HUNT, D.W., SWENNEN, R. Hyperspectral image analysis of different carbonate lithologies (limestone, karst and hydrothermal dolomites): the Pozalagua Quarry case study (Cantabria, North-west Spain). **Sedimentology**, v. 59, p. 623-645. 2012.

LAND, L.S. 1980. The isotopic and trace element geochemistry of dolomite: the state of the art. In: Zenger, D.H., Dunham, J.B., Ethington, R.L. (Eds.). Concepts and Models of Dolomitization. SEPM Special Publication, 28: 87–110.

LANG, H.R. Spectral stratigraphy. **Earth and Atmospheric Remote Sensing**, v. 1492, p. 1-8. 1991

LIMA FILHO, M.F. **Análise Estrutural e Estratigráfica da Bacia Pernambuco.** 1998. Tese (Doutorado) –Universidade de São Paulo: São Paulo, 1998. 200p

LIMA FILHO, M.F., & SZATIMARI, P. Ar-Ar geocronology of volcanic rocks of the Cabo magmatic province (CMP)-Pernambuco basin. *In*: **II Simpósio de vulcanismo e ambientes associados**. **Anais** [...] SBG: Belém, v.2 p.65. 2002

LIMA FILHO, M.F., AGOSTINHO, S., ARAÚJO, I.G., PEDROSA, F.A., MELO, R.M., GOMES, C.R., BARROS, C.L. Revisão da Carta Estratigráfica da Bacia Pernambuco baseado em Novos Dados Bioestratigráficos. *In:* 48. CONGRESSO BRASILEIRO DE GEOCIÊNCIAS. **Anais** [...], Porto Alegre: SBG, v.48. 1p. 2017.

LIMA FILHO, M.F., PEDROSA, F.A, ARAÚJO. I.G.. Reativação cretácica na Zona de Cisalhamento Pernambuco resultados iniciais em dados bioestratigráficos. *In:* **28 Simpósio de Geologia do Nordeste**. Atas [...] SBG: Aracaju , v.28, p.96. 2019

LIMA FILHO, M.F., SILVA SANTOS. P.R. Biocronoestratigrafia da Bacia Pernambuco: Implicações paleoambientais e paleogeográficas, **Revista Brasileira de Paleontologia**, v.2, p. 1-16. 2001

LONG, L. E., SIAL, A. N., NEKVASIL, H., BORBA, G. S. Origin of granite at Cabo de Santo Agostinho, northeast Brazil. **Contributions to mineralogy and petrology**, V.*92*(3), p.341-350. 1986.

MABESOONE, J.M.; NEUMANN, V.H.L.M (Ed.). **Cyclic development of sedimentary basins**. Elsevier, 2005. 516p.

MACHEL, H.G. 2004. Concepts and models of dolomitization- a critical reappraisal. In: Braithwaite C.J.R., Rizzi, G., Darke, G. (Eds.). The geometry and petrogenesis of dolomite hydrocarbon reservoirs. Geological Society of London Speciall Publications, 235: 7-63.

MAIA, M.F.B., 2012. **Revisão da estratigrafia do intervalo Aptiano-Albiano da Bacia de Pernambuco. Nordeste do Brasil**. Dissertação (Mestrado) - Universidade Federal de Pernambuco, Recife, 2012. 226p

MATOS, R.M.D. History of the Northeast Brazilian rift system: Kinematic implications of the break-up between Brazil and West Africa. **Geological Society of London, Special Publications**, v.153, p. 55-73. 1999

MORAIS, D.F.M. **Sismoestratigrafia do Cretáceo Superior/Neógeno nas bacias de Pernambuco e Paraíba, NE do Brasil**. 2008. Dissertação (Mestrado), Universidade Federal de Pernambuco, Recife, 2008. 79p.

MOULIN, M., ASLANIAN, D., UNTERNEHR, P. 2010. A new started point for the South Equatorial Altlantic Ocean. **Earth-Science Reviews**, v. 98, p.1-37. 2010.

MOURA, W.A.L., ARAÚJO, I.G. LÚCIO, T., PAIVA, A.C., SOUZA NETO, J.A. LIMA FILHO, M.F. Folhelhos Negros da Formação Estiva (Cenomaniano Superior-Turoniano) da Bacia Pernambuco: implicações no potencial petrolífero. **Anuário do Instituto de Geociências**, v.43, p.35-46. 2020

NASCIMENTO, G.H. 2018. **Estudo geoquímico e geocronológico de novas ocorrências das rochas vulcânicas Albianas e Maastrichtinias da Suite Magmática Ipojuca, bacia Pernambuco**. Tese (Doutorado) - Universidade Federal de Pernambuco, Recife, 2018. 124p

NASCIMENTO, M.A.L. 2003. **Geologia. Geoquímica Geocronologia e Petrogênese das Rochas Ígneas Cretácicas da Província Magmática do Cabo e as suas Relações com as Unidades Sedimentares da Bacia de Pernambuco (NE do Brasil)**. 2003. Tese (Doutorado) - Universidade Federal do Rio Grande do Norte, Natal, 2003. 264p.

NASCIMENTO, M.A.L., VASCONCELOS, P.M., SOUZA, Z.S., JARDIM DE SÁ, E.F., CARMO, I.O., THIEDE, D. ^{40}Ar-^{39}Ar geochronology of the Cabo Magmatic Province, Pernambuco Basin, NE Brazil. *In*: SOUTH AMERICAN SYMPOSIUM ON ISOTOPE GEOLOGY, **Anais** […] V.4, p. 624-628. 2004

OLIVEIRA, A.I. & LEONARDOS, O.H. Geologia do Brasil. Rio de Janeiro, In: Serviço de Informação Agricola, v. 2, 1943. 813p.

OLIVEIRA, Jefferson Tavares Cruz Oliveira. **Avaliação integrada de dados geofísicos da transição Crustal (continente-oceano) da Bacia de Pernambuco, NE do Brasil**. 2013. Dissertação (Mestrado). Universidade Federal de Pernambuco, Recife, 2013. 72p.

PONTE, F.C. & PONTE FILHO, F.C.1996. Estrutura geológica e evolução tectônica da Bacia do Araripe. Recife, PE, DNPM/DMME (Pernambuco e Ceará). 68 p

RAMÍREZ, J.D.V. **Inferências Paleoambientais na Bacia Pernambuco (Furo IATE 1 LABIO-PE3. Albiano-Maastrichtiano) com base em análise de Palinofácies**. 2017. Dissertação (Mestrado) - Universidade Federal de Pernambuco, Recife, 2017. 73p.

Riedel, P.R., 2017. Mapeamento Geológico Baseado em Dados de Campo e de Poços da Área Norte da Bacia Pernambuco e Quimioestratigrafia de Fósforo do Testemunho de Sondagem 1-LABIO PE 3 (Furo IATE): Investigação sobre Evento de Anoxia. BSc Monograph, Federal University of Pernambuco.

RIEDEL, P.R., LIMA FILHO, M.F., MORT, H.P. Quimioestratigrafia de Fósforo do testemunho de sondagem 1-LABIO-PE-3 (Furo Iate): Investigação do evento de anoxia oceânica na Bacia Pernambuco. **Estudos Geológicos**, v. 29, p. 120-134. 2019

ROSSETTI, D.F., BEZERRA, F.H.R., DOMINGUEZ, J.M.L., Late Oligocene-Miocene transgressions along the equatorial and eastern margins of Brazil. **Earth-Science Reviews**, v. 132, p. 87-112. 2013.

SANTANA, F.R. Análise dos depósitos da sequência vulcanoclástica Albiana da Faixa costeira da Bacia Pernambuco. 2016. Dissertação (Mestrado) - Universidade Federal de Pernambuco, Recife, 2016. 96p.

SIAL, A. N., LONG, L. E., BORBA, G. S. Field trip guide excursion: cretaceous magmatic province of Cabo, Pernambuco, Northeast Brazil. **Revista Brasileira de Geociências**, v.*17*(4), p. 667-673. 1987.

SIBLEY D. 1978. Dolomite textures. In: Sedimentology. Encyclopedia of Earth Science. Springer, Berlin, Heidelberg.

SIBLEY, D.F., GREGG, J.M. Classification of dolomite rock textures. **Journal of Sedimentary Petrology**, v. 57, p. 967-975. 1987.

SILVA FILHO, A.F., GUIMARÃES, I.P., FERREIRA, V.P., ARMSTRONG, R., SIAL, A.N. The Águas Belas pluton, Northeastern Brazil: Evidence on age, emplacement, and magma sources during Gondwana amalgamation. **Precambrian Research**, v.17, p. 676-687. 2010.

TOMÉ, M.E.T.R., LIMA FILHO, M.F., NEUMANN, V.H.M.L. Análise Estratigráfica do Albiano Turoniano da Bacia Pernambuco: Considerações sobre a Paleogeografia e Geração de Hidrocarbonetos. **Geociências**, v.25, p. 1-10. 2006

WARREN, J. Dolomite: occurrence, evolution and economically important associations. **Earth-Science Reviews**, v. 52 p.1-81. 2000

ZAINI, N., VAN DER MEER, F., VAN DER WERFF. Determination of Carbonate Rock Geochemistry Using Loboratory-Based Hyperspectral Imagery. **Remote Sensing**, v. 6, p. 4149-4172. 2014